DEVELOPMENT OF A NEW VELOCITY MEASUREMENT TECHNIQUE: THE LASER BESSEL VELOCIMETRY

By

Mahmud Ali Sakah

A thesis submitted in partial fulfillment
of the requirements for the degree of
Master of Science (MASc) in Engineering

The Faculty of Graduate Studies
Laurentian University
Sudbury, Ontario, Canada

THESIS DEFENCE COMMITTEE/COMITÉ DE SOUTENANCE DE THÈSE
Laurentian Université/Université Laurentienne
Faculty of Graduate Studies/Faculté des études supérieures

Title of Thesis
Titre de la thèse DEVELOPMENT OF A NEW VELOCITY MEASUREMENT TECHNIQUE: THE LASER BESSEL VELOCIMETRY

Name of Candidate
Nom du candidat Sakah, Mahmud

Degree
Diplôme Master of Applied Science

Department/Program
Département/Programme Natural Resources Engineering

Date of Defence
Date de la soutenance June 23, 2015

APPROVED/APPROUVÉ

Thesis Examiners/Examinateurs de thèse:

Dr. Brahim Chebbi
(Supervisor/Directeur de thèse)

Dr. Meysar Zeinali
(Committee member/Membre du comité)

Dr. Ramesh Subramanian
(Committee member/Membre du comité)

Dr. Mohsen Ferchichi
(External Examiner/Examinateur externe)

Approved for the Faculty of Graduate Studies
Approuvé pour la Faculté des études supérieures
Dr. David Lesbarrères
Monsieur David Lesbarrères
Acting Dean, Faculty of Graduate Studies
Doyen intérimaire, Faculté des études supérieures

ACCESSIBILITY CLAUSE AND PERMISSION TO USE

Abstract

The present thesis describes the design, construction and testing of a new velocity measurement optical technique system. The technique has similarities with the laser Doppler velocimetry (LDV) in that it uses scattered light detection, in order to measure one component of the velocity vector of moving flows or solid surfaces. It uses the fringes of a Bessel beam produced by an axicon to generate the measurement volume. This technique, which we call Laser Bessel velocimetry (LBV), is noninvasive and permits continuous velocity measurements of moving particles. The experimental measurement set-up including the laser source, the optical devices, a moving stage with known velocities, a photodetector to capture scattered light and signal processing and data acquisition components, was developed and used to provide a proof of concept of this new technique. The set-up was also tested with a commercial LDV system.

Two types of refractive linear axicons have been used to generate a Bessel type beam by illuminating the axicons with blue and red collimated and coherent laser light of dissimilar wavelengths, λ. The linear axicons offer the advantage of simplicity. The software tools for measurements, acquisition and analysis of the data are developed using NI Labview and MATLAB. Results from both theoretical simulation and experimental measurements are presented and compared.

Acknowledgements

First and primary, I would like to thank my supervisor Dr. Brahim Chebbi for continuous support, encouragement and motivation throughout the work on my thesis. I was very fortunate to have such a good supervisor for my Master studies. I am also grateful for the support in the experiment and discussions we have had. I have benefited not only from his deep knowledge in the field of measurements, but also from his constant interest and enthusiasm, and input throughout this effort.

My thanks are also extended to Greg Lakanen and Adam Walli for their help in the lab. I am grateful for the continuous support of my wife throughout this endeavor. To all my family and friends who have supported me through the course of this work I am thankful for everything.

Table of Contents

List of Tables

List of Figures

Nomenclature

c	Speed of light
C	Capacitor
d	Diameter of laser beam before expansion defined to $1/e^2$ of maximum intensity
d_f	Fringe spacing (μm)
d_p	Particle diameter
D	Expanded laser beam diameter
f	frequency
f_D	Doppler Frequency
f_b	Bessel frequency in Hz
f_c	Cutoff frequency
f_s	Sampling frequency
f_{max}	Maximum frequency
Δf	Change in frequency
F	Focal length of lens (mm)
F_s	Frequency shift
I_0	The incident on- axis intensity
I	Intensity
I_{max}	maximum intensity
J_0	Bessel function of order 0
k	Wavenumber
m	Iteration of Bessel zeros
n	Refraction index of lens
P	Distance from object to lens
q	Distance from lens to photodetector
r	radius in cylindrical coordinates
r_o	Bessel beam spot radius (mm)
R	Resistance
R_f	Feedback resistance
R_i	Input resistance
t_m	Particle arrival time
Δt	Sampling interval

T	Period
u_f	Fluid velocity
u_p	particle velocity
v	Velocity
V	Voltage
V_{in}	input voltage
V_{out}	output voltage
W_0	Laser beam waist
z	longitudinal distance in cylindrical coordinates
Z_{max}	Maximum on-axis intensity

Greek symbols

α	Angle of axicon lens
β	Beam deviation angle of axicon
λ	Wavelength
ρ	Fluid density
ρ_p	Particle density
τ_p	Time constant
μ_f	Fluid viscously
ω_b	Bessel frequency in rad/s

Abbreviations

DOF	Depth of field
SNR	Signal to noise ratio
LBV	Laser Bessel Velocimetry
LPF	Low pass filter
μF	Micro Farad
Ω	Ohm

Chapter 1

INTRODUCTION

Since its invention in 1960 [1], laser has opened new ways in scientific research, and its enormous potential in measurements was soon recognized by researchers. The properties of laser light, such as mono-chromaticity, coherence, low divergence and high intensity are ideal for velocity measurements. Moreover, measurement of movement of objects is possible at relatively low velocities. Generally, optical measurement techniques have more advantages because they are relatively easy to use, fast, and non-intrusive. Furthermore, these methods are safe to use, since there is no direct electrical contact between the measurement devices and or direct contact with laser beams. All the information needed is transferred via light with laser powers in milliwatts. One of the most widely used optical techniques of flow velocity measurement is the laser Doppler velocimetry technique. The first demonstration of measuring velocities with the Doppler shift of laser light was invented by Yeh and Cummins [2] in 1964 who employed it to measure laminar water flow, by observing the shift of light frequencies scattered from particles seeded in water flow. Since then, as equipment that provide higher precisions was invented, the Doppler Velocimetry method became more accurate and reliable as well as numerous experimental applications of laser Doppler technique have been demonstrated. In this thesis we develop a new velocity measurement technique, which, similarly to the LDV, uses light scattered from moving particles crossing fringes, but makes use of the fringes of a single nearly non-diffracting beam. The theory of non-diffraction beams was first demonstrated by J.Durnin in 1987 [3]. These beams have large depth of field and have proved useful for many applications including optical sorting [4] and imaging [5]. In this research, limited diffraction beams, specifically Bessel beam [3], are used for velocity measurement using the fringes they generate. Because the Bessel beam has a long depth of field (DOF), the scattered frequency is less dependent on the distance of moving particles. The Laser Bessel Velocimetry system relies on measuring the characteristics of light scattered from particles seeded in a flow or on the surface of a solid object. The idea of using a single beam to generate the measuring volume and the fringes is promising but several outstanding technical challenges need to be addressed before robust systems can be developed. A major challenge for this application is to have adequate light

scattering from small particles and a strong signal-to-noise ratio (SNR). Although, the Bessel beam fringes generated by axisymmetric intersection of different rays refracted through the axicon do not have uniform fringe spacing which might make the LBV less advantageous than LDV in determining flow direction and velocity components. Yet the proposed LBV method has very simple components setup and can be used in fluids and solid surface measurements. An experiment for a rough surface scatterer moving along the horizontal direction was performed. This investigation is expected to provide key theoretical support and practical guidance for the techniques of laser detection of particles with Bessel beam. The measurements of velocity will be described and results will be compared with those calculated by theory. Measurements have been performed with (0.5°, 5°) axicons and taken on 400, 150, 220 and 1500 grit sandpaper cases shown in table 5-2. The theoretical and experimental results are presented and compared.

It is important to note that similar to the LDV technique, the present technique is expected to be mostly used for fluid flow velocity measurement. In the present thesis we test this technique with the solid surface velocity measurement and since the proposed system provides good control on the velocity to be measured.

1.1 Motivations

Bessel beams offer many advantages such as a narrow long DOF, near diffraction-less properties and ease of generation of fringes. The endeavor of the present research is to explore the use of axicons to generate Bessel beams and use them in measurement of velocities of flows and solid surfaces. It is anticipated that the obtained system will be simple and lead to less expensive focusing capability than other optical measuring systems. Using Bessel beams for velocity measurement is a new concept, and in view of its possibility and advantages, it may provide an important and valuable tool in many applications**.** For example, it is well known that Bessel beams are better suited for use in turbid media like tissue because of their self-healing properties and their ability to reconstruct compared to Gaussian beams. The decision to start the development of such a technique is at the basis for the work of this thesis, and the goal of the research is to contribute to the continuous growing knowledge and research on the topic. Since the LBV technique has a simple and compact configuration, it can offer alternative advantageous in some applications such as Laser Doppler Flowmetry where a single laser beam is used to

measure the Doppler frequency which is more difficult to measure the frequency difference as in the dual beam configuration.

1.2 Objectives

The objective of this thesis is to provide a proof of concept of the laser Bessel velocimetry technique. The research work involves the development, construction and testing of the system with Bessel beam generated with axicons. The equipment setup is tested with LDV to determine the validity of the optical measurement system. Previous investigations on applications of Bessel beam do not report direct measurements of velocities of flows with the exception of a Bessel beam LDV reported by [6] which comprises an axicon and a diffracting grating producing two Bessel beams intersecting on the measurement volume. This is an LDV system and different from the system we report in this thesis. The second system is using Bessel beam in ultrasound Doppler velocity estimation [7]. Both systems are described in chapter 3.

In order to gain good understanding of the measurements with Bessel beam, it is important to study the individual properties of non-diffracting beams, how they are generated and to characterize their effects on the measurement systems. Though a Bessel beam is generated and formed right after an axicon, its size can be manipulated through lenses. It is our goal to find how lenses can affect the dimension of a Bessel beam, that a Bessel beam with desired dimensions can be created and incorporated into the measurement system. We will be using the Bessel beam fringes generated with axicon and collect scattered light from particles crossing these fringes and analyzing the time variation and frequency content of the signal for information about the particles velocity. The final objective is to collect a consistent set of experimental data of velocity measurement that is sufficient for evaluating the theory and assumptions of particle measured velocity with Bessel beam.

1.3 Thesis Outline

The thesis is organized as follows:

- Chapter 1 provides a brief overview of the proposed system, applications, motivation and objective for this work.
- Chapter 2 describes the theoretical background that is relevant in this work.
- Chapter 3 provides a literature review of relevant work applicable to this thesis. This review includes laser Doppler Velocimetry, Axicons, Bessel beams and their applications in measurements in previous research.
- Chapter 4 describes the experimental setup, instrumentation and data acquisition of the system that is used to perform the measurements.
- Chapter 5 presents the Laser Doppler Velocimetry (LDV) validation procedure of the developed system and results of the measurements with LDV and displays examples of the results.
- Chapter 6 describes the procedure and measurements performed with the measurement system and the measurement techniques.
- Chapter 7 presents the results obtained and describes the analysis of the measurement results.
- Chapter 8 discusses the conclusion for this work and recommendations including suggestions for future work.

Chapter 2

BACKGROUND THEORY

This Chapter covers the background theory of relevant topics to develop the measurement system setup. Section 2.1 is meant to give the reader a basic understanding of the laser Doppler velocimetry with a brief overview of light scattering and the Doppler effect. Section 2.2 presents a brief discerption of particles seeding in flow.
Section 2.3 describes the optical characteristics of axicons. Section 2.4 discusses the Bessel beams which are typically used to describe the intensity profiles generated from axicons including illustration figures.

2.1 Laser Doppler Velocimetry

2.1.1 The Doppler Effect

The Doppler effect was discovered by the Austrian physicist named Christian Doppler in 1842 and it was named after him [8]. It specifies that there is a change in frequency of a wave for an observer moving relative to its source. It occurs because the waves transmitted by the source are either compressed if the source and observer are moving towards each other or spread out if they are moving away from each other. The most known daily example of the Doppler effect is the drop in pitch as a sound source moves past an observer. For example, when an emergency vehicle with a siren passes an observer, the pitch of the siren sound is high; and then after the car passes by, the pitch of the siren sound becomes low. Compared to the emitted frequency, the received frequency is higher during the approach, identical at the instant of passing by, and then becomes lower [9]. Since this frequency change is dependent on the observer and relative source velocities, this effect can be used to measure velocities. The Doppler effect can be observed for any type of wave such as water wave, sound wave, light wave, etc. The relative motion of light waves source and observer (detector) leads to a corresponding Doppler effect for light. However, the frequencies of light waves are very high and difficult to measure directly. This problem is resolved by using the phenomenon of beats; the effect produced when two waves of slightly different frequencies are superimposed. When two waves come in and out of phase with each

other, a resulting frequency is equal to the difference in frequencies between the two waves. In combining the Doppler shifted wave with original frequency reference wave, a frequency is formed which is lower than either of the two fundamental wave frequencies and hence much easier to measure. L. E. Drain et al. presented the relationship between frequency change, the detector and the source relative velocity [10].

2.1.2 Scattering light

For a review of some basic theoretical characteristics of the scattered light, the reader is referred to references [11] [12] [13]. Figure 2.1 shows a particle in vacuum or fluid and the incident light scatters in all directions. The scattering light from a particle may depend on some parameters such as:

- Wavelength λ of incident light
- Size of the particle
- The particle index of refraction

Light can be described as an electromagnetic wave, and the source of light waves relative motion with respect to an observer leads to a corresponding Doppler effect. The wavelength of light is shifted to a higher value if the source motion is away from the observer and shifted to a lower value if source motion is toward the observer. Blue light is scattered more efficiently than red because blue light has smaller wavelength than red.

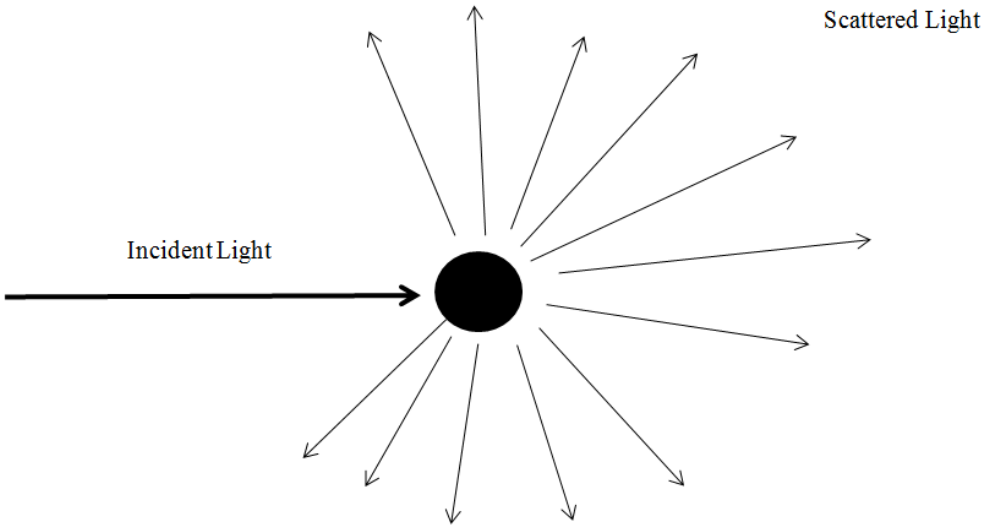

Figure 2.1: Scattering of incident light off a particle in fluid or in vacuum

2.1.3 Doppler Velocimetry

Laser Doppler Velocimetry is a technique to measure the instantaneous velocity of small particles moving in a flow field by measuring the Doppler shift of light scattered by these particles in the fringe region [14] [15]**.** This technique is non-intrusive and can measure all the three velocity components. The particles seeded in the flow are generally in micron size (d<50 micron), small enough to follow the flow velocity and large enough to scatter light to the photodetector to produce a strong signal. LDV uses laser to illuminate a moving particle in the flow. In general, a laser source has the following properties: it is well-collimated, highly coherent (meaning its electromagnetic wave fronts are all in phase), and it is nearly monochromatic meaning it is composed of very narrow range of wavelengths.

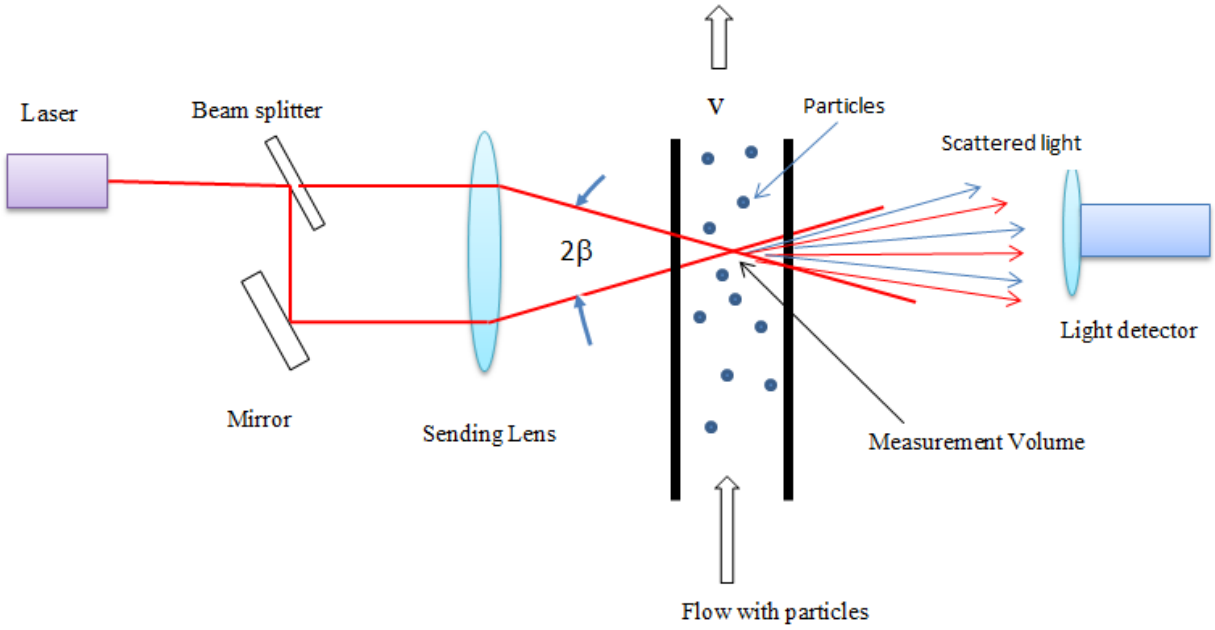

Figure 2.2: Basic components of a complete LDV system for velocity measurements

The two common configurations of this technique are the dual beam configuration and the reference beam configuration [16]. The diagram in the above figure shows the basic components of an LDV system in the dual beam mode which is the most widely used. The laser beam is split into two parallel coherent beams by a beam splitter and a mirror. A lens focuses the beams on the measuring volume with an angle 2β. When the two beams cross each other, they form interference fringes in the measuring volume. When a particle passes through the measurement

volume and crosses the fringes it scatters light when it passes a bright fringe, and scatters no light as it passes a dark fringe. This results in a shifting pattern of scattered light intensity with a frequency directly proportional to the particle velocity. The scattered light is collected by a photodetector and converted to time varying signals (voltage). The distance between fringes can be calculated and the time for the particle to travel from one fringe to the other is measured (inverse of signal frequency). The measured signal frequency can be converted to velocity [2] [17] [18]**.** Hence, the velocity of the particle can be obtained by measuring the change in frequency of the scattered laser light. One important requirement is that the particle velocity is equal to the flow velocity. The fringe spacing d_f depends simply on the half angle β and the laser light wavelength λ.

$$d_f = \frac{\lambda}{2\sin\beta} \qquad (2.1)$$

The wavelength of lasers is known accurately (approximately 0.01% or better) and with high quality optical components one can get an accurate measurement of the beam angle. This results in an accurate value of d_f which relates the particle velocity to the signal frequency. The frequency of the detected signal is directly proportional to the velocity component and inversely proportional to the fringe pacing d_f.

$$f_D = \frac{v}{d_f} = \frac{2v\sin\beta}{\lambda} \qquad (2.2)$$

Where v is the velocity component perpendicular to the fringes, and the flow velocity is the only parameter that depends on the flow; the other parameters (β, λ) depend on the instrument, therefore the LDV requires no calibration

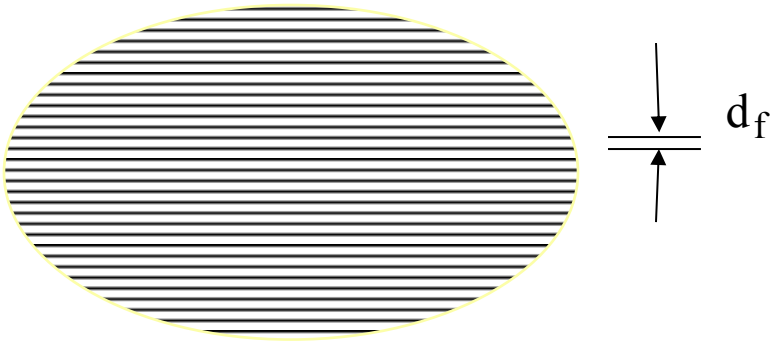

Figure 2.3: LDV fringes

2.2 Seeding in Flow

The correct selection of seeding particles is important to have adequate velocity measurement using the LDV. It must be small enough to follow the flow speed being measured and large enough to reflect a strong signal. Several seeding particle materials available are listed in table 2-1 [19]. The particle size, shape, composition density and concentrations are important parameters for selecting the seeding particles. A greater index of refraction and large geometric particle size can increase the signal quality and signal strength.

Table 2-1: Common Seeding materials and their refractive indices

Seed Material	**n**	**ρ_p (kg/m^3)**	**Fluid**
Polystyrene	1.59	$1.05x10^3$	Gas-liquid
Polyamid	1.5	$1.03x10^3$	Gas-liquid
NaCl crystals	1.54	$2.16x10^3$	Gas
Al_2O_3	1.76	$3.96x10^3$	Gas-liquid
SiC	2.6	$3.2x10^3$	Gas-liquid
Oil mists	1.4-1.5	$\cong 0.9x10^3$	Gas
Hollow glass beads	1.52	$1.1x10^3$	Liquid

The seeding particles follow the flow according to a time constant τ_p [19]

$$\tau_p = \frac{\rho_p d_p}{18\mu_f} \qquad (2.3)$$

Where ρ_p density of particle, d_p diameter of particle and μ_f is viscosity of fluid, and the system behaves as a first order one

$$\tau_p = \frac{du_p}{dt} + u_p = u_f \qquad (2.4)$$

Where u_f is fluid velocity, so that if a particle is injected with zero initial velocity at time t=0, its velocity becomes

$$u_p = u_f(1 - e^{-\frac{t}{\tau}}) \qquad (2.5)$$

Most fluid flows contain natural seeding such as dust, lint, aerosols etc. However, because size, density and index of refraction and shape of these particles are not known, flows can be filtered and seeded with particles with known characteristic for suitable measurements [19].

2.3 Axicons

Axicons are optical elements that produce a Bessel beam. An axicon can be a cone of glass, which creates long and narrow focal lines along the optical axis which makes them suitable in many applications. A property of an axicon is that a point source on its axis of revolution is imaged to a range of points along the axis. The principle of an axicon is illustrated in figure 2.4 parallel rays are refracted at approximately the same angle, independent of position in the axicon, thus producing a conical wave in a ring shaped beam which creates the Bessel beam

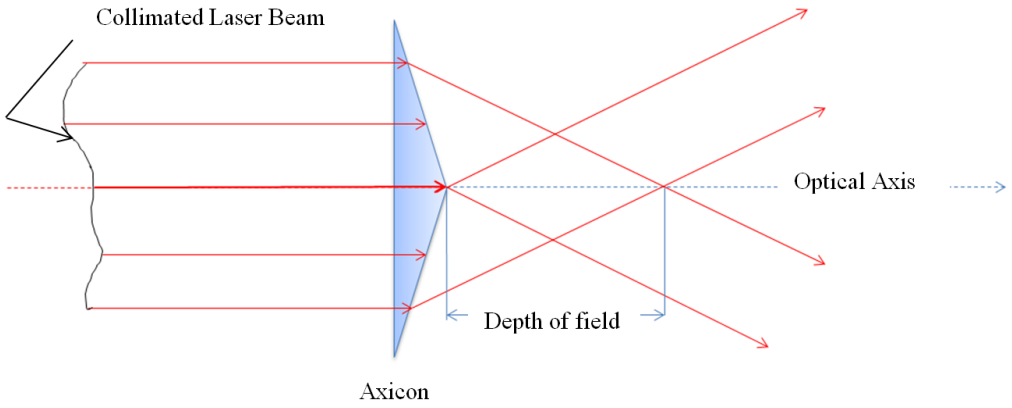

Figure 2.4: Ray tracing for an Axicon

In 1954, J.H. McLeod conducted the first experiments on axicons. Since then, many new researches, construction methods, design methods and applications have been presented depending on the type of axicon [20]. For further reading on axicons, there are several reviews [21] [22] [23] [24]. Whereas a normal lens generates a point focus, an axicon produces focal lines stretched along the optical axis. The length of the line can vary from one millimeter up to several kilometers depending on the type and design of the axicon [25] [20]. When an axicon is illuminated with a collimated Gaussian beam, it produces a non-diffractive Bessel-type beam retaining a constant ring thickness within the axicon's depth of field (DOF) and a ring shaped beam that increases in diameter over the beam propagation distance. The Bessel beam is ideal for

a range of applications in medical research, measurement, and instrumentation fields [26], which will be discussed in the next chapter. The state of the incident light is important for the performance of the axicon, and in this thesis, two axicons (0.5° and 5°) are used to generate the Bessel beam. If the laser beam directed on the axicon was not parallel and coherent, in other word oblique illumination, the Bessel focus is destroyed. Fully coherent and collimated light is required to generate Bessel beam which will produce the measurement volume of the moving particles. For incoming light beam of plane waves, simple geometric optics results in an uneven spreading of the light energy along the axis. Moreover any increase in the angle of refraction makes the energy of light to be spread over a shorter distance becoming denser. The angle of refraction β is related to the angle of the axicon α which is the base or apex angle of a prism or a cone by:

$$\beta = \arcsin(n_{lens} * \sin\alpha) - \alpha \qquad (2.6)$$

This can be written for small angles as $\beta = (n - 1)\alpha$

2.4 Bessel Beam and Bessel-Gaussian Beam

In 1987, J. Durnin showed that a Bessel beam distribution is a solution to the Helmholtz wave equation [27]**.** The non-diffraction property of this beam is in stark contrast to a Gaussian beam change as it propagates through space [28]. A Bessel beam gets its name from a Bessel function, and this leads to a predicted cross-sectional profile consisting of a set of concentric rings. When a Gaussian beam is incident on an axicon, a conical wave front is generated that interferes to produce a zero order Bessel beam profile function, $J_{0,}$ for the electric field. Higher order Bessel beams J_n can be generated by illuminating an axicon with a Laguerre Gaussian beam [29]. In this thesis, we are only concerned with zero order Bessel beams. In addition to being non-diffractive, Bessel beams also have the property of self-regeneration when obstructed [30] [31]. This is one of the most prominent qualities of the Bessel beam. It can reconstruct around obstructions placed in the beam propagation direction. The obstruction blocks some of the incoming waves, but the waves that pass the obstruction are able to interfere and reform the Bessel beam. This is also known as the self-healing property. The Bessel beam has its energy evenly distributed between its rings [32] [33], so the more rings the beam has the lower the energy in the central core or spot

intensity, although a larger number of rings comes with an increased propagation distance [34]. Ideally, the Electric field of a Bessel beam can be described by equation [35]:

$$E(r, \phi, z, t) = E_0 \exp(i(-\omega t + k_z z)) J_0(k_r r) \quad (2.7)$$

$$k_z = (\frac{2\pi}{\lambda})\cos\beta \quad (2.8)$$

$$k_r = (\frac{2\pi}{\lambda})\sin\beta \quad (2.9)$$

Where J_0 is the zeroth-order Bessel function, k_z and k_r are the longitudinal and radial wave vectors. The wavenumber can be determined

$$k = \sqrt{{k_z}^2 + {k_r}^2} = \frac{2\pi}{\lambda} \quad (2.10)$$

By multiplying the electric field by its conjugate (assuming k is real) the transverse intensity $I=E*E^*$ is proportional to: $J_0^2(k\beta r)$

Higher order Bessel beams also have a transverse intensity profile of concentric rings but without the central bright spot. In theory, the intensity profile of a zero order Bessel beam propagates for an infinite distance without spreading in propagation direction and the Bessel beam can contain an infinite number of rings illustrated in figure 2.6. The amount of energy contained in each ring of the Bessel beam distribution is almost equal to the amount of energy contained in the central lobe, that is over an infinite area would carry infinite power. In practice, the beam can propagate diffraction-free for only a finite distance. This is because an infinite diffraction-free propagation distance would require the Bessel beam to have an infinite number of intensity rings and therefore the beam would require infinite energy. Since this is impossible, however, a finite approximation to the ideal Bessel beam, which has diffraction-free propagation distance and finite energy, can be produced experimentally [34]. The maximum diffraction-free propagation distance in free space of a beam generated by axicon depends on the material index of refraction, n, the angle of the axicon, α, and the incident beam waist, W_0. The Bessel beam form is illustrated in figure 2.6 showing the concentric rings and the central spot.

When the beam is projected further from the axicon, within the depth of field (DOF) a ring-shaped beam is formed as illustrated in (Fig 2.5), with its diameter increasing with distance, the

beam is actually conical. The thickness of the beam remains constant since the rays are non-diverging. The thickness of the ring is half of the input laser beam diameter.

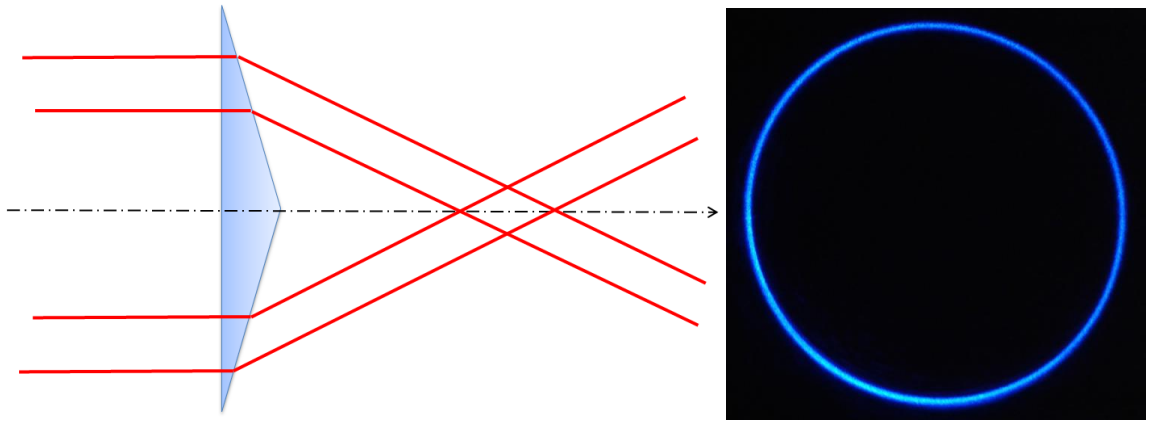

Figure 2.5: Ring formed after an axicon illuminated with Gaussian beam

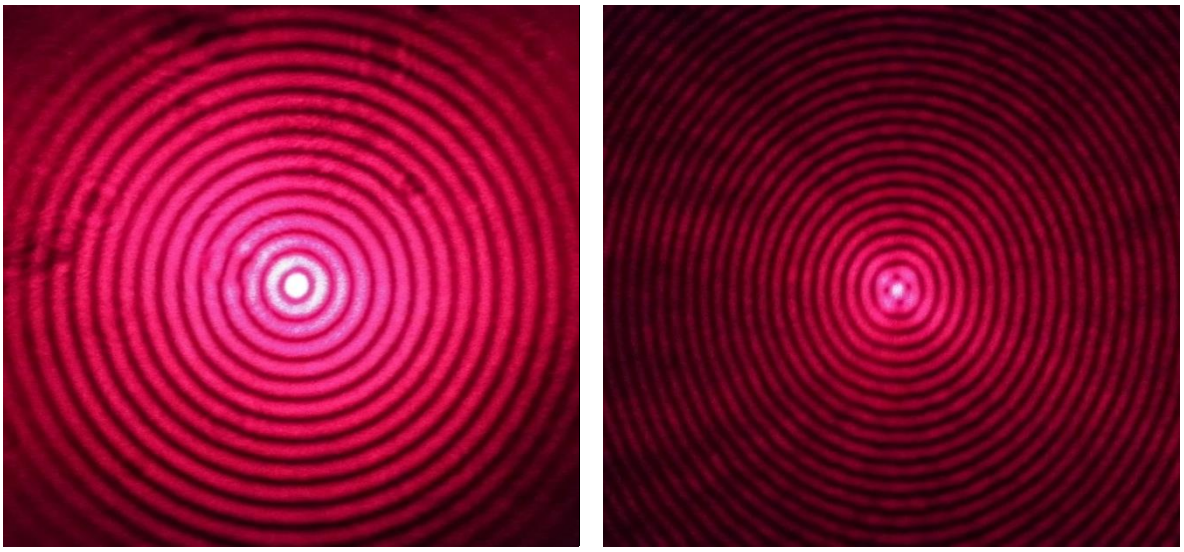

Figure 2.6: Bessel beam generated by 0.5° Axicon and 5° Axicon

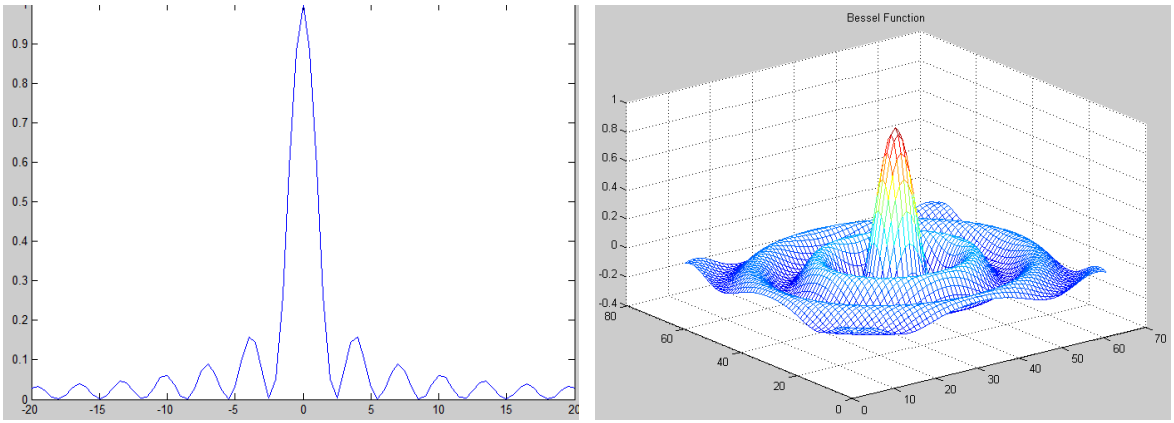

Figure 2.7: Bessel beam profile generated with Matlab

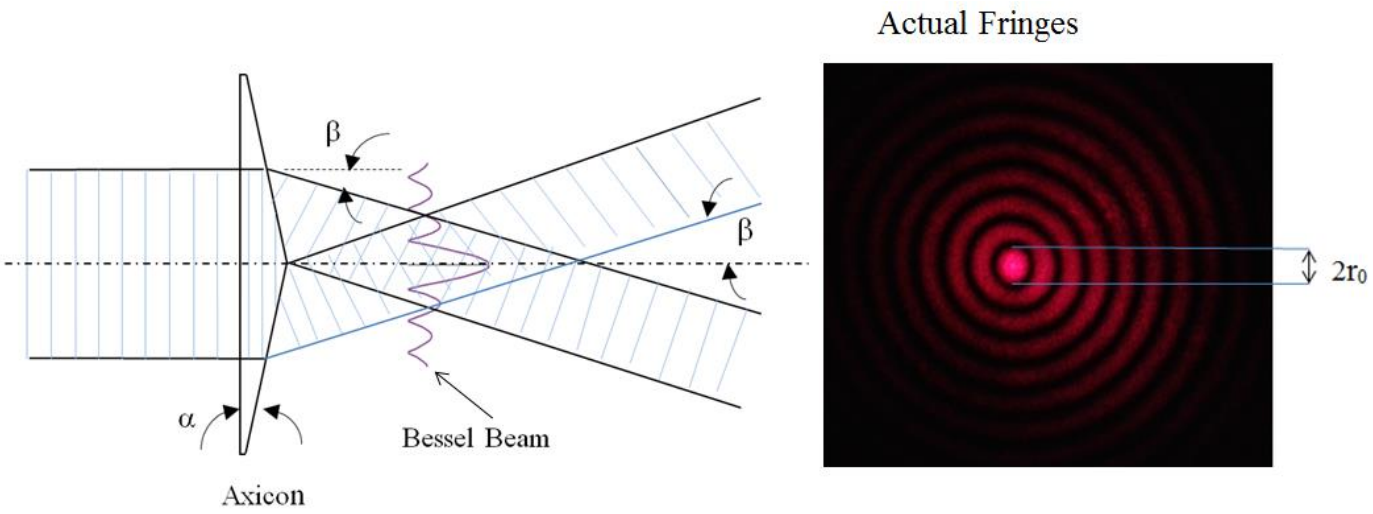

Figure 2.8: Bessel Beam which propagates in horizontal direction

The Bessel function described above is characterized by intense spot in the center encircled by rings of less intensity. The size of the central spot is given by its radius:

$$\mathrm{ro} = \frac{2.4048\lambda}{2\pi \sin\beta} \qquad (2.11)$$

Since $\sin\beta \approx \beta$ from the small angle approximation $\mathrm{ro} = \frac{2.4048\lambda}{2\pi\beta}$

However, if collimated Gaussian beam is used to illuminate an axicon, the beam generated is called Bessel-Gaussian beam. The following variation of intensity distribution [36] [6] is obtained:

$$I(r,z) = I_0 \left(4\pi^2\beta^2 \frac{z}{\lambda}\right) * \exp\left[\frac{2(\beta z)^2}{w_0}\right] * J_0{}^2(k\beta r) \qquad (2.12)$$

Where r,z are radial and longitudinal coordinates, I_0 is incident on-axis intensity, w_0 is the beam waist, and k is the wavenumber in free space.

The above equation (2.12) gives the variation of the intensity in a cylindrical coordinate system (z,r,ϕ), but since the lenses considered are symmetric about the z axis there is no variation with ϕ. The on-axis intensity is obtained by setting $\boldsymbol{r} = 0$:

$$I(0,z) = I_0 \left(4\pi^2\beta^2 \frac{z}{\lambda}\right) * \exp\left[\frac{2(\beta z)^2}{w_0}\right] \qquad (2.13)$$

The radial/transverse distribution can also be obtained by setting **z** to a constant value along the axis. When the axicon is illuminated with laser beam the on-axis intensity increases linearly with distance until the end of the focal range (or depth of field) where it drops off dramatically. The depth of field (DOF) is defined by the distance where the on-axis intensity is greater than half the maximum intensity, which can be found from the geometry of the axicon in figure 2.9 by
The original beam with diameter d is magnified by a two-lens telescope, with magnification factor, $M = \frac{F2}{F1}$, where F_2 and F_1 are the focal lengths of the two lenses. The new diameter D is:

$D = d\left(\frac{F1}{F2}\right)$ and $W_0 = \frac{D}{2}$

$$DOF = \frac{W_0}{\tan\beta} \qquad (2.14)$$

The on-axis maximum intensity can be found from the axicon and Gaussian beam properties

$$Z_{max} = \frac{W_0}{2\beta} \qquad (2.15)$$

And the value of the maximum intensity I_{max}:

$$I_{max} = \left(\frac{2\pi^2\beta}{\lambda}\right) * \exp(-0.5) I_0 \qquad (2.16)$$

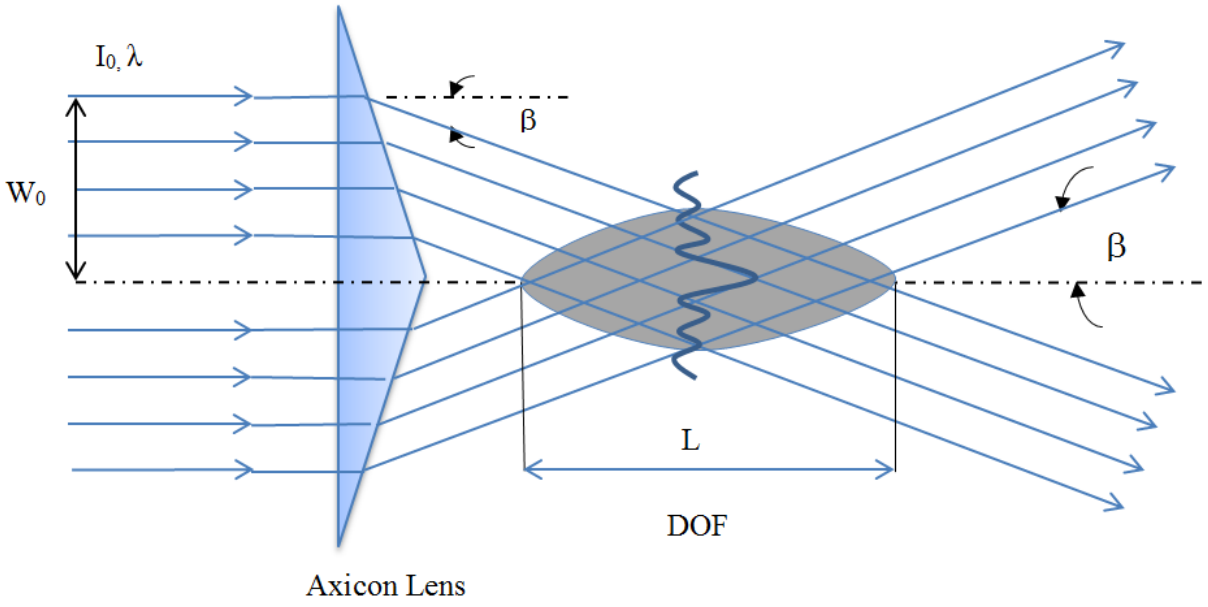

Figure 2.9: Bessel beam depth of field

Chapter 3

LITERATURE REVIEW

This Chapter contains a review of relevant investigations related to this thesis. Section 3.1 reviews different optical techniques to measure velocity with an emphasis on the LDV technique. Section 3.2 reviews the axicons in details and their properties and the different kinds. Section 3.3 reviews the Bessel beams. Section 3.4 outlines briefly some of the axicon and Bessel beam applications and section 3.5 outlines the axicon extension of depth of field. Since laser Bessel velocimetry is a new technique, there is no related literature available.

3.1 Optical techniques to measure velocity

We restrict this review to the techniques relevant for fluid velocity measurement. There are different optical encoders to measure rotational and rectilinear solid velocities, and some of the techniques reviewed in this section, such as the LDV, can also be used for solid surface velocity measurement [37] [38].

3.1.1 Laser Doppler Velocimetry

Laser Doppler Velocimetry [39] [40] is very well established and commonly used optical velocity measuring technique with some unique features for applications in fluid dynamics velocity measurement. It uses the Doppler shift of light scattered from moving particles in the measurement region [14] [15]. The value of this frequency shift is small compared to the laser frequency so different configurations were proposed such as the reference beam configuration and the dual beam configuration. The first application of laser Doppler velocimetry in flow measurement was performed by Yeh and Cummins in 1964 [2] to measure velocity of water in a pipe flow soon after the invention of the first laser in 1960. They split HeNe laser beam into two beams with a beam splitter with one beam illuminating the particles seeded in the flow and the other beam acts as a reference. With the reference beam, the scattered light from the particles was focused and recombined on a photomultiplier, making this arrangement acting as an optical heterodyne detection set-up of the frequency difference between the two light beams and restricting the collection of light to the direction of the reference beam. The frequency difference

is recorded by the photomultiplier as a beat signal which has a frequency proportional to the particle velocity. Additionally, since the beat signal is a function of the scattering angle, small solid angles are necessary to collect the scattered light in order to avoid broadening the frequency spectrum. Different approaches to measure scattered light and frequency shift with LDV were developed by many researchers leading to several advances. This technique became widely used and commercially available.

The LDV was successfully applied for solid surface measurements for different applications, for example Yuen et al [37] developed and applied a scanning LDV system for the measurements and investigation of the metal flow velocity distribution in the plate rolling process. The scanning mechanism was based on beam displacement by a rotating transparent plate. Multi-point LDV measurement was possible by adding a scanning mirror to the LDV optics. Rotating mirrors can generate a curved scanning trace and a large scanning range [38]. The LDV unique features, for instance high special resolution, high accuracy and fast response were favorable to detect the velocity distribution in the roll bite and the instantaneous relative velocity between the strip and the work roll. The scanning LDV was first tested with a rotating disk and then applied in the rolling process. The test results have demonstrated the feasibility of the scanning LDV and the velocity distribution in the deformation zone could be found.

3.1.2 Other techniques

Particle image velocimetry (PIV) is a nonintrusive optical measurement technique used to obtain velocities over a planar cross-section of a flow field [41]. The system works with seeding the fluid with small particles. The fluid is illuminated so the particles become visible. An image of moving particles in the illuminated region is captured by a camera at time t. After a short time another image is taken at time $t+\Delta t$. Then, a velocity vector map of the flow area can be generated provided the time interval between image captures is known. The motion of these particles is used to calculate the speed and direction of the flow being studied. The PIV technique consists of image acquisition and image evaluation. The main difference between PIV and the LDV technique is that PIV produces two-dimensional or even three-dimensional vector fields, while the LDV technique measure the velocity at a point.

Other techniques include the Doppler Global Velocimetry (DGV) and the Laser Induced Fluorescence (LIF) [42].

3.2 Axicons

John H. McLeod [26] was the first to use axicons which are optical conical elements generating a narrow focal line along the optical axis instead of the usual point focus [27]**.** He mentioned in his work the name axicon to describe diffractive or refractive optical elements that image along their axis a point source over a range of points. Axicons are different from the widely used spherical lenses which have shorter depth of field (DOF) and generate a Gaussian like diffracting transverse distribution. The extended DOF and specific properties of axicons makes them attractive in many applications. In general, there are many different types of axicons or optical elements generating nearly non-diffractive Bessel-type beams and they can be diffractive, refractive or reflective, but probably the most important one is the conical lenses described by McLeod [27] which are used extensively and are commercially available. For generating diffraction-free beam, refractive axicons are more energy efficient than diffractive axicons. The axicons and their derived elements were studied extensively in recent years [36] [43]. A glass cone will refract all rays at the same angle relative to the optical axis, hence creating a Bessel-type beam. It is also referred to as a linear axicon. Linear axicons have a varying on-axis intensity distribution. In order to obtain other types of axicons, for example a logarithmic axicon, the shape of the glass cone has to be slightly modified. Some examples of investigations using these elements include [44] and [45]**.**

Durnin [3] has shown that passing a collimated laser beam through the axicon center, the traverse intensity along the focal line can be approximated by a zero-order Bessel-type beam which propagates without diffraction and preserves its transverse distribution along the axis**.** Combining an axicon with an spherical lens can produce a varying ring pattern along its optical axis and extends the depth of field (DOF) [46]**,** which is one the main characteristics of axicons. This property specifically differentiates the axicons from typical spherical lenses which have shorter Gaussian like DOF, diffracting transverse distribution beams. Jaroszewicz [21] [47] offered a comprehensive review on the different types of axicons, their design, construction and properties. A hollow beam was created with the use of axicon combined with two lenses [48]. The hollow beam would be shown as a ring with constant intensity and its diameter increases as

it propagates. When the axicon is illuminated by a collimated laser beam, then at a known distance from axis the incident rays intersect at a point along the propagation axis and the incident rays at another known distance intersect at another point on the propagation axis and so on. This generates an image focused at all positions up to a maximum distance. This maximum distance is the depth of field and can be determined by the axicon angle α, its refractive index and its aperture [48]. In addition, the incident laser beam characterized by a waist w_0 where the beam spot size is minimum, its waist w_0 location and size can be controlled by a convergent lens which is usually inserted before the conical lens [49].

3.3 Bessel beam

By illuminating an axicon with a collimated Gaussian light beam, a narrow focal line is generated along its optical axis [27]**.** The intensity along the focal line can be approximated by zero-order Bessel-type non-diffracting beam preserving its transvers distribution along the propagation axis increasing depth of field (DOF) [3].

In optics, several methods for creating Bessel-type beams have been suggested such as narrow annular slit [3]**,** optical refracting systems [50], Fabry-Perot cavity [51], axicons [52]**,** diffractive phase elements [53], and computer-generated holograms [54]**.** Bessel-type beams (diffraction-free) were also generated by other types of axicons such as lens axicons, reflective axicons [55] and holographic axicons [54] [56]. However, the most efficient method of generating Bessel beam has been proposed using axicons**.** The Bessel beam does not break the laws of diffraction, but nonetheless it is very useful in alignment [57], due to the long and narrow line of light. Bessel beams have been theoretically investigated by many researchers [3] [58] [59] [60].

3.4 Applications of axicons

Perhaps the most common application of axicons is in imaging [61]. Other applications include microscopy [62] [63] [64], scanning optical systems [65], laser Doppler velocimetry [6], shearing interferometry with radial displacement [66], laser-machining [67], hole drilling [46], generation of intense non-diffracting beams [68] [69], laser trapping [44] [70] [71], optical coherence tomography [72] and telescopy for long-range alignment [26]. A variety of papers

were devoted to the focusing scheme consisting of a thin lens and an axicon [46] [48] [73] [74] [75]. The combination can be used to obtain a high-quality focal ring and diffraction-free beams in a region beyond the focal plane where the two waves overlap [76] [77]. To create a Bessel beam in this region, another lens is required to rectify the diverging wave front [73] [76] that can be reconstructed with a transverse profile expanding while propagating. The axicon is also used in laser diagnostics of the mechanical properties of thin films and solids by surface wave spectroscopy which helps study the mechanical properties of materials under extreme conditions. Axicons can also be used to increase the range of depth in triangulation [78]. The benefit and application of the extended DOF of axicons will be reviewed in detail in the next section. Saikaley investigated the use of different axicons in imaging applications [79]. Three types of refractive axicons were investigated: a linear axicon, a logarithmic axicon and a Fresnel axicon. Also their performance and a number of restoration techniques were demonstrated and compared.

3.5 Extended depth of field of axicons

Many applications can benefit greatly from extended depth of field of axicons. Optical devices with extended and controllable DOF are uncommon and are expensive because of the requirement of special lenses or movable mechanical parts. Consequently, affordable devices with a controllable extended DOF are needed to enable their utilization in a wider range of applications. Many methods have been proposed to extend the DOF, such as the use of wave front coding [80] and optical power-absorbing apodizers [81]. Chebbi et al [82] showed experimentally an optical system that produces a variable position and extends focal depth utilizing axicons. The proposed system consisted of three axicons. The first two axicons are identical and they create an annular beam propagating in free space or in a fiber bundle. This beam was focused by a third axicon generating a controllable DOF. By adjusting the distance between the two external axicons the focal distance can be controlled which depends on the diameter of annular beam. This system setup allows a simple and cost effective adjustable focus capability in many applications such as laser Doppler velocimetry, endoscopy and tomography [82]**.** Zhai et al. used an axicon with a common lens to extend its depth of field (DOF) [83].

3.6 Applications of Bessel beam

In optical area application, diffraction-free Bessel beams have attracted great interest over the years and have been broadly investigated. Their novel properties have many substantial applications [84]. To our knowledge, a single laser Bessel beam has never been previously used for velocity measurement applications, with the exception of the work of Andreas Voigt et al who suggested the limited divergence of Bessel beams can be used as a means of improving the spatial resolution in laser Doppler velocimetry [6]. The paper suggests two intersecting Bessel beams to form the measurement volume based on LDV principles instead of the conventionally used Gaussian beams. The LDV system as investigated by Voigt et al. employed the plane wave front property of Bessel beams to generate a small measurement volume minimizing the velocity uncertainty resulting from variations of fringe spacing. Greenleaf et al. [7] showed that an ultrasonic Bessel beam can be applied to estimate velocity using the Doppler effect. Because of the large depth of field, velocity estimation is depth independent. Because Bessel beams have the property of propagation invariance and extremely narrow intensity profile, they are applicable in scanning optical systems and metrology. Recently, Bessel beams were used to manipulate micrometer-sized particles [85]. Using the self-regeneration property of Bessel beam, it is likely to manipulate tiny particles (of micron-sized) simultaneously in multiple planes. Li and Aruga [86] argued that a diffraction-free Bessel beam is applicable in imaging providing a longer focal depth compared with Gaussian beams and improving the resolution of images system [87]. Since Bessel beams can stand the atmospheric turbulence more than other beams they were used for large-scale measurement and straightness [88], Bessel beams were used to accelerate the particles of the electron beam when radially polarized [89]. Li et al [90] applied Bessel beams to optical interconnection and promotion of free electron laser gain. Tewari et al [91] proposed the use of Bessel beam in nonlinear optics to generate third harmonic which is usually only observed at very high intensities of light such as those provided by lasers. The increase of Z-scan sensitivity in measurement using Bessel beams was demonstrated in [92].

Chapter 4

INSTRUMENTATION AND EXPERIMENTAL TECHNIQUES

This Chapter describes the instrumentation and optical components used in the LBV experimental work along with their purpose and any operating and usage guidelines. It outlines the fundamental procedure employed to develop and build the optical system used for the measurements reported in subsequent Chapters. The experimental configuration is described in details in section 4.1.

4.1 Experimental Apparatus

The experimental apparatus designed and built for velocity measurement is presented in figure 4.1. A red laser diode with an output power of 107 mW and a wavelength of 658 nm mounted horizontally on the lab bench was used for most measurements. A blue laser with an output power of 10 mW and a wavelength of 473 nm was also available for the measurements. Two spherical lenses of 50 mm and 400 mm focal length were mounted in front of the laser beam to expand it to a diameter of 8mm. This is given by D=8 mm with the relationship $D = d\left(\frac{F2}{F1}\right)$ as shown more clearly in figure 4.2. The expanded laser beam was aligned and centered on the axicon. Two axicons of 0.5° and 5° were available for all measurements. All lenses and axicons used in this thesis have a diameter of 25.4 mm. Four sandpapers with abrasive rough surface with different grit sizes (table 6.1) were used in the measurements. Copper wires of a diameter approximately 150 μm were used in the second test. The rough surface testing plate is attached to a linear stage (Zaber Technologies, T-LSR) mounted horizontally as shown in figure 4.3**.** This stage was used to control the speed of a moving surface and controlled with an NI Labview graphical user interface (GUI) shown in figure 4.7. A Thorlabs photodetector (PDA10A) was used to detect scattered light from the moving plate rough surface once it crosses the fringes of the Bessel beam and also detect scattered light from wires crossing the fringes. The photodetector was used in connection with 20 mm focal length lens to collect the scattered light from the measuring volume and provided a voltage with frequency proportional to the scattered light frequency. The signal from the photodetector was passed through an amplifier and low pass filter circuits. An Oscilloscope (2542 Digital Storage Oscilloscope, BK Precision) was used for

adjusting and monitoring the signal. A power supply voltage (BK Precision 1671) used to supply a 12-Volt DC to the low pass filter circuit and the amplifier. The amplified and filtered signal was digitized with an (A/D) converter connected to a personal computer and the obtained data files were stored for processing. An NI LabVIEW © program permitted selecting the sampling rate, the number of samples and the velocity of the linear stage. The data files were processed using Matlab. The spectra of the signal were determined using the Fast Fourier Transform (FFT) to determine its frequency content. The laser, the lenses, the axicon and the photodetector were mounted on posts and holders and secured into an optical breadboard bench. Proper adjustment and alignment procedures of each component were followed.

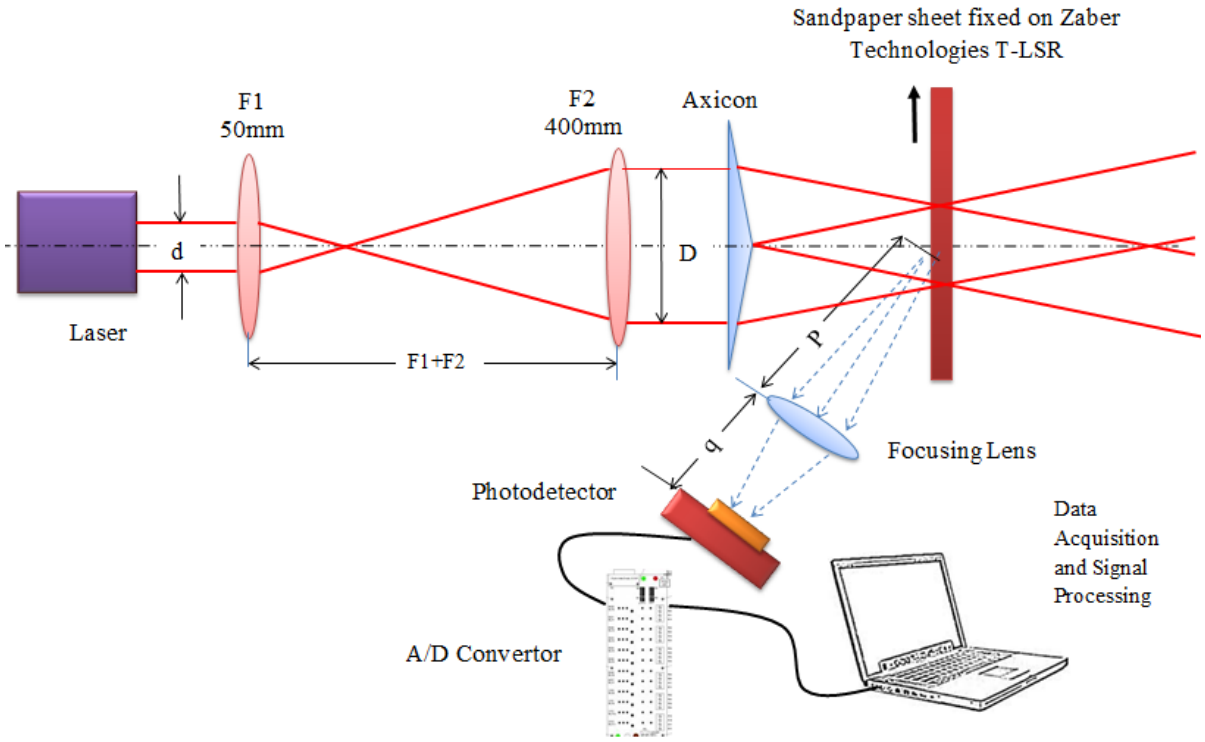

Figure 4.1: Equipment setup

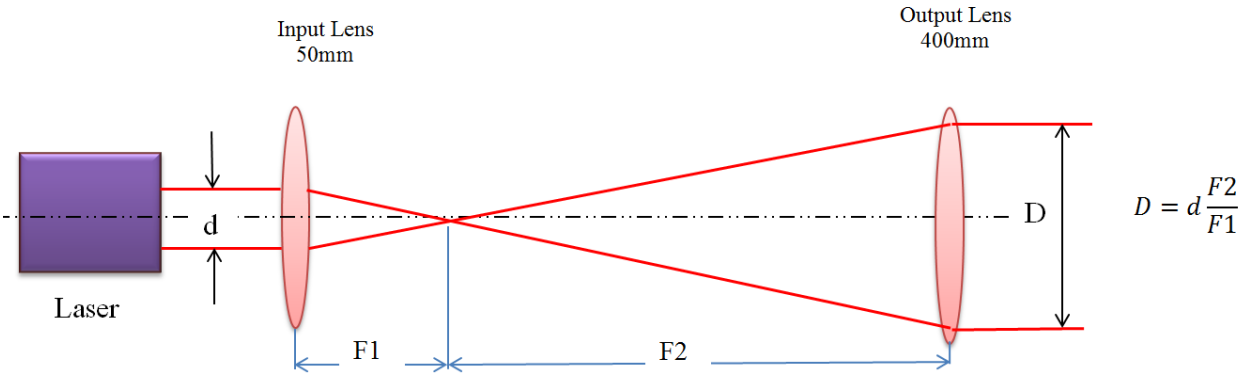

Figure 4.2: Laser beam magnification with lens setup

4.2 Zaber Technologies T-LSR160D

The Zaber motor stage was operated by software written in NI Labview to control the position and the speed of up to a maximum of 80 mm/s.

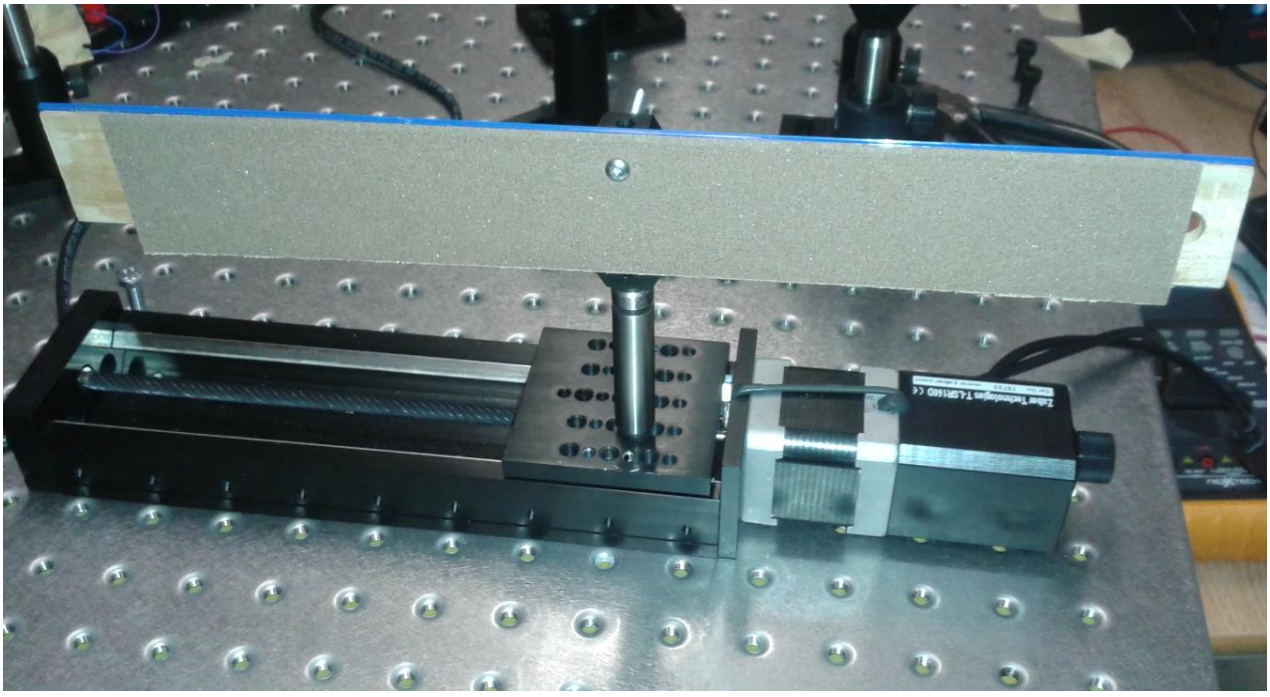

Figure 4.3: Sandpaper sheet mounted on Zaber Motor Stage

4.3 Thorlabs Photodetector (PDF10A)

The photodetector (PD) is a silicon photodiode of 150 MHz bandwidth at wavelength=220-1100 nm and a responsivity of 0.47 A/W. It has a fixed gain of 10kV/A with high-Z load and a maximum output current of 100mA. The detection size is 1.0mm in diameter with an area of $0.8mm^2$. It converts the scattered light into electric current. From there a load resistance of 5 kΩ was connected to the photodetector to convert the generated current to an output voltage signal. The voltage is amplified, filtered and collected by A/D converter. The amplified and filtered voltage has a frequency proportional to the frequency of the scattered light from the measurement volume. The voltage signal was digitized using an analog to digital converter controlled by a program written with NI Labview. The data was stored in a text files that were processed by a program written in Matlab.

4.4 Photomultiplier (H9306 Hamamatsu)

A Hamamatsu HC120-05, PMT (R3823) Photomultiplier detector was used with the setup to collect the scattered light. It has a bandwidth of 20 KHz and a wavelength detection range of 185-900nm.

4.5 Amplifier and Low Pass filter

The first portion of the circuit is a simple amplifier with a gain of approximately 11. The circuit is shown in figure 4.4 and was built with R_f =10kΩ resistor and R_i=1kΩ. The second stage of the circuit consists of low pass filter, shown in figure 4.5, and was built with R_f =10kΩ resistor, R_i=1kΩ, R=10kΩ, and a capacitor C=0.001μF when using 5° axicon. When using the 0.5° axicon the capacitor was replaced with C=0.01μF. The LPF has cut-off frequency 1.59 kHz when using 0.5° axicon and 15.92 kHz when using 5° axicon. When using 5° axicon fringes and based on the theoretical prediction, the maximum Bessel frequency f_b is 11300Hz which occurs at v=80mm/s. Based on the Nyquist criteria the maximum frequency will be twice the sampling frequency ($f_s \geq 2f_{max}$) where f_{max} is the highest frequency contained in the signal which is 11300Hz. Thus the sampling frequency f_s was set to 30000Hz. When using 0.5° axicon, the maximum Bessel frequency f_b at maximum velocity is 1130Hz thus, the sampling frequency was

set to 5000Hz. The LPF allows only frequencies below the cut-off frequency f_c to pass and above f_c are attenuated. It reduces high frequency noise but also eliminates aliasing.

$$\text{Gain} = \frac{\text{Rf}}{\text{Ri}} + 1 = 11 \qquad (4.1)$$

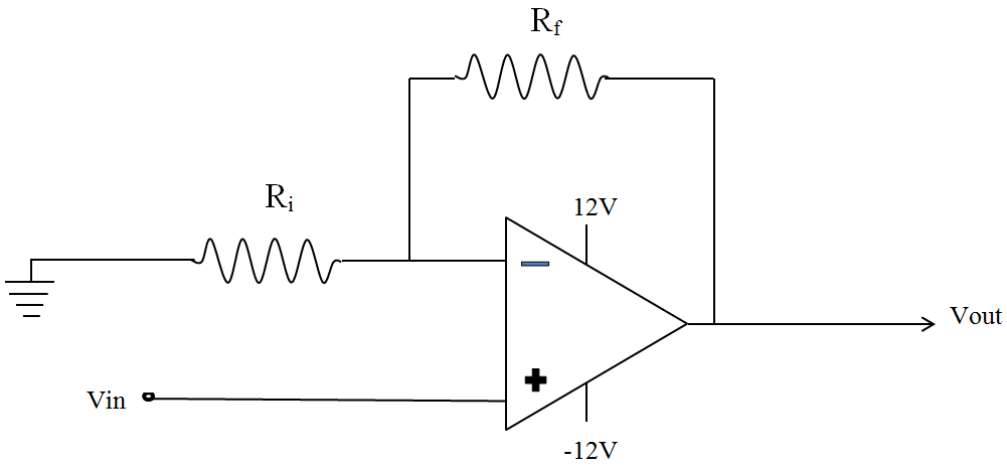

Figure 4.4: Non-inverting Amplifier Circuit

The cutoff frequency $f_c = \frac{1}{2\pi RC}$ (4.2)

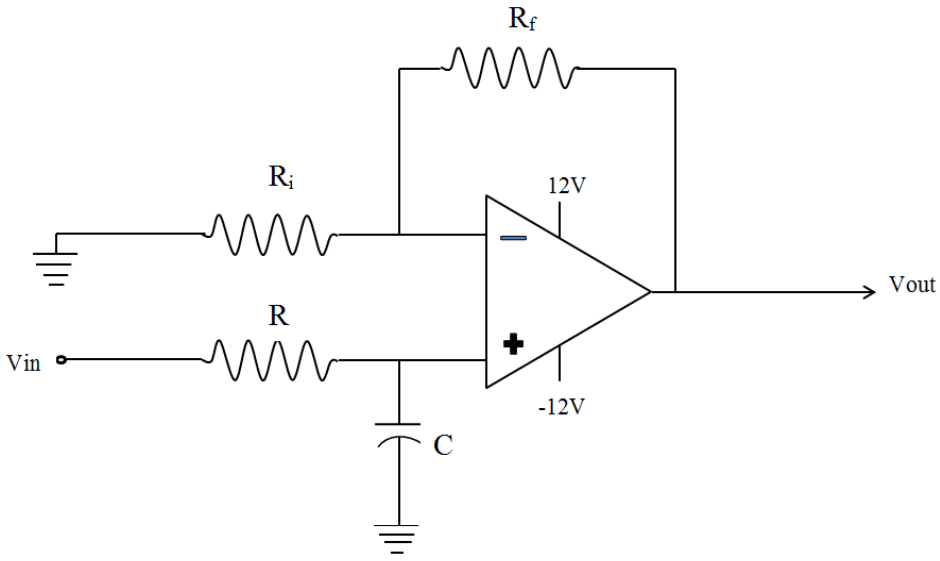

Figure 4.5: Low Pass Filter Circuit

When using the 5° axicon the capacitor C=0.001μF and the cutoff frequency

$$f_c = \frac{1}{2\pi RC} = \frac{1}{2\pi * 10 * 10^3 * 1 * 10^{-9}} = 15.92KHz$$

When using the 0.5° axicon the capacitor C=0.01μF and the cutoff frequency

$$f_c = \frac{1}{2\pi RC} = \frac{1}{2\pi * 10 * 10^3 * 10 * 10^{-9}} = 1.59KHz$$

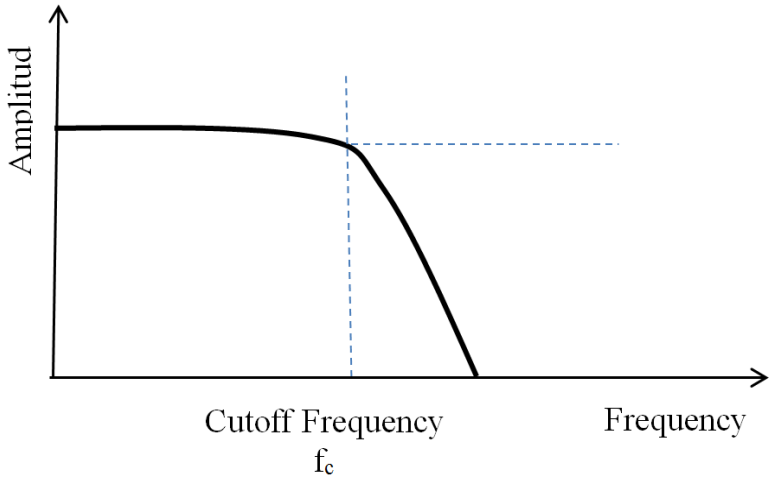

Figure 4.6: Low Pass Filter

4.6 Data Acquisition

An Omega-DAQ Board-3000 is used for data acquisition and programmed using NI Labview. It digitizes the amplified and filtered signal from the photodetector or photomultiplier. An oscilloscope was used to monitor the signal. A Graphic User Interface was developed using NI Labview and used for each of the experimental measurements (Figure 4.7). It includes all the required controls such as scan rate, number of scans and speed. A detailed explanation of each component is described in figure 4.7 and figure 4.8. Velocity was set in LabVIEW figure 4.8 with ±0.1 mm/s uncertainty. Each velocity corresponds to a set value as shown in figure 4.8, for example 40mm/s corresponds to 2150 set in window (12). The position is set in window (14) which corresponding to the distance the linear actuate will move.

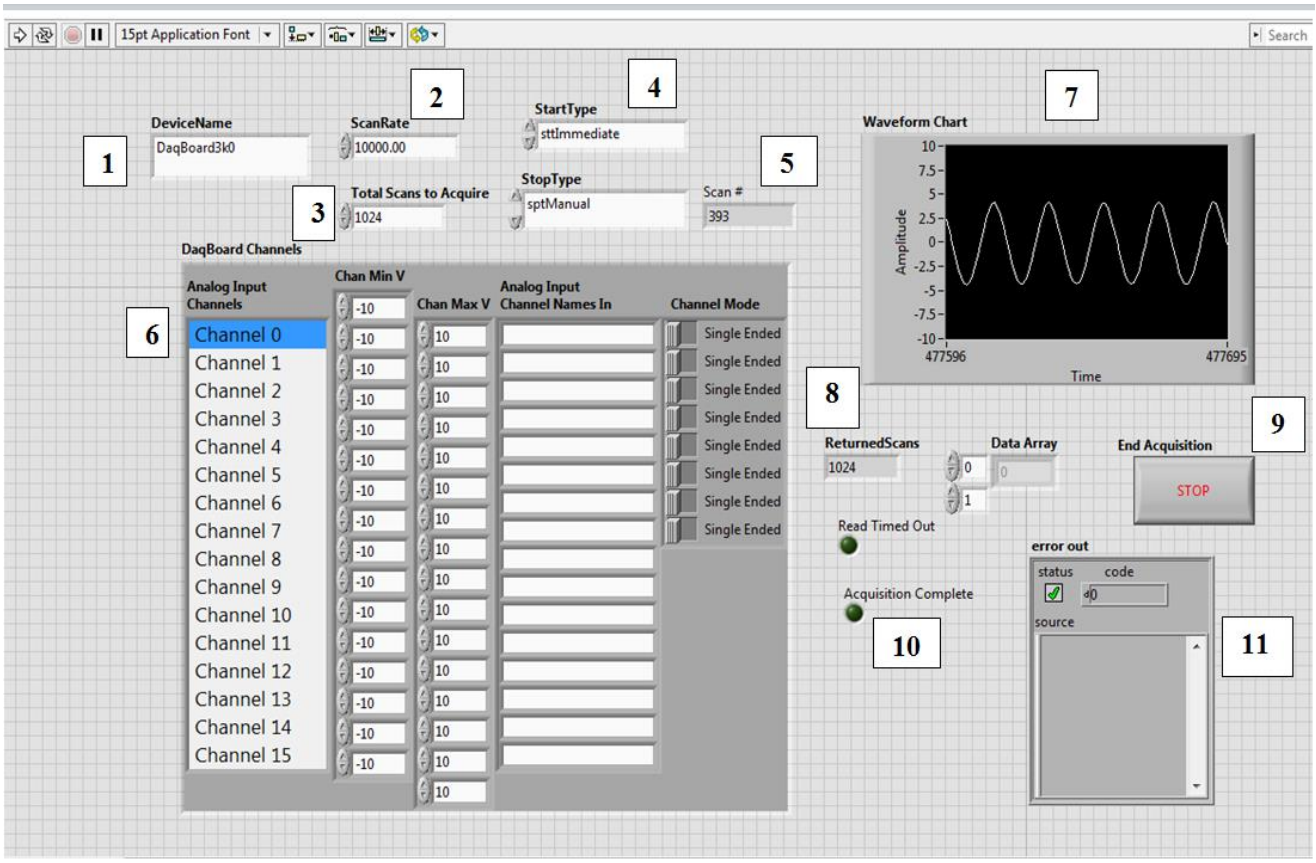

Figure 4.7: Labview Graphic-User Interface of Experimental Apparatus

(1) Device name of Data acquisition card

(2) Sampling rate adjustment

(3) Total number of scans

(4) Scan type

(5) Number of scans

(6) Channel used in acquisition

(7) Auto-update waveform of the measuring signal

(8) Number of returned scanned samples

(9) Ending acquisition control

(10) Acquisition status feedback

(11) Output error

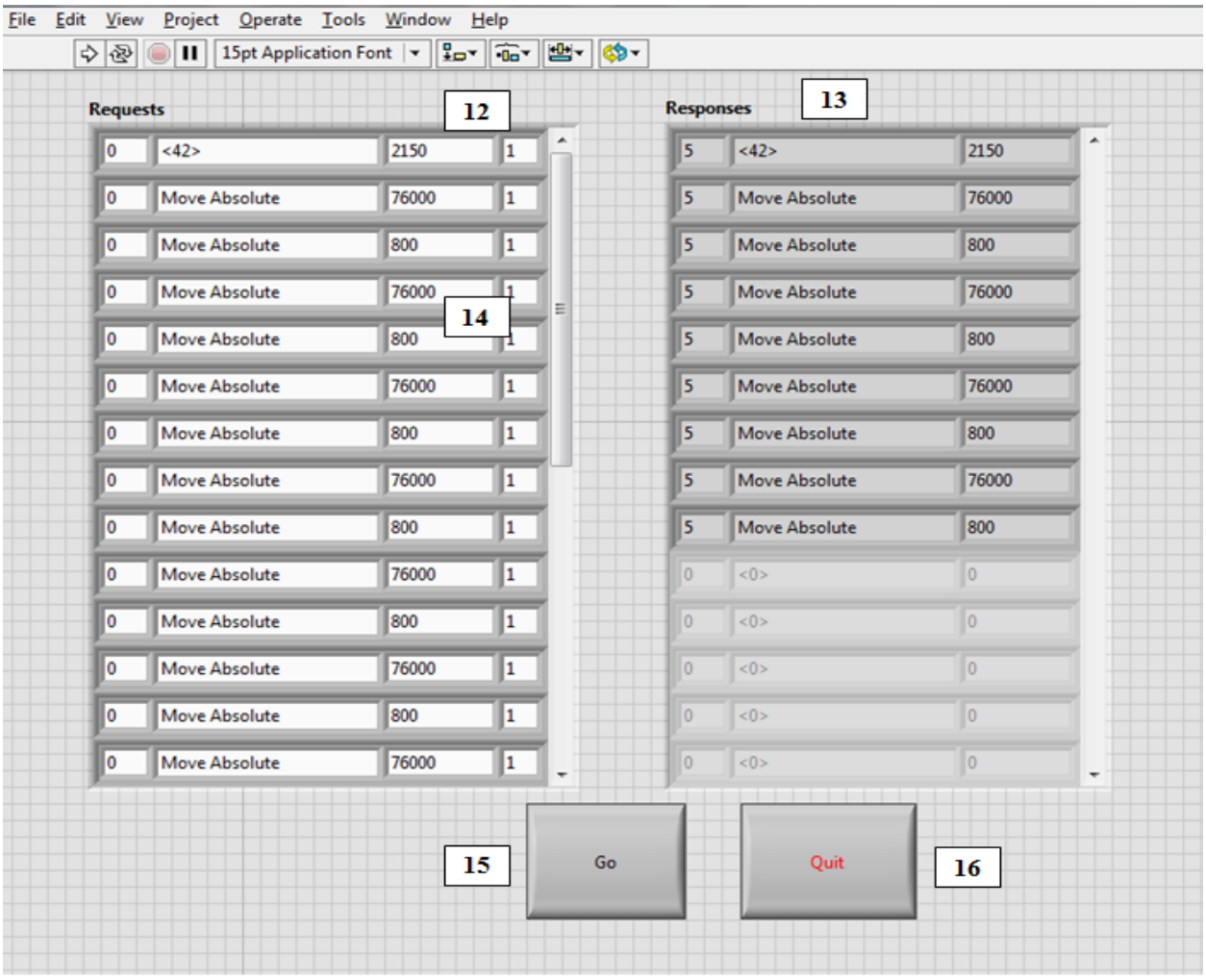

Figure 4.8: Labview diagram (photo) of Zaber motor stage speed control

(12) Linear actuator controls of speed

(13) Linear actuator status feedback

(14) Parameter sets position of actuator

(15) Send data to actuator to start indentation cycle

(16) Send data to actuator to stop indentation cycle

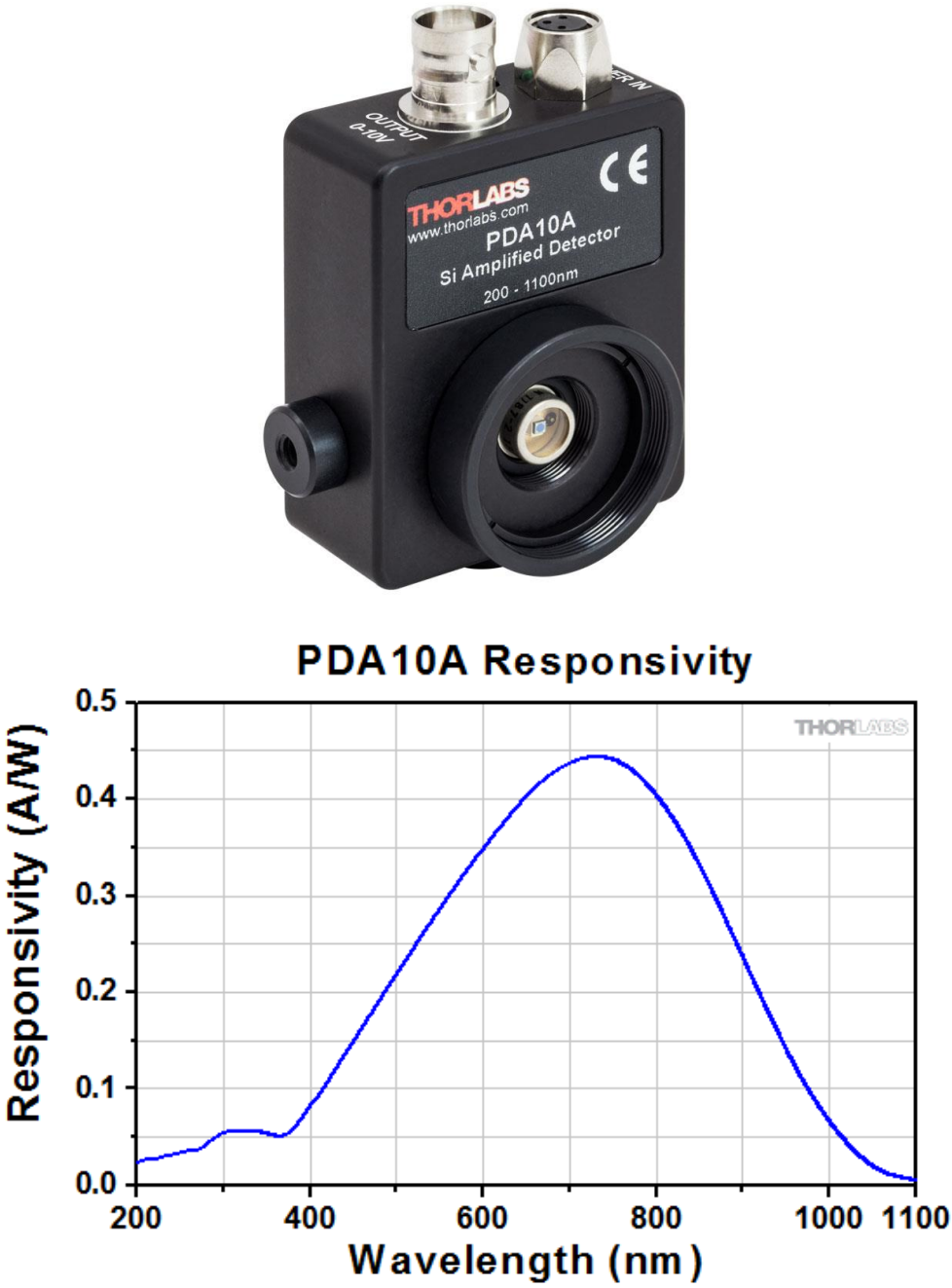

Figure 4.9: PDA10A detector responsivity (Thorlabs) [93]

4.7 Equipment List

Table 4-1: Equipment list

Component	Description
Axicon,	0.5 degrees , n=1.53
Axicon	5 degrees , n=1.53
Spherical lens1	focal length=50mm
Spherical lens2	focal length=400mm
Spherical lens3	focal length=20mm
Lab Jack	Hand operated manually with adjustable height (maximum height 25cm) and a platform of 150x150mm for lab use.
Various Newport post holders & posts.	
Various lens holders, plastic screws with plastic hands.	
Vernier caliper (+/-0.5mm).	
Microscope objective	(Olympus Plan 20x, 50x).
Zaber Technology T-LSR160D (motor stage)	operated with NI Labview
Photomultiplier	H9306 Hamamatsu
Photodetector (PDA10A).	Thorlabs
Power supply	BK Precision Model 1671A Triple output, DC power supply (-15/+15 DC Volt)

Chapter 5

TESTING OF THE SETUP WITH LASER DOPPLER VELOCIMETRY

The aim of the experiments described in this Chapter was to test the proposed measurement technique with a commercial LDV system. The laser Doppler technique is used to measure a velocity of the moving particles of a sandpaper sheet. The setup consisted of MiniLDV and sandpaper sheets fixed on motorized stage. The testing was simply performed to characterize and validate the proposed measurement system experimentally for the purpose of analyzing the impact of the sandpaper surface roughness with different particle sizes on measurement accuracy. The test samples were four sandpaper sheets with known grit sizes randomly distributed. Velocities from 10-80 mm/sec were used for each test sample. The objective was to obtain measurements with all four samples. Comparison of the velocities measured with the velocity signal is presented in table 5-3. Results of the measurement with 50mm/sec are presented. Diagram outputs from Measurement Science Enterprise (MSE) software and data corresponding to multiple speeds performed on the setup are in next sections. All measurements in this Chapter were performed with MSE.

5.1 MiniLDV (Miniature Laser Doppler Velocimeter)

The MiniLDV probe consists of laser, miniature beam shaping optics, receiving optics, a detection system and signal conditioning electronic circuits and processing software. The system operates with red laser (wavelength λ=658nm) and requires no calibration. The sensor is 32 mm diameter x 165 mm long. The fixed distance between the probe volume and the sensor was selected to be 250 mm. The MiniLDV is able to capture velocity measurements in the low and high ranges. It is reported to have a repeatability uncertainty of 0.1% [94] with typical accuracy of 99.7%. It is operated with MSE software which is 1D Burst Processor Acquisition Manager software package. The probe must be rotated to measure multiple components of velocity. The Processing Engine combines driver electronics, a band-pass filter, and a PCI acquisition card into one device, providing a USB 2.0 connection to the host computer and the Burst Processor Acquisition Manager software.

Table 5-1: MiniLDV laser specifications

Laser Characterization Sheet	
Part number	MiniLDV-G5-240
Serial number	P002427
Fringe separation	9.14 μm
Frequency shifting slope	284.25 Hz/RPM
Frequency shifting @3000 rpm	852.8 KHz
Frequency shifting @4000rpm	1137.0KHz
Frequency shifting @5000rpm	1421.3KHz
Driver used for Frequency shifting	FSA
Probe volume distance	255mm
Power in the probe volume	107mW
Transmission efficiency	76%
Wavelength at	658 nm
Probe volume size at FWHM	150x300 μm
Probe volume length at FWHM	2.5mm
Colour	Red

5.2 LDV Testing with MSE Software

The Burst Processor Acquisition Manager is the software interface that controls and receives data from MSE processing engine. To perform acquisition tasks, the acquisition parameters were set to the desired values in MSE software, initially a single point acquisition tab was triggered to configure the processing engine and to start and stop acquisition manually. The measurement volume is set at 25cm from the point of measurement which is the exact required distance for

MiniLDV from the probe to the measurement volume. A drawing of the experimental setup is given in figure 5.1.

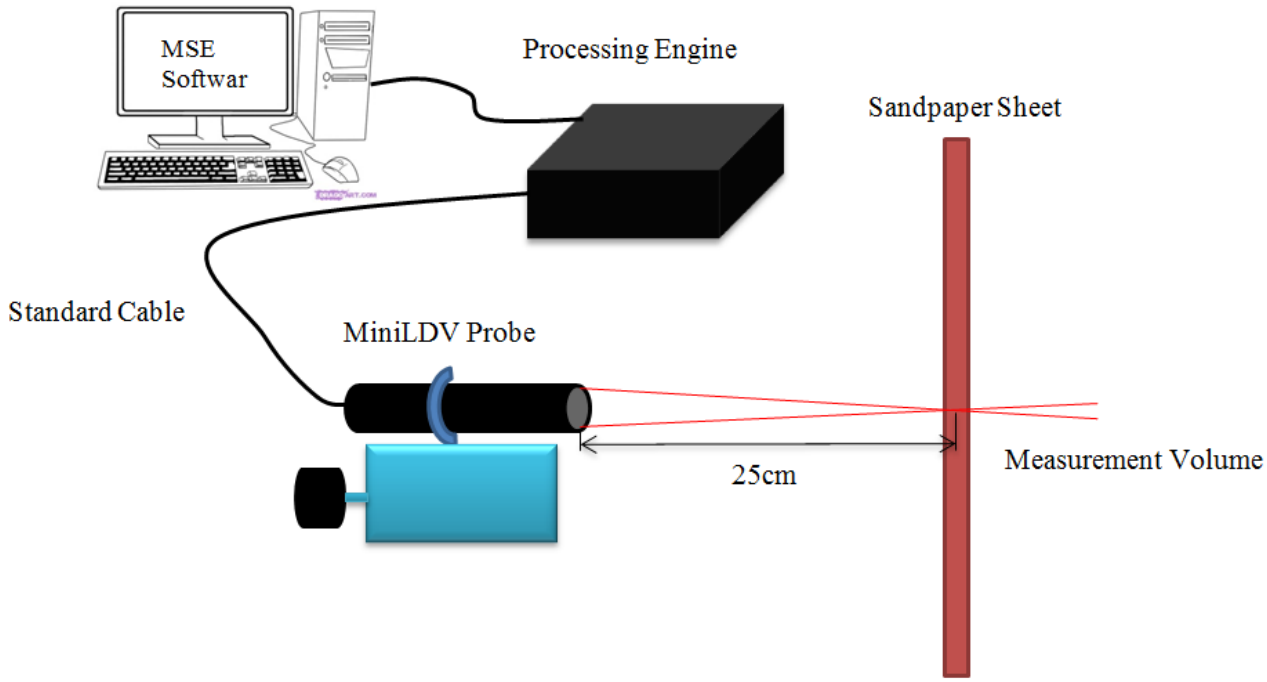

Figure 5.1: MiniLDV Testing setup

The MiniLDV probe was successfully mounted on an adjustable lab jack as shown in figure 5.1 and placed on the test bench which allowed for precise positioning of the probe.

5.2.1 MSE Burst Processor Acquisition Manager

LDV measurement with MSE software is described in details in figure 5.2. The system parameters were set according to the LDV setup, and to the desired speed to be measured (in this window the measured speed=65 mm/sec).

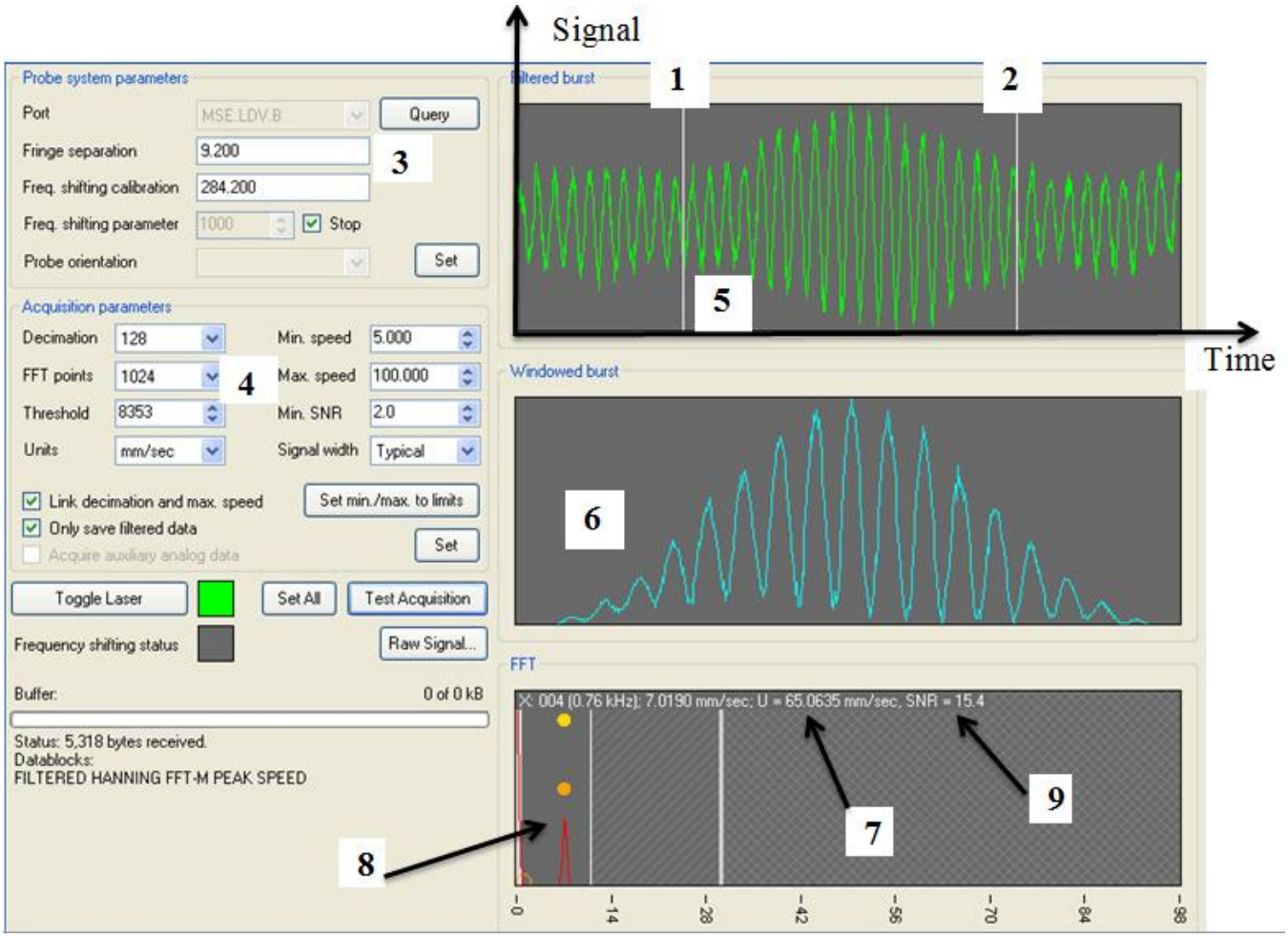

Figure 5.2: MSE Burst Processor Acquisition Manager

1. Minimum speed line
2. Maximum speed line
3. Fringe spacing
4. Acquisition parameters
5. Doppler signal

6 Burst signal of light scattered by a particle passing through LDV fringes.

7 Measured speed indicator.

8 FFT signal.

9 SNR (signal to noise ratio).

The key requirement is that the sensor probe volume is at the measurement location where the two beams intersect forming parallel fringes as shown in figure 5.3. For beams with Gaussian intensity profile, the measuring volume is ellipsoidal in shape. The scattered light from the surface of moving particle passing through the fringes oscillates with a specific frequency that is related to the velocity of the small particles in sandpaper. When a particle passes through the fringes of the measurement volume, a burst Doppler signal occurs as shown in the representative sketch in figure 5.4. The burst Doppler signal oscillates at Doppler frequency and the amplitude is modulated by the Gaussian intensity profile.

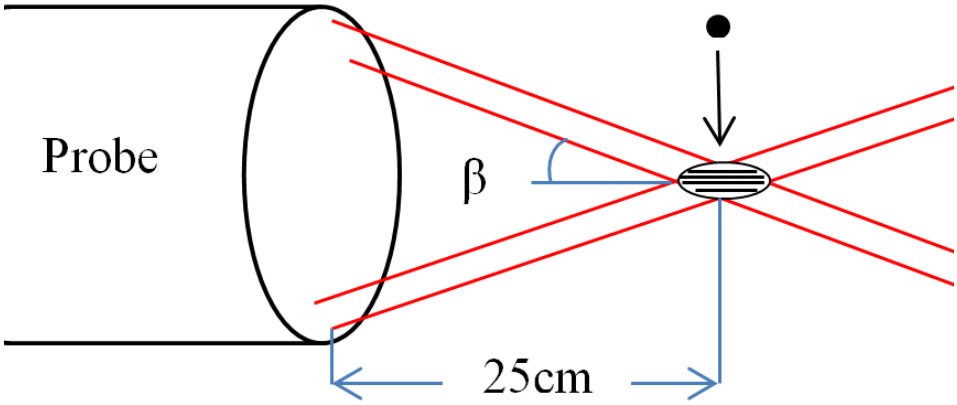

Figure 5.3: Particle crossing fringes of LDV

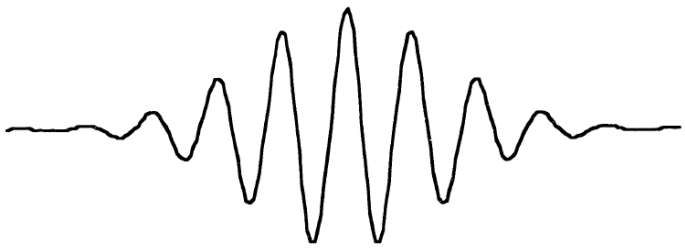

Figure 5.4: Burst Doppler signal

5.3 Sandpaper Selection

Four sandpaper types, shown in figure 5.5, were chosen and used in the measurements. They have equal dimensions, different material and surface roughness. The sandpapers were grit 400, 150, 220 and 1500. The selection was based on grit size matching small particles normally seeded in flow which are listed in table 5.2. These particles of the sandpapers are uniform size and randomly scattered, thus increasing the number of particles passing through the measuring volume and enhancing the data acquisition rate. The sandpaper was found most suited since the sand had evenly distributed grain sizes. Another advantage was the wide range of grain sizes available.

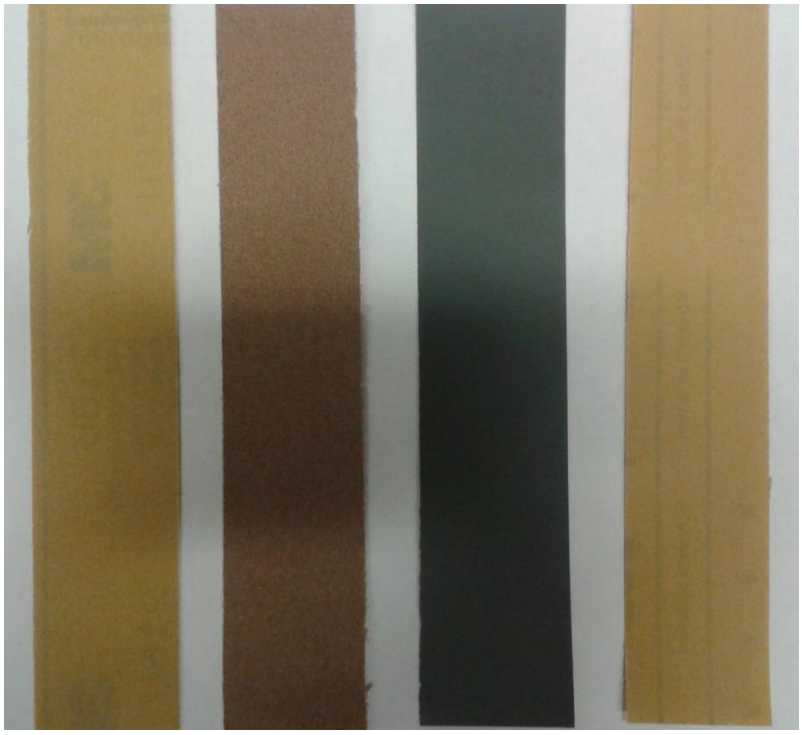

Figure 5.5: Four sandpapers used in the measurement

Values for sandpaper specs parameters are taken from the literature [95] and are summarized in Table 5-2. The particles refractive indices were taken from [96] and depended on the laser wavelength.

Table 5-2: Sandpaper specifications

Sandpaper Type	**Particle diameter d_p (μm)**	**Index of refraction (n) Red Laser (λ= 0.658μm)**	**Color**
Silicon Carbide 400 Extra fine	23	1.76-1.763	Yellow
Aluminum Oxide 150 Fine	93	1.7648–1.772	Brown
Aluminum Oxide 220 very fine	66	1.74-1.89	Yellow
Silicon Carbide 1500 Ultra Fine	8.4	2.6281	Gray

5.4 Measurements

Software provided by Measurement Science Enterprise (MSE) allowed for control of the acquisition. The probe Processing Engine included digital filters for which the high-pass and low-pass cut-off frequencies were set and adjusted by the MSE software. The Burst Processor software collects data from the sandpaper particles of the rough surface and presents signal statistics. The fringe spacing of this probe was set to 9.2 μm. The following parameters were set for data acquisition using the Burst Processor Acquisition software manager: fringe spacing, decimation, number of fast Fourier transform (FFT) points, threshold, units, minimum speed, maximum speed, minimum signal-to-noise ratio, and signal width. These parameters were adjusted depending on the speed of the particles. The decimation parameter adjusts the equivalent digitization rate of the hardware. The analog-to-digital converter hardware has a maximum digitization rate of 25 MHz. A higher decimation parameter was used for all speeds for lower frequency signals. The measured Doppler frequency signal is obtained by performing FFT calculations on the signal. The FFT number of points was typically set to a value of 1024. As the number of FFT points increases there is a corresponding increase in the resolution of the results. The minimum acceptable signal-to-noise ratio SNR was set to a value of 8 for all experiments. The signal width parameter was set to a typical value that allows for processing optimization of the entire Doppler burst. For the threshold parameter**,** when setting up the LDV system, a common way of dealing with constant noise in the raw signal is to set the threshold just above the highest peak in the signal and the threshold was set above the maximum value of noise

to 8353 slightly above the noise level which determines the processor signal trigger. Measurements and acquisition screen files were recorded at velocities ranging from 10 mm/sec up to maximum velocity of 80mm/sec. The parameters are shown in figure 5.6. At first, the sandpaper was cut into 27.5cm long and 5cm wide affixed on a straight wooden bar then secured on the Zaber motor stage and set to move linearly at selected constant speeds in the measurement volume. The laser was turned on and the parameters were set in MSE software to begin acquisition.When the Zaber motor stage started to move at constant speed, data acquisition was recoded. The measurements were recorded for velocities from 10 to 80mm/s. Only those at velocity of 50mm/s are shown in figures 5.7, 5.8, 5.9 and 5.10 corresponding to the 400-grit, 150-grit, 220-grit and 320-grit sandpapers respectively.

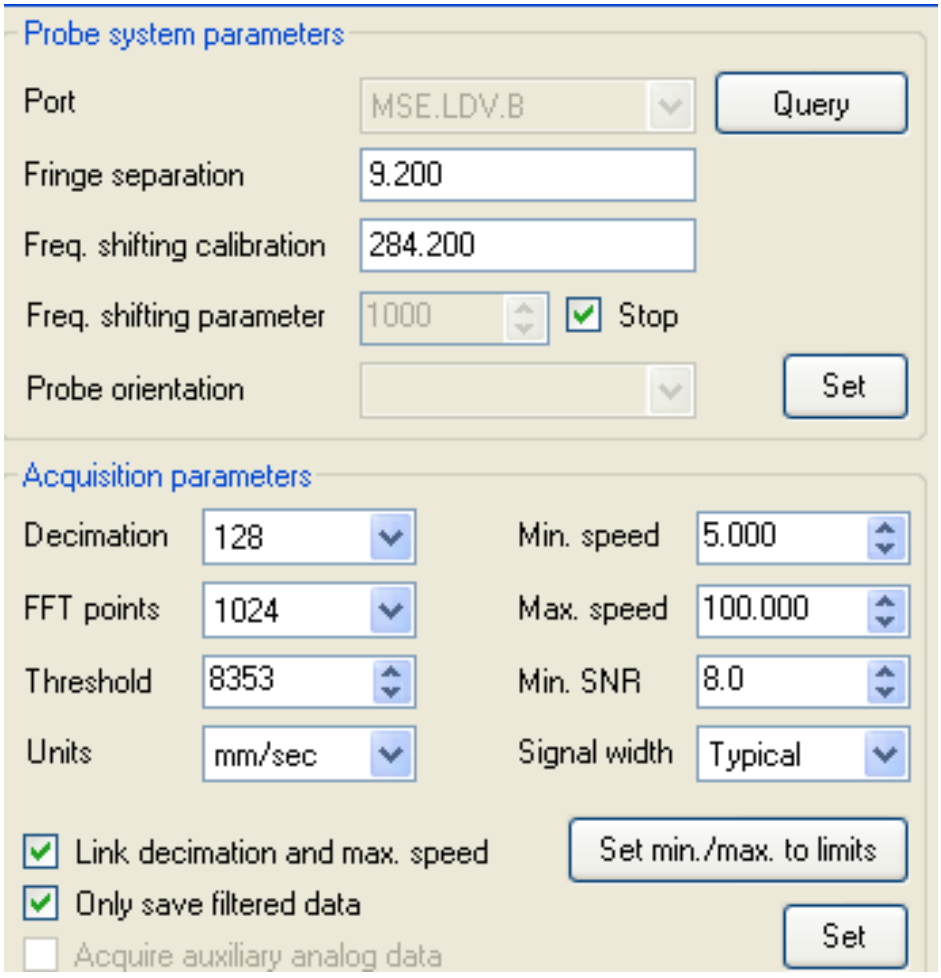

Figure 5.6: System Parameters set in MSE software

5.5 Results and Discussion

In this experiment, extensive tests have been conducted with speeds ranging from 10 to 80 mm/sec. The aim of testing the optical technique with four sandpapers having different surface roughness is to investigate whether the surface roughness affects to the probe measurement. Only samples of the measurements are presented in figures 5.7-5.10 for a speed of 50mm/sec. The results of all the measurements are summarized in table 5-3.

Table 5-3: LDV velocity and SNR measurement results with MSE

Actual Velocity (mm/s) ±0.1	**Measured velocity (mm/s)**			
	Sandpaper 400 Yellow d_p=23 μm	Sandpaper 1500 Grey d_p=8.4 μm	Sandpaper 220 Yellow d_p=66 μm	Sandpaper 150 Brown d_p=93 μm
10	10.1 (SNR=6.5)	10.4 (SNR=32.9)	10.2 (SNR=8.1)	10.6 (SNR=16.8)
20	20.5 (SNR=15.8)	20.2 (SNR=27.8)	20.4 (SNR=13.8)	20.1 (SNR=21.9)
30	30.3 (SNR=16.4)	30.0 (SNR=18.5)	30.3 (SNR=11.4)	30.7 (SNR=15.1)
40	40.3 (SNR=18.2)	40.0 (SNR=15.9)	40.4 (SNR=13.8)	40.0 (SNR=18.6)
50	50.7 (SNR=19)	50.2 (SNR=18.6)	50.1 (SNR=15.6)	50.3 (SNR=16.8)
60	60.7 (SNR=19.1)	60.1 (SNR=16.8)	60.0 (SNR=14.1)	60.1 (SNR=18.7)
70	70.1 (SNR=16)	70.2 (SNR=16.7)	70.1 (SNR=15.7)	70.3 (SNR=12.2)
80	80.3 (SNR=12.3)	80.1 (SNR=12.8)	79.8 (SNR=16.3)	80.0 (SNR=10.9)

Table 5.3 shows that the measurements were performed with MSE software have good accuracies. In general, when the speed was increased the measurement accuracy increased. Figures 5.7 to 5.10 and the results for other speeds show that the burst signals produced represents very well a Doppler signal. The velocity was measured equally on any point on the sandpaper sheet surface giving identical results. From these results, LDV can measure particles velocity accurately with size as large as the sandpaper selected grits. The idea evolved from the results that larger particles would need higher speed to cross fringe formation therefore generating ideal Doppler signal with high SNR. The results show that the rougher surface generates more back-scattered light intensity than the smoother surface. This may occur as the rougher surface provides more scattered points. The measurement signals in figure 5.7-5.10 display the quality of the measured velocity with sandpaper grits. The vertical axis corresponds to signal and the horizontal axis corresponds to time.

In summary, the LDV provided velocity measurement with MSE was very reliable. When measurement was taken with speeds below 10mm/sec the signal was not showing similar accuracy as testing with higher speeds. The same setup will be used for testing with the LBV technique.

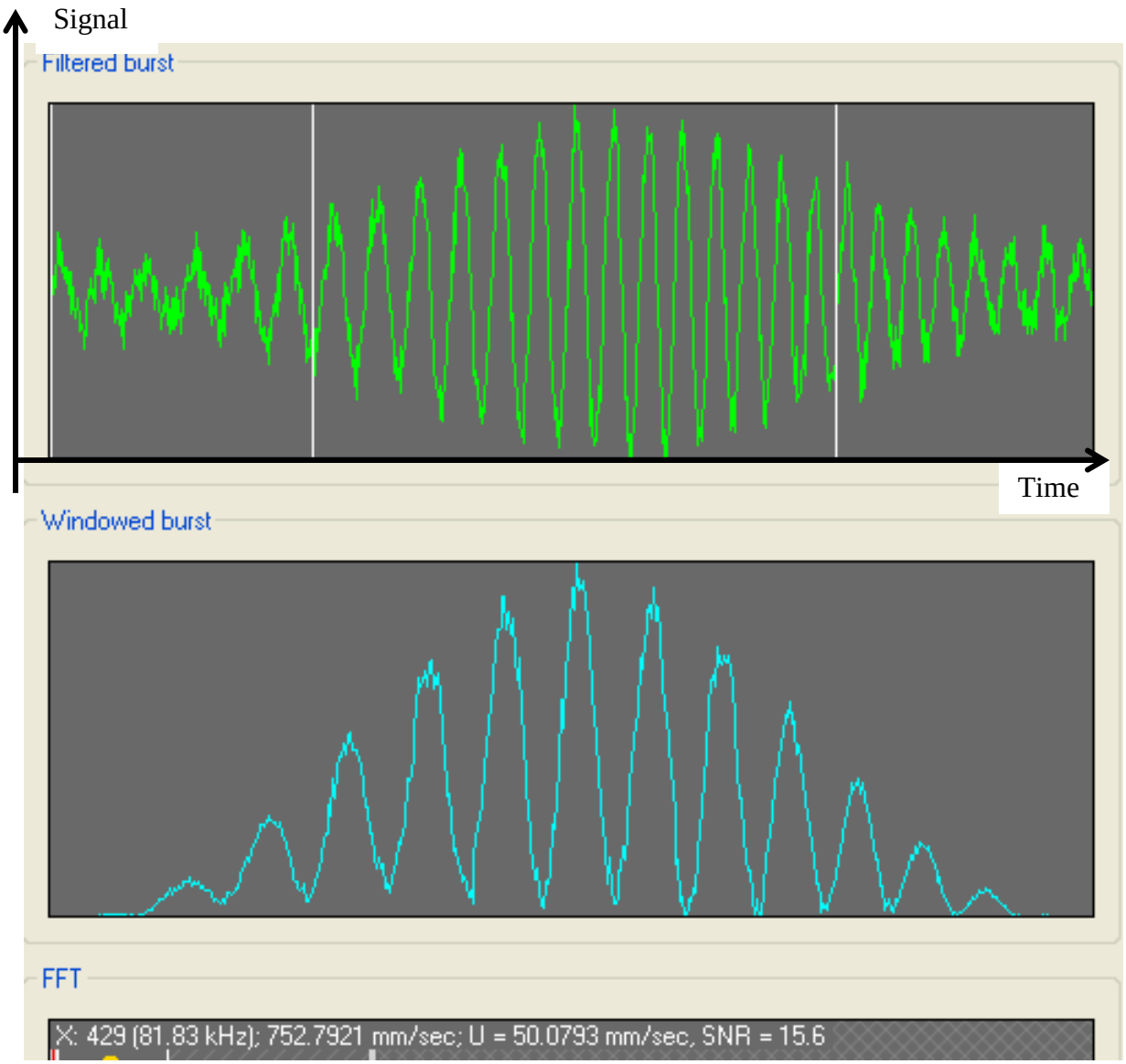

Figure 5.7: LDV measurement of Aluminum Oxide (Yellow sandpaper 220 very fine) particles signal display

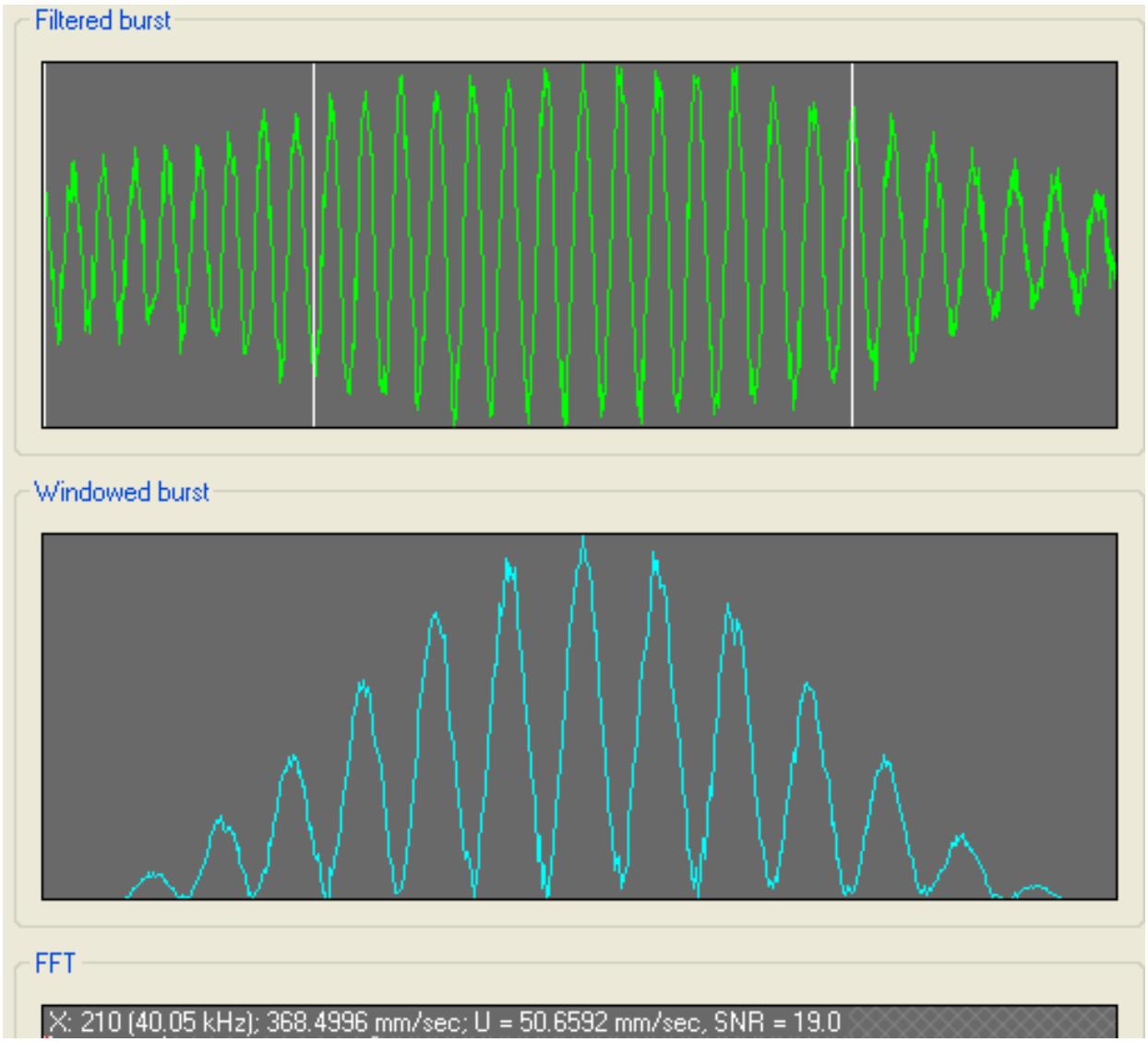

Figure 5.8: LDV measurement of Silicon Carbide (Yellow sandpaper 400 extra fine) particles signal display

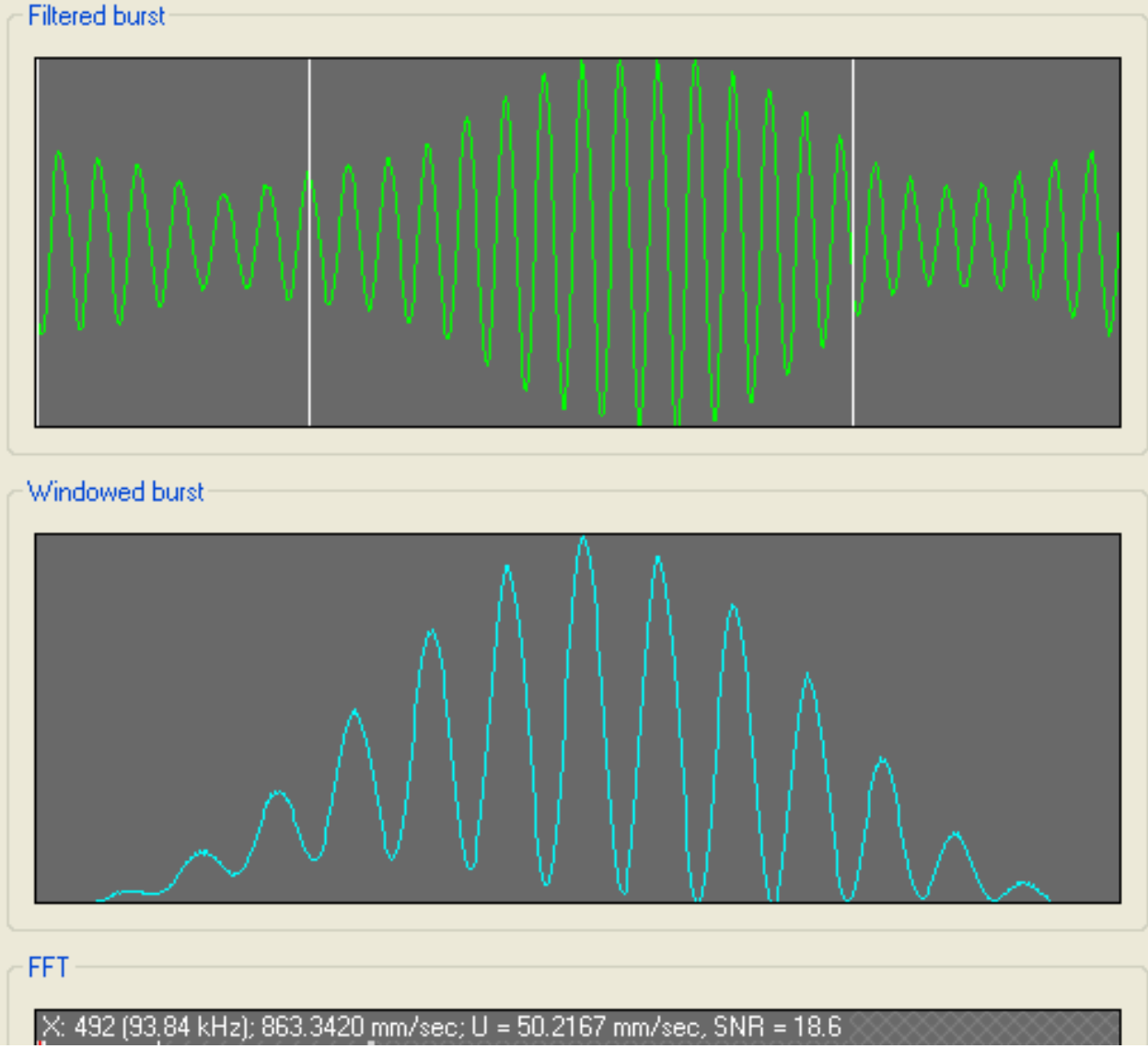

Figure 5.9: LDV measurement of Silicon Carbide (grey sandpaper 1500 Ultra Fine) particles signal display

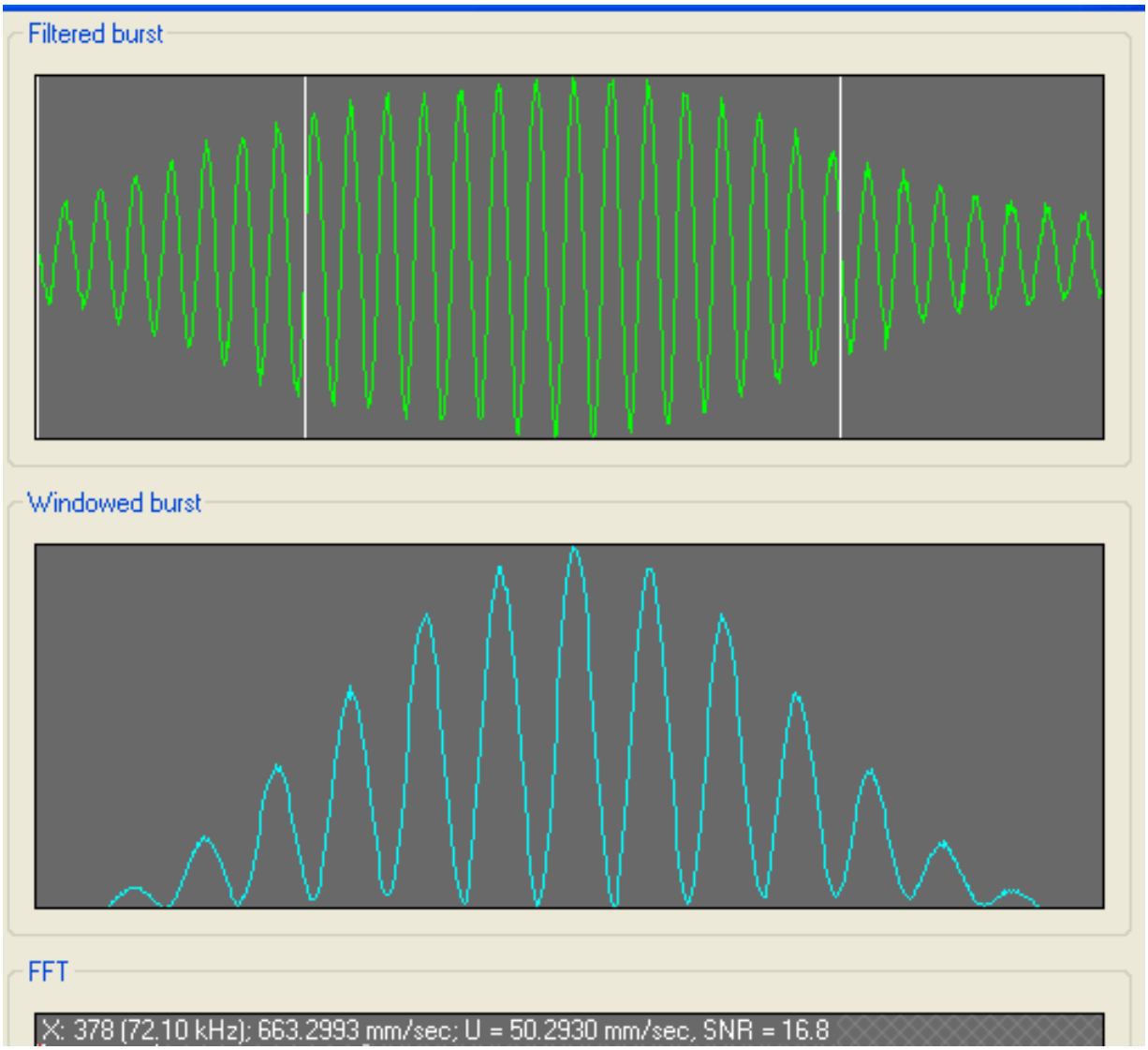

Figure 5.10: LDV measurement of Aluminum Oxide (Brown sandpaper 150 Fine) particles signal display

Chapter 6

MEASUREMENTS AND EXPERIMENTAL TECHNIQUES

In this Chapter, the measurement procedure is described. Section 6.1 describes the procedure used in the measurements including the setup and adjustment of the optical components used with 0.5° and 5° axicons. Section 6.2 describes the measurements with sand paper and how the photodetector was adjusted in measurements to collect scattered light. Section 6.3 describes the measurement with a set of wires and results are presented. Section 6.4 describes how the measurement signal was improved and enhanced for better detection.

6.1 Procedure and Adjustment of Optics

The laser probe was mounted on the hand adjustable lab jack and the laser was turned on. The laser height was adjusted and aligned such that the laser beam was parallel to breadboard test bench. Then the beam was directed and located on the middle of a board which is placed about 3m further from laser source marking a spot indicating the beam center. The laser beam has to be monochromatic, coherent and having high intensity for practical workable measuring process. The spherical lens (F=50mm) was mounted in front of the laser beam with a lens post and holder on the breadboard test bench. The first lens was aligned such that the laser beam passes through its center. The second spherical lens (F=400mm) was mounted with a lens post and holder at a distance 450mm from the first lens which is the summation of the focal length of both lenses (F1+F2) as shown in figure 4.1 and aligned with the first lens such that the laser beam passes through its center. The laser beam diameter was broadened to 8 times its original diameter and collimated.

6.1.1 Adjustment for 0.5° axicon

The 0.5° axicon was mounted with a lens post and holder in front of the second lens. The distance between the axicon and the second lens was not very important since the diameter is collimated. A fine adjustment was made to the alignment to ensure that the beam passing through both lenses and the axicon was still centered and parallel to the breadboard test bench. The

axicon was adjusted to have its axis coincide with that of the beam by examining the ring pattern produced away from the axicon using a whiteboard. The intensity of the ring was examined and it was made sure that it was evenly distributed. It was also made sure that the center of the ring was in the center laser dot on the wall. Finally, the positions of the optics were fine-tuned until the center of the laser head was centered horizontally in each of the lens center. The axicon was not removed or replaced until all required measurements were accomplished. To check that the beam remains in focus, a 50X microscopic objective was required. It was mounted and adjusted after the axicon in the DOF to project the Bessel beam. The image of Bessel beam was observed on a sheet starting at least 10 cm away from the objective lens then picture were taken and are shown in figure 6.1.

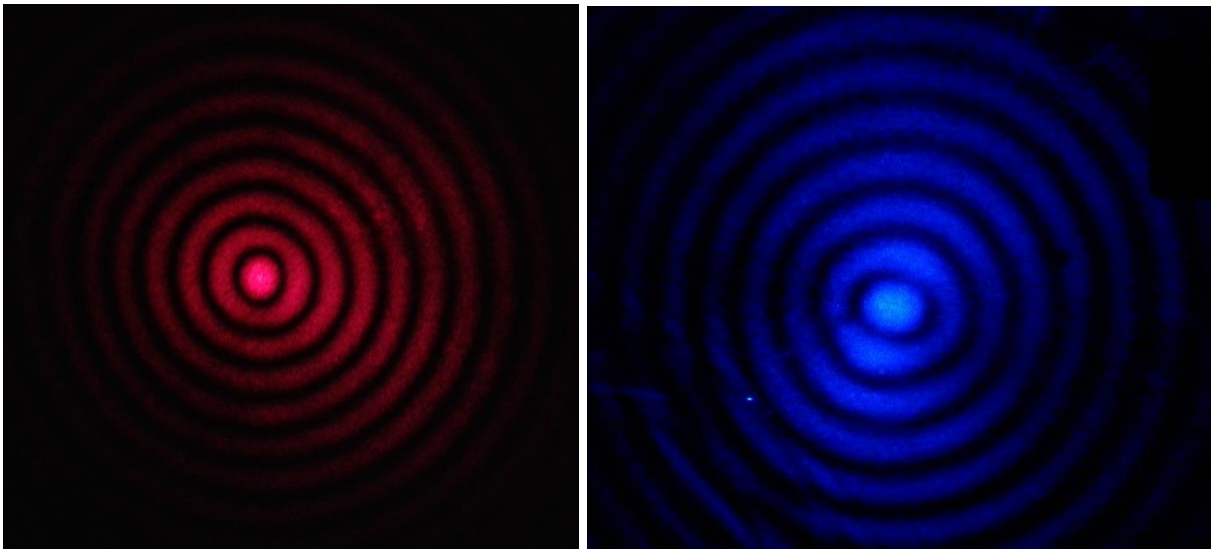

Figure 6.1: Bessel beam produced with (0.5°) Axicon and 50X microscope objective for red and blue laser respectively

Then a 20X microscopic objective lens was also adjusted to project and observe an image of Bessel beam. Then pictures were taken and are shown in figure 6.2.

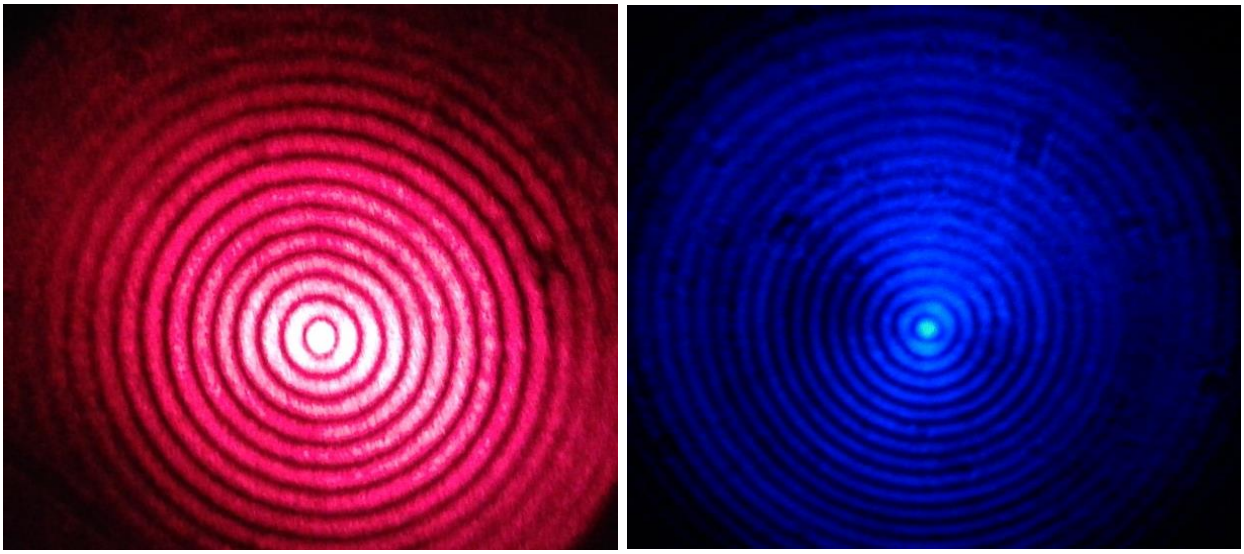

Figure 6.2: Bessel beam produced with (0.5°) Axicon 20X microscope objective for red and blue laser respectively

Each microscopic objective lens displayed the Bessel beam rings in a different size. The Bessel beam DOF was calculated from geometry (Table 6.1) and verified experimentally while adjusting the microscopic objective lens. The sandpaper sheet was affixed on wooden straight flat bar and mounted on the Zaber motorized stage as shown in figure 4.2. The Zaber motorized stage was placed in the DOF temporarily secured via the set of holes on the breadboard test bench with the sandpaper rough surface facing the laser beam. The motor stage was controlled from the desktop computer by the Labview program illustrated in figure 4.8. The movement of the Zaber was tested with the knob to ensure it is free to move properly in the horizontal direction with sufficient movement from end to end. The Thorlabs photodetector was fixed on a square bracket post holder and placed close to the measuring volume to be adjusted with the scattered light from the rough surface. A plano-convex lens (F=20mm) was positioned at a distance q=30mm away from the scattering light of the fringes and the Photodetector was adjusted at a distance p=60mm to focus the scattered light onto its detector as illustrated in figure 4.1. The photodetector was connected to power supply and turned on to begin acquisition. The Zaber motorized stage speed was set initially to move freely with constant speed of 30 mm/s and controlled by LabVIEW GUI shown in figure 4.7.

The sampling frequency was set to 5000 Hz and the number of samples was set to 2048 then the measurements were recorded with LabVIEW and written in a text file. The procedure was repeated with speeds 35, 40, 45, 50, 55, 60, 65, 70, 75 and 80 mm/sec.

6.1.2 Adjustment for 5° axicon

In a similar way, the procedure already described was performed in the second test with 5° axicon for speeds ranging from 30 to 80mm/sec. In the Labview program, the sampling frequency was set to 30000Hz and the number of samples was set to 4096. The Zaber motorized stage with the sandpaper sheet affixed to it was placed in the DOF of the axicon. It was temporarily secured on the breadboard test bench in the DOF with the sandpaper rough surface facing the laser beam. The same procedure was repeated for the four types of sandpaper. The output power of 10mW with the blue laser (wavelength ~ 473 nm) was not sufficient to get any back-scattering from the sandpaper particles. In this regard, the red laser of wavelength ~ 658 nm and an output power of ~107mW were then used to have sufficient back-scattering power. Table 6-1 shows the characteristics of the Bessel beam generated with the red laser (λ=658nm and power=107 mW) and the two axicons used. The 0.5° axicon has larger fringe spacing than the 5° axicon as illustrated in table 6-1.

Table 6-1: Axicons experimental parameters

	β (°)	**DOF (cm)**	**Spot size $2r_0$ (μm)**
0.5° axicon	0.265	86.2	109.90
5° axicon	2.66	8.60	10.853

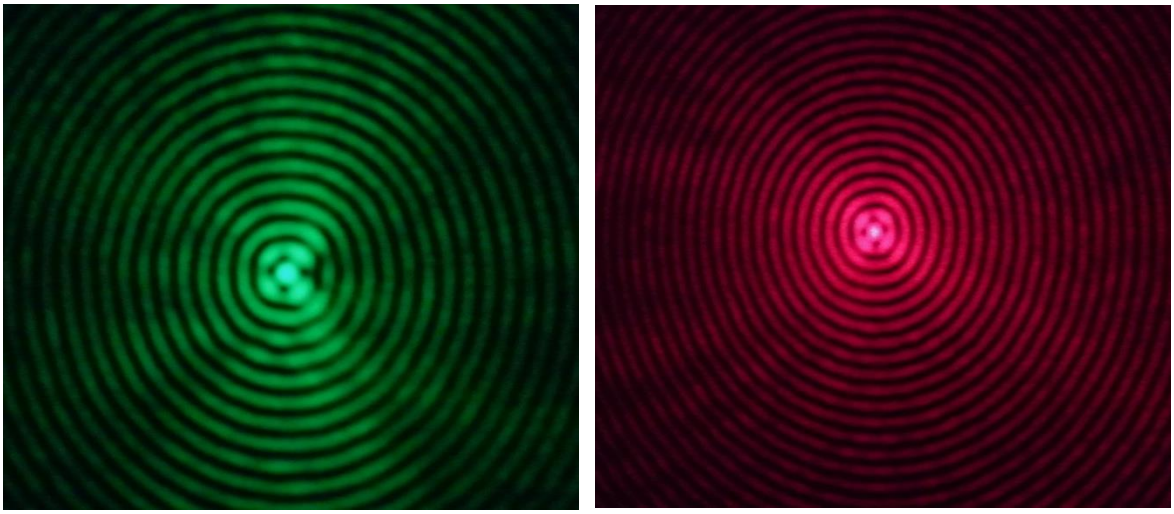

Figure 6.3: Bessel beam Fringes generated with 5° axicon using 50X and 20X microscope objectives with red laser

6.2 Adjustment and Placement of the photodetector

The photodetector collects scattered light from particles passing through the fringes and converts it to an electric signal for processing. Since scattered light radiates in all directions, the photodetector could be in principle positioned anywhere around the measurement region. It was positioned close to the measuring volume to collect scattered light in the backscatter mode as shown in figure 4.1 to ensure that a strong signal can be detected. The scattered light is focused onto the photodiode using a single plano-convex lens of 20 mm focal length. The plano-convex lens was placed at a distance p from the measuring volume and the photodetector was placed away from the lens at a distance q from the lens which is the detection point as shown in figure 6.4. The lens collects the scattered light and focuses it onto the photodetector to improve the sensitivity and increase the signal strength.

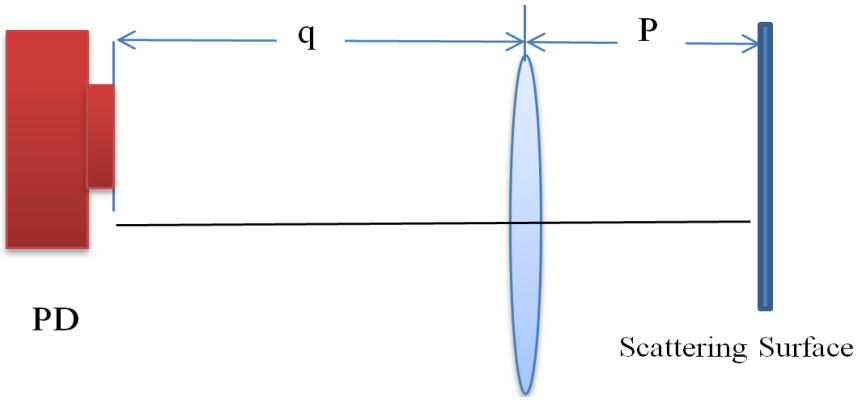

Figure 6.4: Photodetector adjustment

In the second setup using the 5° axicon, it was not possible to align very precisely the lens (plano-convex) near the sandpaper measurement position in order to focus scattered light onto the photodetector. Its location was limited due to the short DOF of the axicon. Every effort was made to fine tune the adjustment of the receiving optics to focus them on the desired measuring location and to produce a good signal. For this reason the signal was slightly lower than the signal generated with 0.5° axicon setup. The 0.5° axicon has longer DOF as described in table 6-2 which was easier in adjustment. The time signals from the sandpaper measurements presented large variations and it was impossible to extract useful information about the velocity in the time domain. A frequency analysis will be performed in the next chapter.

6.3 Measurement with Copper Wires

The measurements with copper wires were performed with a similar technique to the one described for the sandpaper measurements. The same optical configuration shown in figure 4.1 was used to perform the measurements by replacing the sandpaper with copper wires of 150μm in diameter and 5cm long.

6.3.1 Measurement with 0.5° axicon

For the measurements with the 0.5°axicon, three copper wires were affixed vertically on a flat straight plate shown in figure 6.5 and fixed on the Zaber motorized stage. The wires were placed 5 mm apart considering 20mm the maximum distance to record measurements by moving these

wires across Bessel beam in the DOF of the axicon. Having a prior knowledge about the range of velocities to be measured, the sampling rate of the data acquisition was adjusted for each measurement based on the information from the previous velocity measurement. The frequency value is chosen to cover the number of samples and all points of measurements shown in table 6-2. This procedure ensures that every point is measured with the highest possible accuracy. Also in this optical setup, the laser beam did not require any further adjustments throughout the measurements. Rather the axicon is the only piece of equipment required adjustment when changed for measurement purposes which was simple procedure.

Table 6-2: Parameters of wires measurement with 0.5° axicon

Actual set speed (mm/sec) ±0.1	**Sampling Frequency fs (KHz)**	**Number of sampling points**
10	2	4096
20	4	4096
30	6	4096
40	8	4096
50	10	4096
60	12	4096
70	14	4096

The scattered light from the copper wires was focused with the 20mm focal length lens on the Thorlabs photodetector. The measurements were repeated for all velocities in table 6-2.

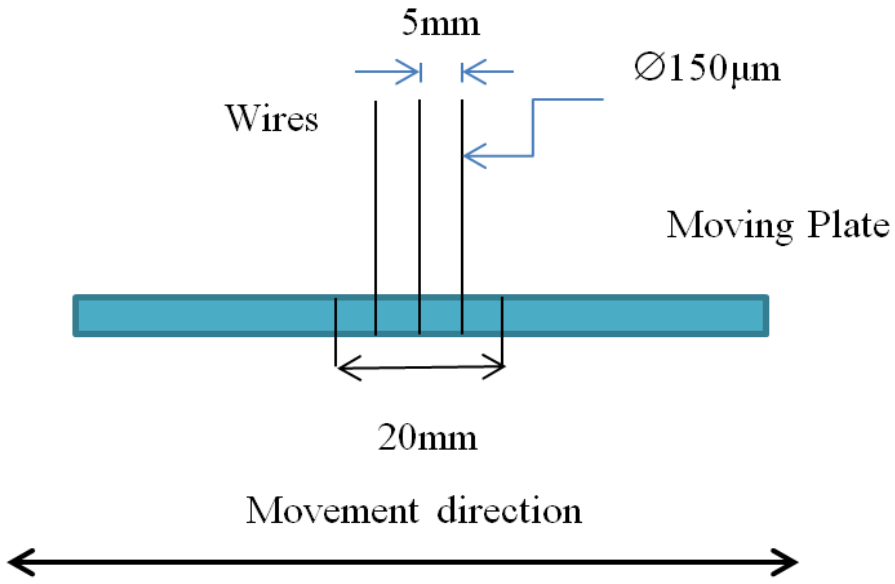

Figure 6.5: The setup of electric wires for testing with 0.5° axicon

The data was recorded with NI Labview, stored in a PC, processed and analyzed with Matlab to investigate the time signal. When the three wires pass through the Bessel beam, three peaks were generated 5 mm apart as shown in figure 6.6. When each single wire crosses the Bessel beam, it emits a single signal burst with well-defined peaks as shown in figure 6.7. The highest peak indicates when the wire crosses the central spot of Bessel beam then each fringe is represented with a peak. Results of measurements at different speeds are presented in figure 6.6.

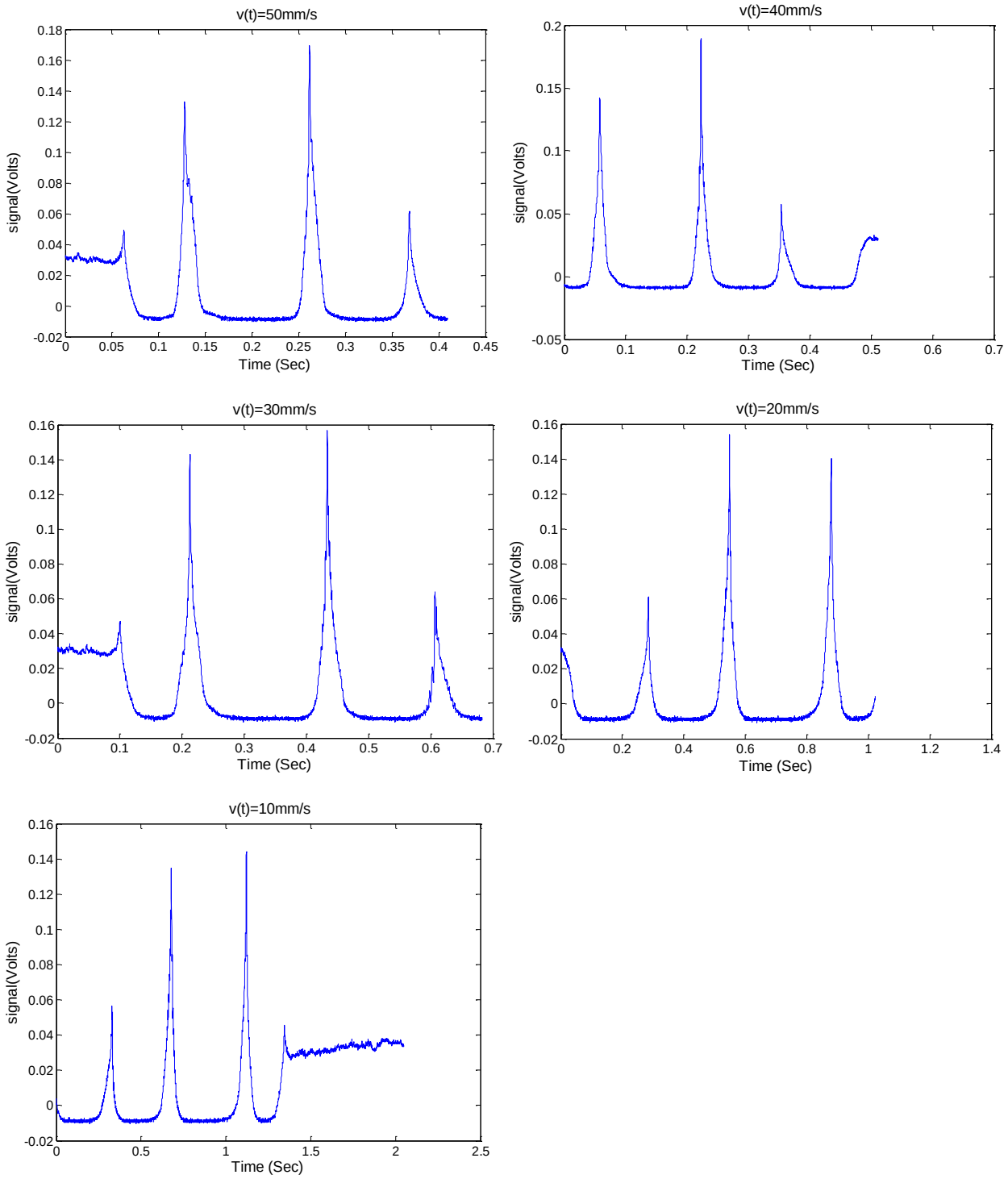

Figure 6.6: Time signals of the three wires when passing through Bessel beam fringes at constant speed for 0.5° Axicon

As can be seen from figure 6.9, the signal emitted from the different wires has different magnitudes. This is probably due to the different in their shapes and surface roughness.

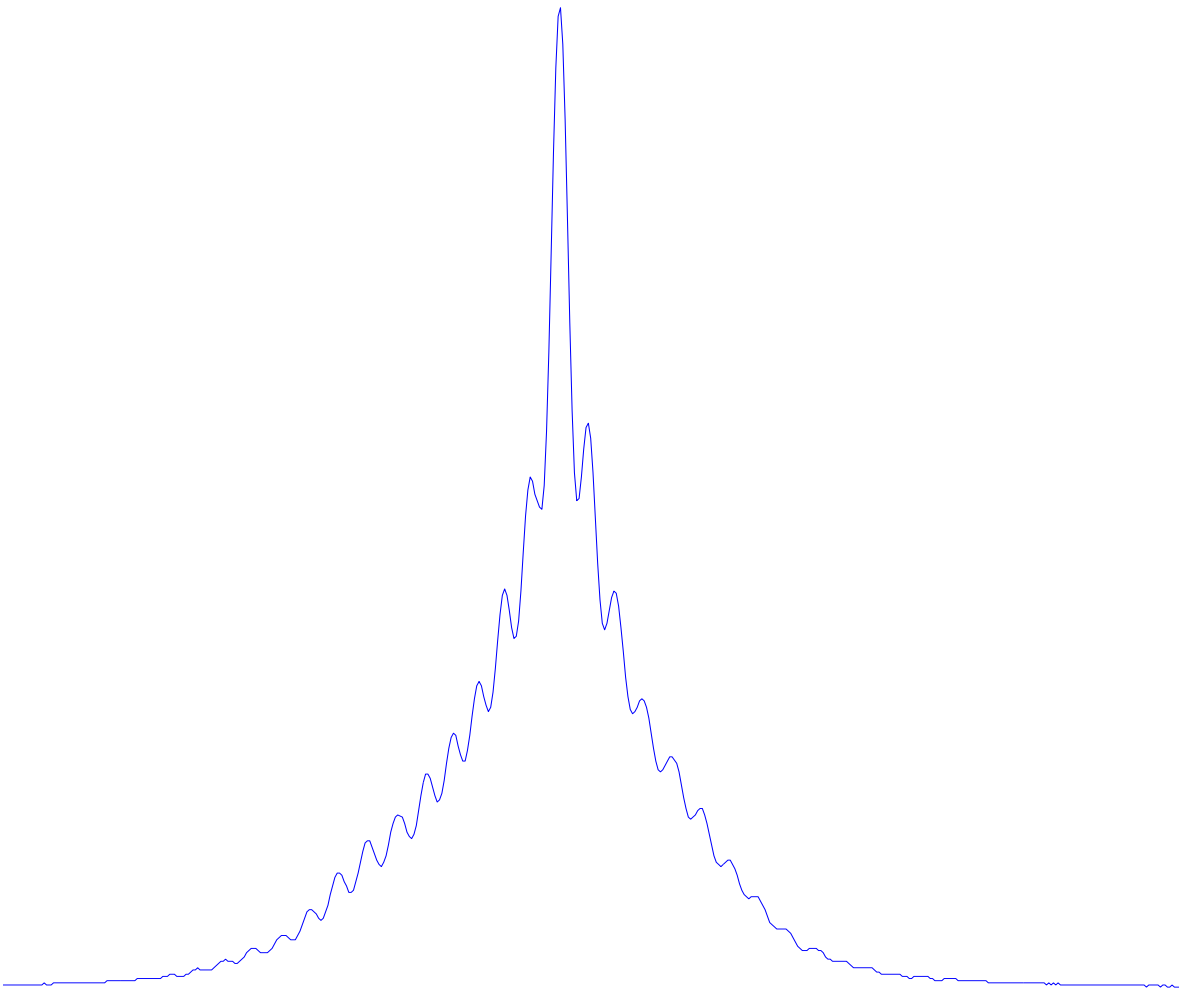

Figure 6.7: A peak of 150μm wire passing through Bessel beam generated with 0.5° Axicon using Matlab clearly showing the different peaks when the wire crosses each fringe in Bessel beam

6.3.2 Measurement with 5 axicon

The procedure was repeated with the 5° axicon, with two copper wires fixed 5mm apart as shown in figure 6.8. With the speeds listed in table 6-3 the measurements were recorded and processed in Matlab. Two peaks were generated when the two wires cross the Bessel beam. The results are presented in figure 6.9. Table 6-3 shows the sampling frequency and number of points used in the measurement.

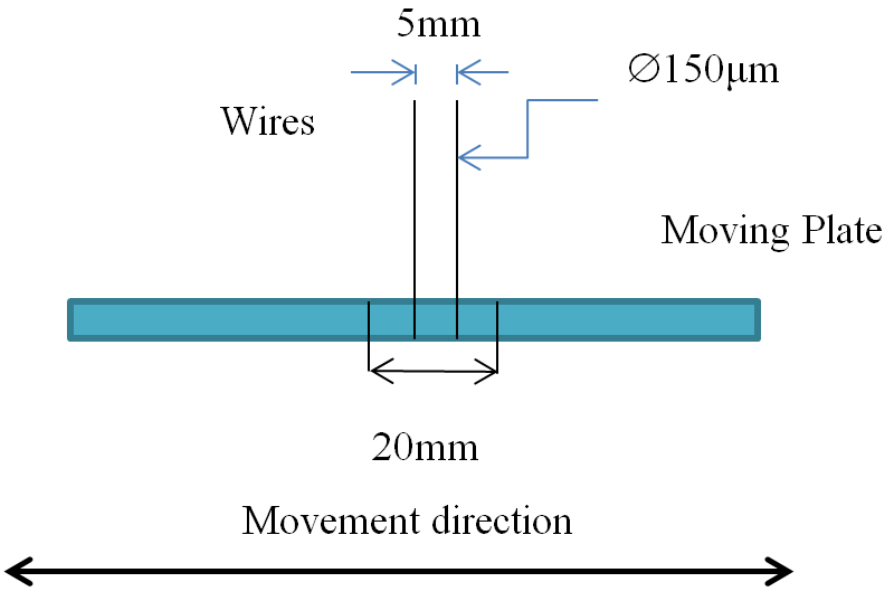

Figure 6.8: The setup of electric wires for testing with 5° axicon

Table 6-3: Parameters of wire measurement with 5° axicon

Actual set speed (mm/sec) ±0.1	Sampling Frequency fs (kHz)	Number of sampling points
10	10	10000
20	20	10000
30	30	10000
40	40	10000
50	50	10000
60	60	10000
70	70	10000

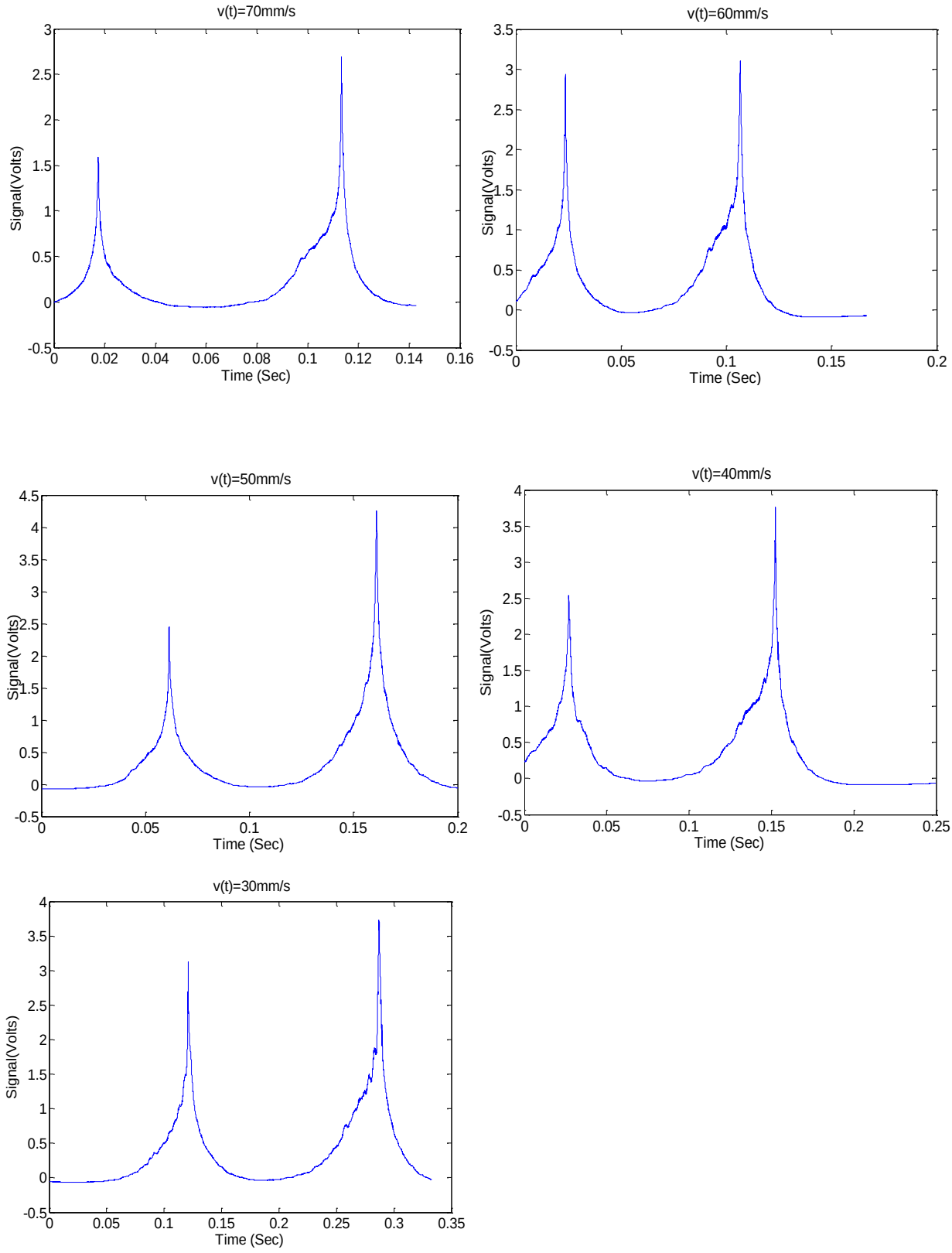

Figure 6.9: Time signals of the two wires passing through Bessel beam fringes at constant speed for 5° Axicon

6.4 Improving the signal detection

Initially, the photodetector was plugged into a power source and the voltage was measured from the scattered light. The maximum measured voltage was 370 millivolts. This voltage level was sufficient to show results with 0.5° axicon measurement, but was not sufficiently high to produce a signal variation using the 5° axicon. The signal was amplified to about 3.5 volts and filtered to reduce the noise. Measurements were also performed with the photomultiplier (PMT) several times. When the data was processed, the signal was very noisy. This is because the PMT is very sensitive to all sources of light including nearby ambient light and other reflections from the equipment. The output signal was found always smaller than noise and was difficult to discern. Also, the expected frequency produced with measurements using 5° axicon is out of the bandwidth range of PMT and the high velocity using 5° axicon induced a frequency above the frequency response of the photomultiplier.

Chapter 7

ANALYSIS

In this Chapter a theory of the variation of the signal from the scattered light of particles crossing the fringes of the Bessel beam is developed. A frequency analysis is performed on the velocity signals from the moving sandpaper measurements. A time domain analysis is performed on the velocity signals of the moving wires. The Chapter is divided into three sections with subsections. Section1 describes the theoretical analysis and presents the simulation results. Section 2 is divided into two subsections. Subsection 1 describes the experimental analysis of velocity measurement with sandpapers using the 5° axicon and presents the results. Subsection 2 describes the experimental analysis measurements with 0.5° axicon and presents the results. Section 3 describes the time signal generated with the set of wires and presents the analysis of the velocity using this time signal with the fringe spacing of Bessel beam. All theoretical and experimental analysis is based on constant velocity. Experimental results for the measurement of velocity with sandpaper will be described and analysis will be compared with those predicted by theory.

7.1 Theoretical Analysis and Simulation

The theoretical simulation results are based on the assumption that there is only one particle passing through the center of the Bessel beam and scattering light when crossing the fringes as illustrated in figure 7.1. We keep in mind that there are multiple scatterers and that they cross the fringes at different positions in real situations. The particle size is assumed to be less than the fringe spacing and the intensity of the scattered light is proportional to the intensity of light of the fringes. A moving particle placed at a distance r from the center of the spot scatters light with intensity given by $I = I_0 {J_0}^2(k\beta r)$, where I_0 is reference intensity. The scattered light from the particle is collected by the photodetector producing a proportional current which is converted to a voltage. The frequency content of the voltage signal is analyzed by Fourier transform which will give the spectrum of the signal. This theoretical analysis assumes constant velocity. it is understood that if one extends this analysis to fluid flow measurements, the velocity of different

particles might vary in magnitude and direction. Similar to the LDV technique, the average the effect should be close to these predictions.

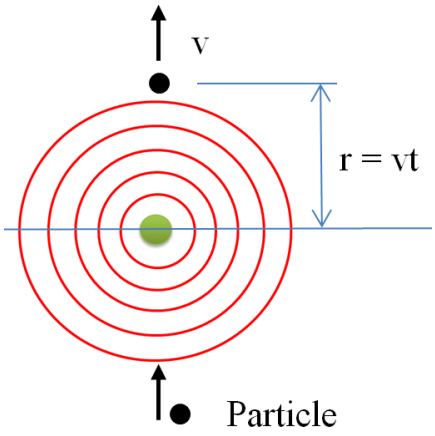

Figure 7.1: A particle passing through the center of Bessel beam with constant velocity

The Fourier transform of the Bessel function squared, $J_0(t)^2$, is obtained from Wolfram© [97], :

$$F(\omega) = F\left(J_0(t).J_0(t)\right) = \begin{cases} \frac{\sqrt{2}K\left(1-\frac{\omega^2}{4}\right)}{\pi^{3/2}} & -2 < \omega < 2 \\ 0 & otherwise \end{cases} \qquad (7.1)$$

Where K is the complete elliptic integral of the first kind given for a parameter m by **:**

$$K(m) = \int_0^1 \frac{dt}{(1-t^2)(1-mt^2)} \qquad (7.2)$$

In our case we need the Fourier transform of the function $J_0{}^2(k\beta r)$, which can be written as $J_0{}^2(k\beta vt)$, by substituting the radius r as a function of the velocity of the particle (r=vt). .
The Fourier transform of a function $J_0{}^2(at)$ is found from:

$$F(f(at)) = \frac{1}{|a|} F\left(\frac{\omega}{a}\right) \qquad (7.3)$$

in the present case, $a = k\beta v$.

Equation 7.1 is plotted using WolframAlpha [97] in figure 7.2. At low frequencies it has higher values and as the frequency increases the value decreases until the frequency $\omega_b = 2\ (rad/s)$, after which F(ω) becomes zero. This frequency ω_b is called the Bessel frequency [6].

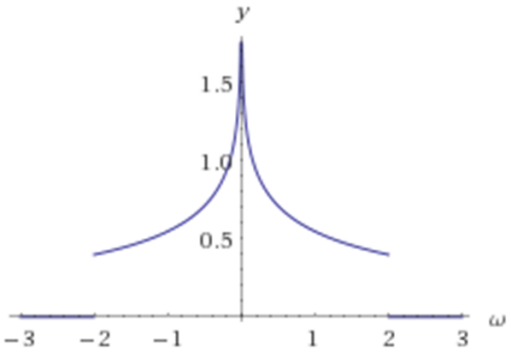

Figure 7.2: Plot of $J_0^2(k\beta r)$ from Wolfram Alpha [97]

The Bessel frequency of the spectra can be related to the velocity from equation (7.3) and from the variation shown in figure 7.2

$$\frac{\omega_b}{k\beta v} = 2\ (\text{rad/s}) \quad \text{or} \quad f_b = \frac{2\beta v}{\lambda}\ (\text{Hz}). \tag{7.4}$$

Using (7.1) and (7.3) we can plot the spectra of $J_0^2(k\beta vt)$ for different values of the velocity v. Figure 7.3 shows these plots when a particle is passing through Bessel beam generated with 0.5° axicon for velocities between 30mm/s and 80mm/s. Figures 7.4 shows the plots of frequency spectra generated with 5° axicons for velocities from 30-80mm/s.

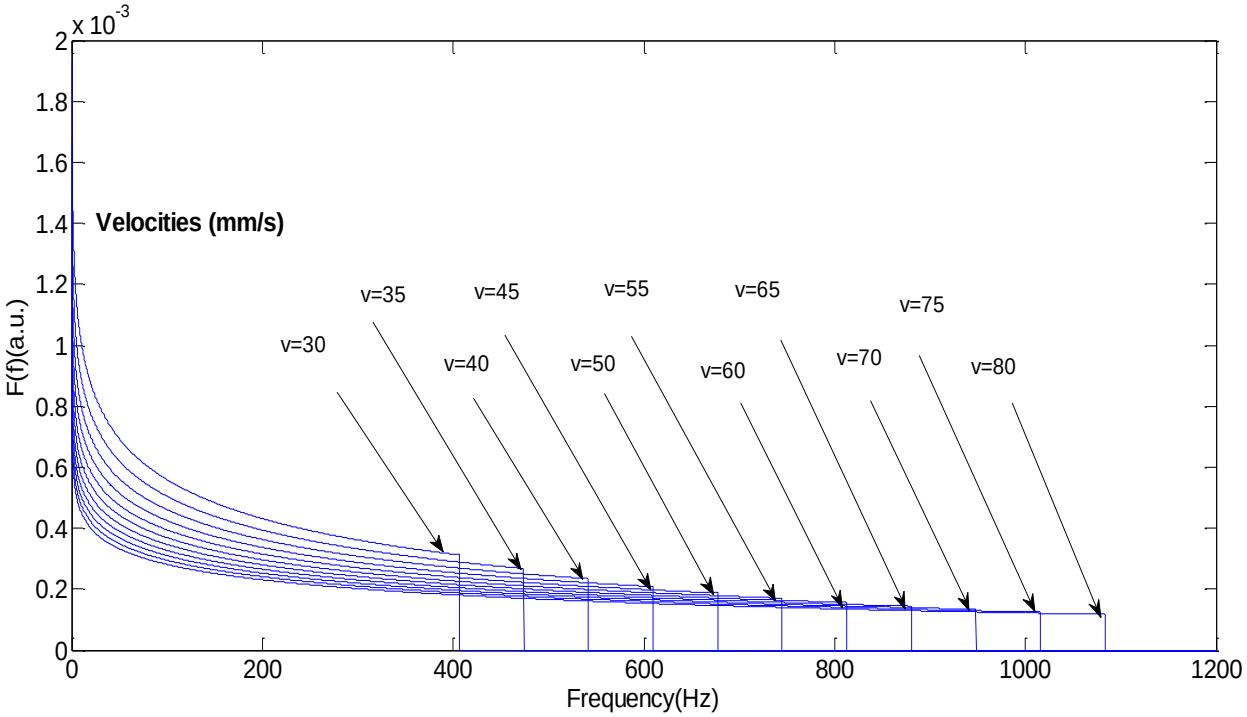

Figure 7.3: Theoretical calculation of scattered light from particles crossing Bessel beam at its center of measurements with 0.5° axicon of velocity measurements 30-80mm/s

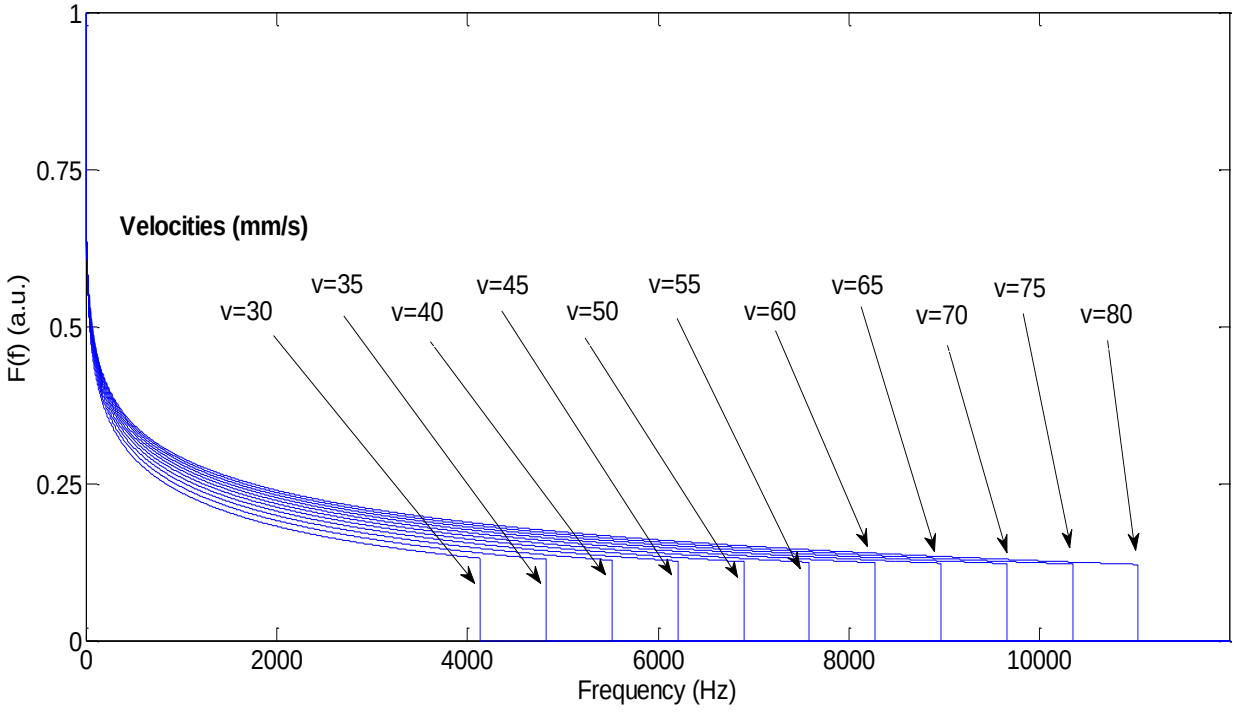

Figure 7.4: Theoretical calculation of scattered light from particles crossing Bessel beam at its center of measurements with 5° axicon of velocity measurements from 30-80mm/s

7.2 Experimental analysis for sandpaper velocity measurements

The measurements were analyzed with Matlab using the Fast Fourier Transform (FFT) algorithm which was used to perform the frequency analysis on the signal. Figure 7.5 represents a typical variation of the obtained spectrum of the signal. Based on the obtained spectra and the theoretical calculations, we opted to determine the experimental Bessel frequency, f_b, as the value at which the spectrum starts to decrease after presenting a nearly constant value. This value was consistently close to the theoretical value of f_b for most measurements.

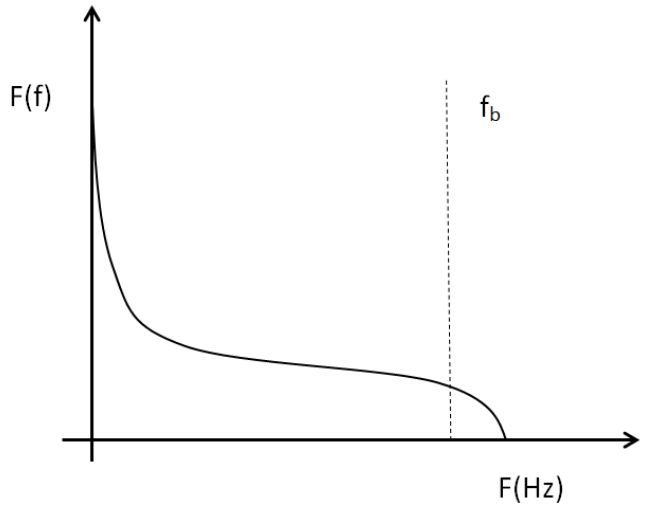

Figure 7.5: Spectra and Bessel frequency

7.2.1 Measurements results with 5° axicon

The results with sandpapers 150-grit, 400-grit, 220-grit and 1500-grit are presented in figures 7.6, 7.7, 7.8 and 7.9 respectively**.** Polynomial curve fitting for the spectra was used. From the plots the Bessel frequency obtained experimentally is in agreement with the theoretical value obtained using equation (7.4) and the spectra versus frequency profiles have consistently distributed trend. By examining each plot the trend of measured Bessel frequency is approximately located at the same value of the theoretical with only small differences along the horizontal axis as the trend starts to curve towards the horizontal axis. The difference can be more apparent in higher velocities**.** This frequency change with similar trend is evidence of frequency change observed experimentally. These experimental results are generally in good agreement with the theoretical analysis and numerical simulations in terms of the dependence of

the spectra on the velocity. The main difference in the plot is that for the theoretical and numerical simulation the spectrum marks the edge of the frequency axis vertically at the f_b of the desired frequency while experimentally it marks the edge gradually. The polynomial curve fitting was used to indicate the trend of the spectra. Measurements were taken with velocities less than 30mm/s were not very reliable and were discarded from the analysis because on careful inspection, the change in frequency was particularly difficult to discern. By comparing the experimental results corresponding to the four sandpapers, it appears that the light scattering and strength of the signal depends on the grit size and the colour of sandpaper sheet used.

The 150 grit plots shown in figure 7.6 and which has a particle diameter of 93 μm, gave a slight decrease in oscillation. This is more likely due to particles size and surface of reflection. Also the type of material and brown colour was found experimentally to generate the highest signal.

The results in figure 7.9 using 1500 grits size (8.4μm) are essentially identical to theoretical results in figure 7.3, with some small differences along the frequency axis. Although when using 1500 grit the maximum signal obtained was about 800 mV which was less than signals generated with the other grit sizes which was about 2000mV-2800mV. It is likely because the sandpaper 1500 grits has particles size of 8.4μm close to the fringe spacing (7μm).

In figure 7.10, where the velocity vs. frequency is plotted for two sets of repeated experiments, the % error between the measurements is also displayed and shows that the experiments have good repeatability.

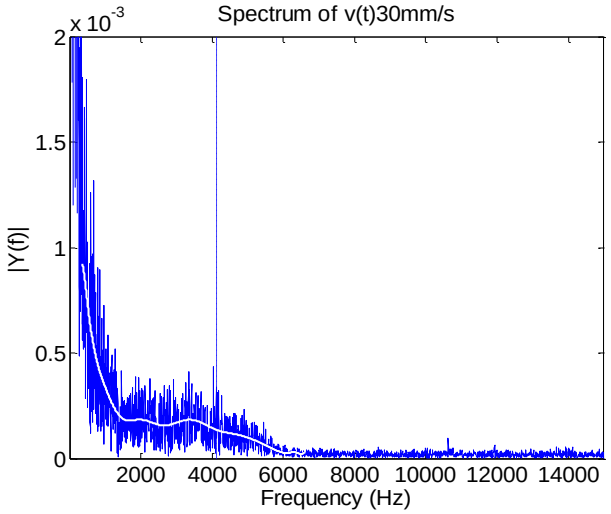
Spectrum of v(t)30mm/s
x 10^-3
|Y(f)|
Frequency (Hz)

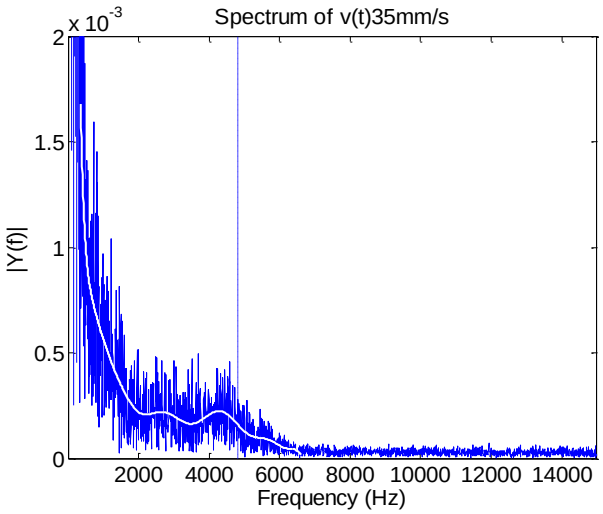
Spectrum of v(t)35mm/s
x 10^-3
|Y(f)|
Frequency (Hz)

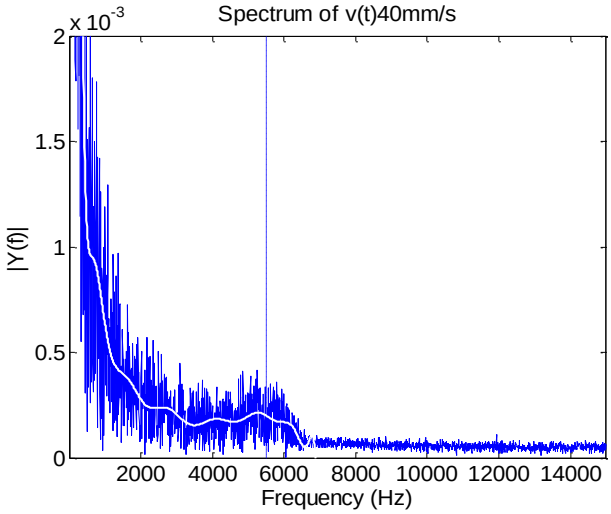
Spectrum of v(t)40mm/s
x 10^-3
|Y(f)|
Frequency (Hz)

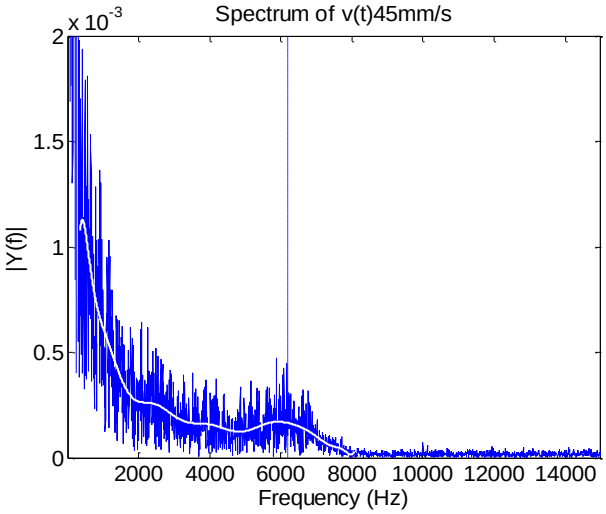
Spectrum of v(t)45mm/s
x 10^-3
|Y(f)|
Frequency (Hz)

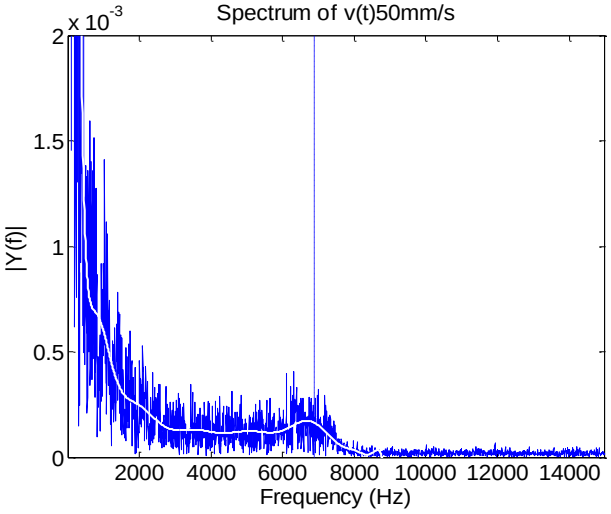
Spectrum of v(t)50mm/s
x 10^-3
|Y(f)|
Frequency (Hz)

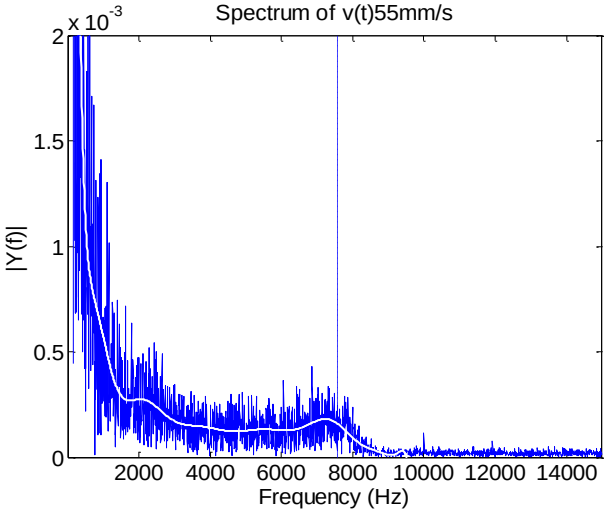
Spectrum of v(t)55mm/s
x 10^-3
|Y(f)|
Frequency (Hz)

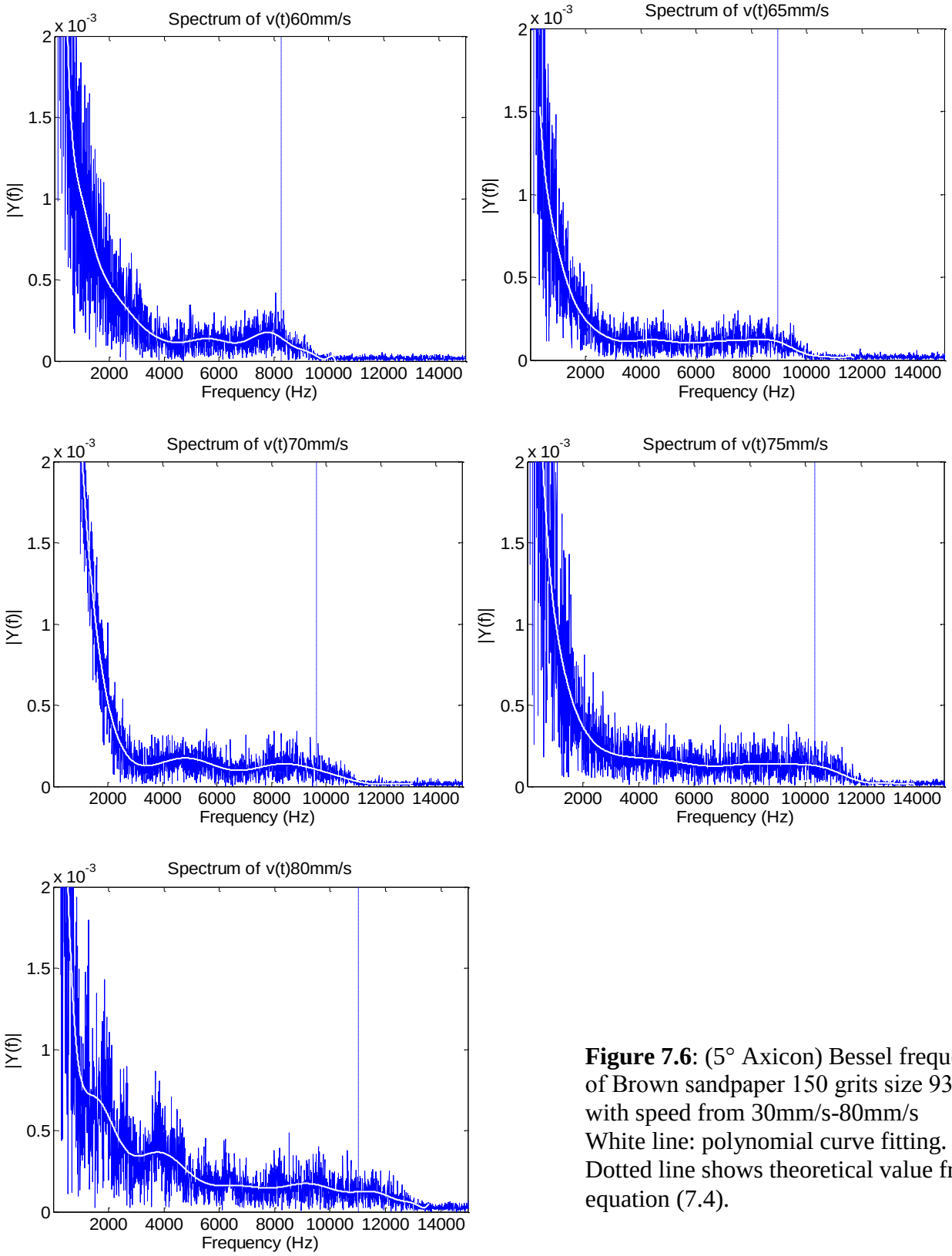

Figure 7.6: (5° Axicon) Bessel frequency of Brown sandpaper 150 grits size 93μm with speed from 30mm/s-80mm/s
White line: polynomial curve fitting.
Dotted line shows theoretical value from equation (7.4).

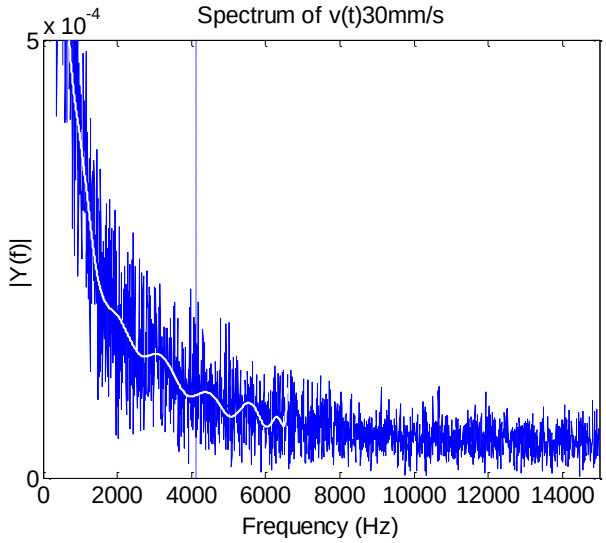
Spectrum of v(t)30mm/s
x 10^-4
5
0
|Y(f)|
0 2000 4000 6000 8000 10000 12000 14000
Frequency (Hz)

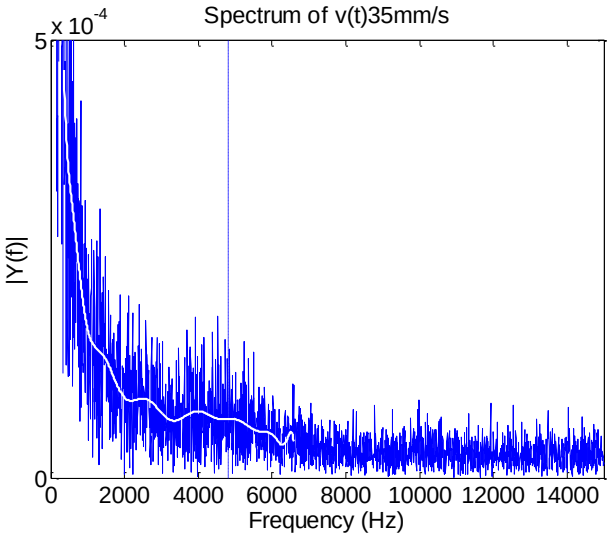
Spectrum of v(t)35mm/s
x 10^-4
5
0
|Y(f)|
0 2000 4000 6000 8000 10000 12000 14000
Frequency (Hz)

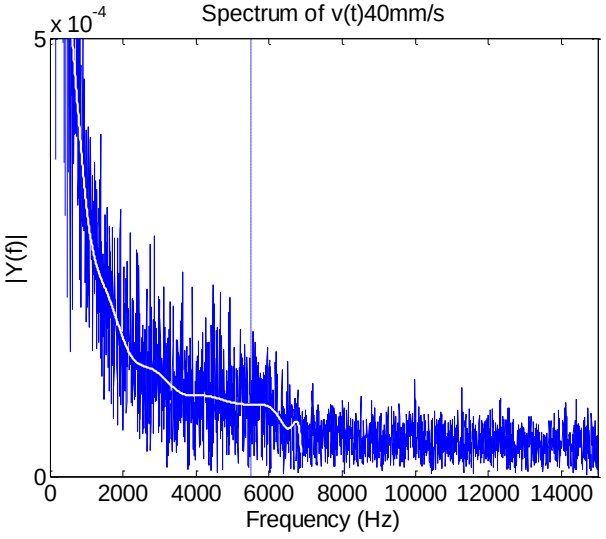
Spectrum of v(t)40mm/s
x 10^-4
5
0
|Y(f)|
0 2000 4000 6000 8000 10000 12000 14000
Frequency (Hz)

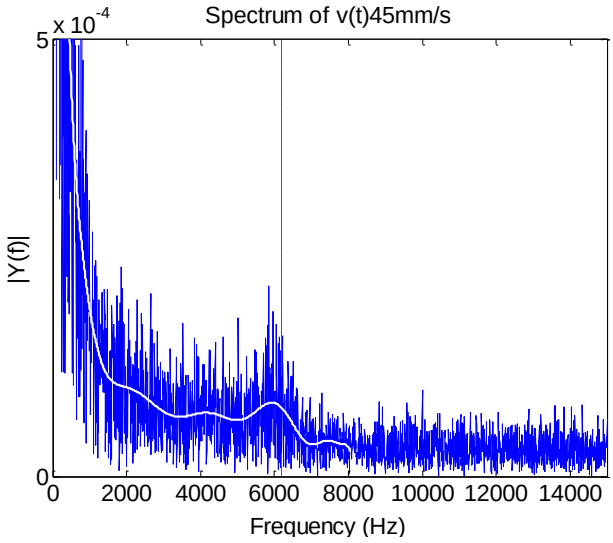
Spectrum of v(t)45mm/s
x 10^-4
5
0
|Y(f)|
0 2000 4000 6000 8000 10000 12000 14000
Frequency (Hz)

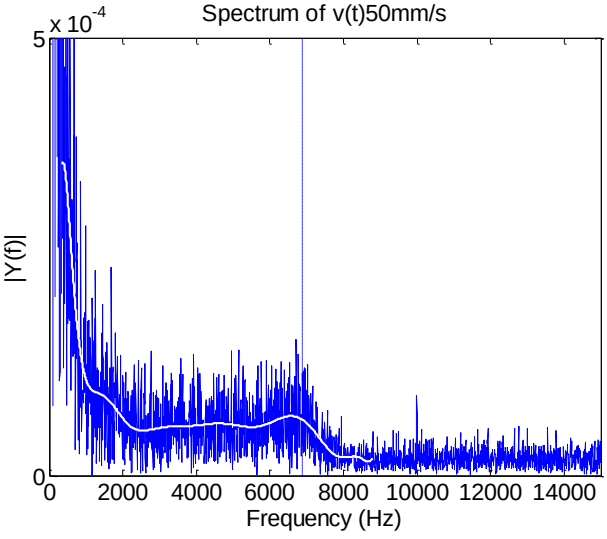
Spectrum of v(t)50mm/s
x 10^-4
5
0
|Y(f)|
0 2000 4000 6000 8000 10000 12000 14000
Frequency (Hz)

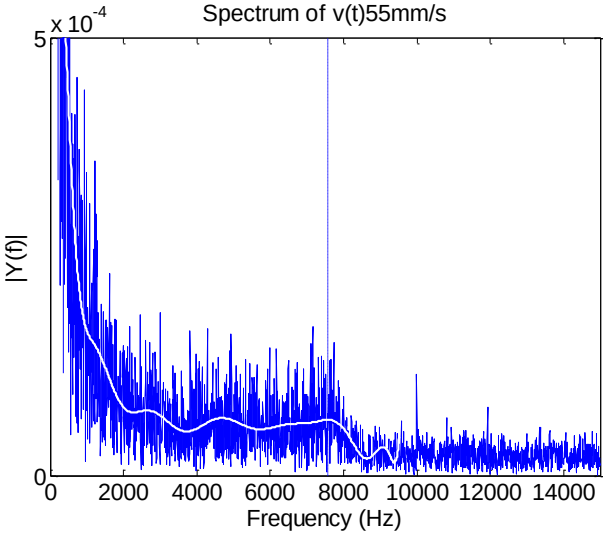
Spectrum of v(t)55mm/s
x 10^-4
5
0
|Y(f)|
0 2000 4000 6000 8000 10000 12000 14000
Frequency (Hz)

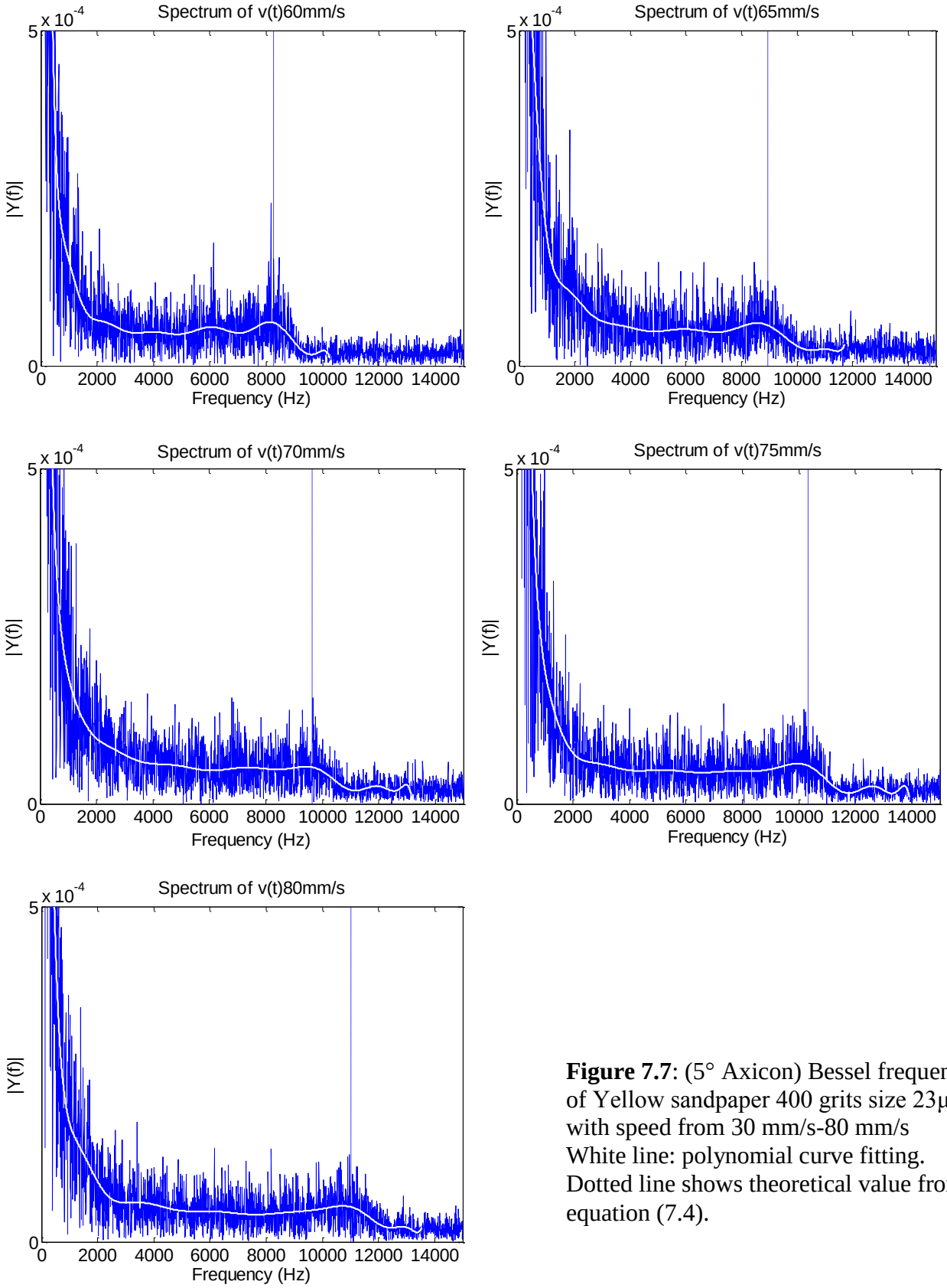

Figure 7.7: (5° Axicon) Bessel frequency of Yellow sandpaper 400 grits size 23μm with speed from 30 mm/s-80 mm/s White line: polynomial curve fitting. Dotted line shows theoretical value from equation (7.4).

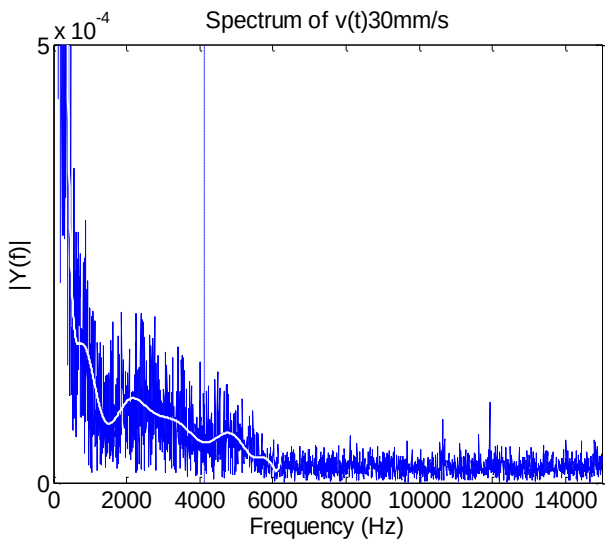
Spectrum of v(t)30mm/s
x 10^-4
5
0
|Y(f)|
0 2000 4000 6000 8000 10000 12000 14000
Frequency (Hz)

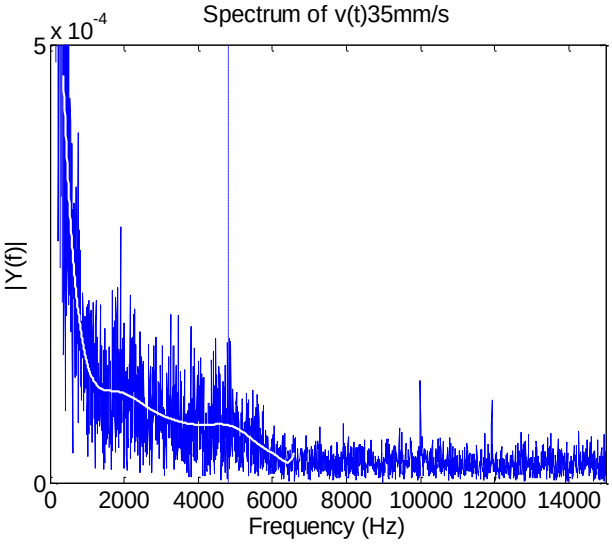
Spectrum of v(t)35mm/s
x 10^-4
5
0
|Y(f)|
0 2000 4000 6000 8000 10000 12000 14000
Frequency (Hz)

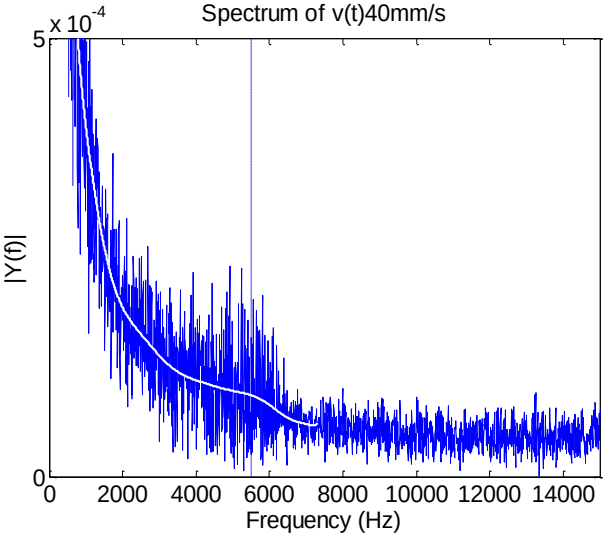
Spectrum of v(t)40mm/s
x 10^-4
5
0
|Y(f)|
0 2000 4000 6000 8000 10000 12000 14000
Frequency (Hz)

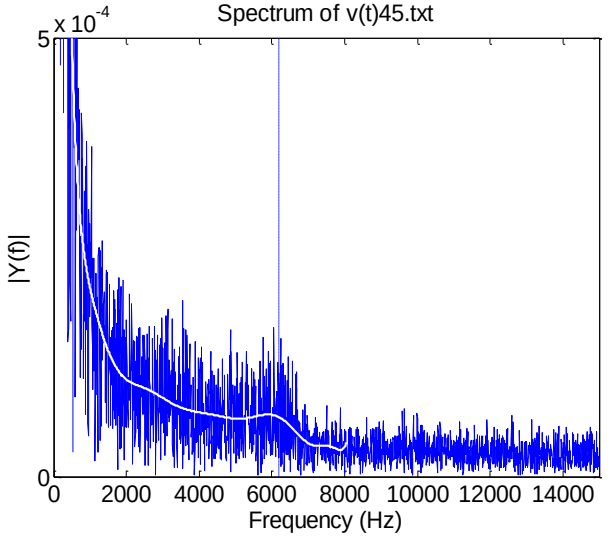
Spectrum of v(t)45.txt
x 10^-4
5
0
|Y(f)|
0 2000 4000 6000 8000 10000 12000 14000
Frequency (Hz)

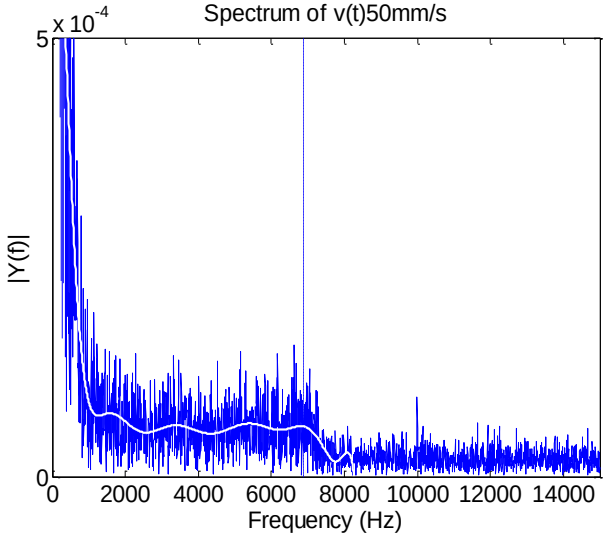
Spectrum of v(t)50mm/s
x 10^-4
5
0
|Y(f)|
0 2000 4000 6000 8000 10000 12000 14000
Frequency (Hz)

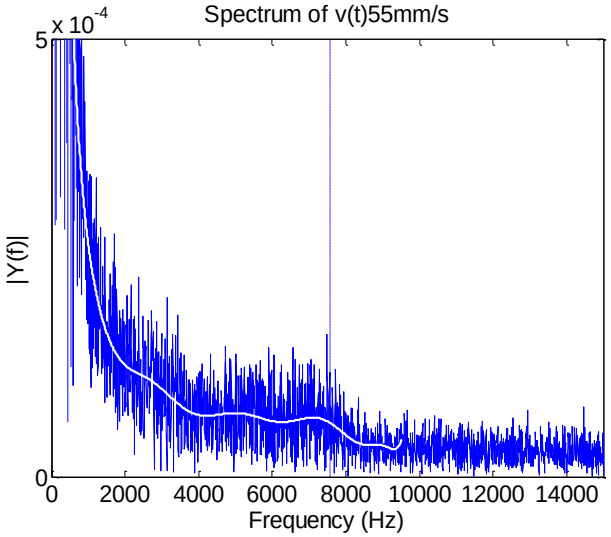
Spectrum of v(t)55mm/s
x 10^-4
5
0
|Y(f)|
0 2000 4000 6000 8000 10000 12000 14000
Frequency (Hz)

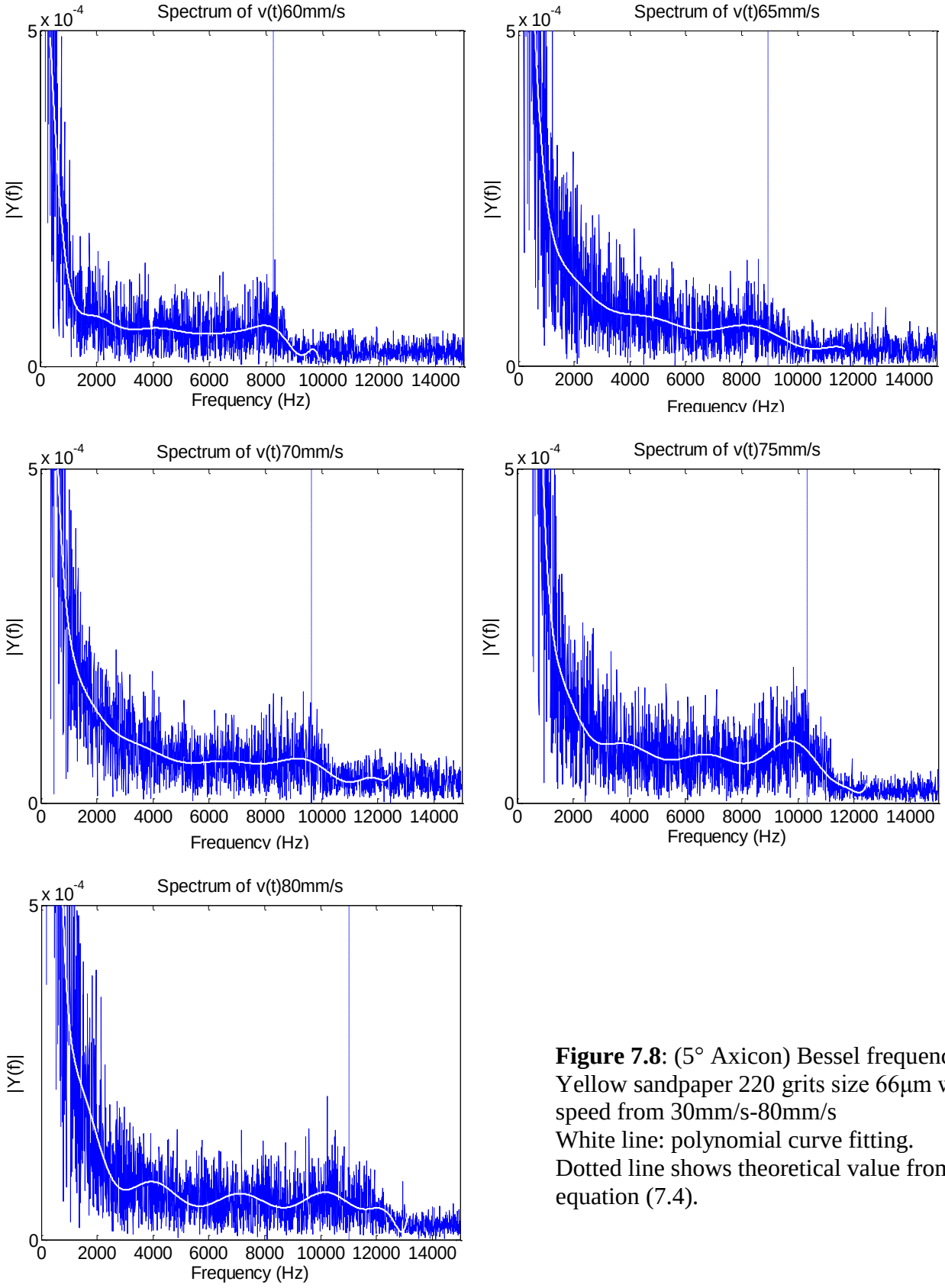

Figure 7.8: (5° Axicon) Bessel frequency of Yellow sandpaper 220 grits size 66μm with speed from 30mm/s-80mm/s
White line: polynomial curve fitting.
Dotted line shows theoretical value from equation (7.4).

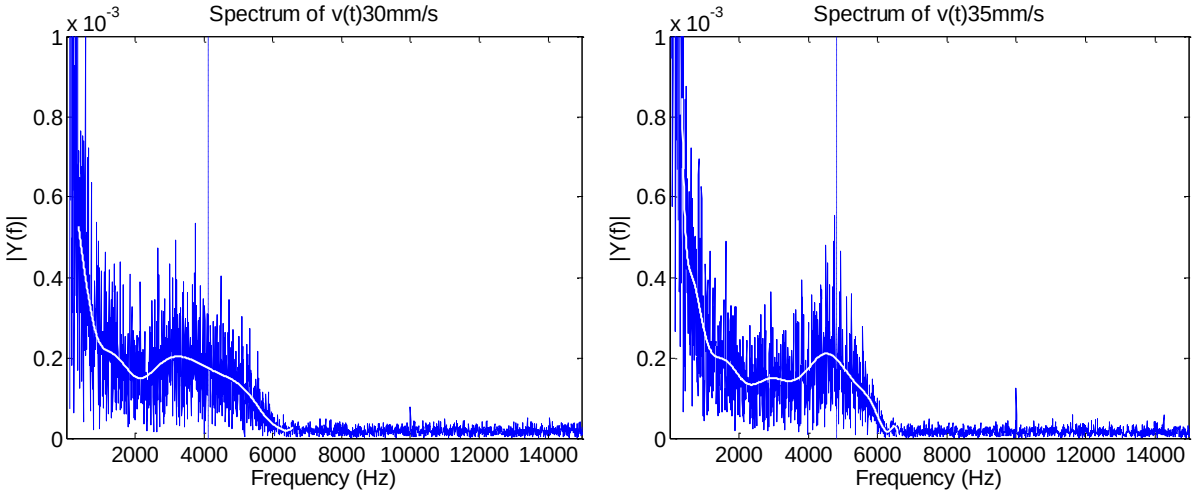
Spectrum of v(t)30mm/s
x 10^-3
|Y(f)|
Frequency (Hz)
0
0.2
0.4
0.6
0.8
1
2000 4000 6000 8000 10000 12000 14000

Spectrum of v(t)35mm/s
x 10^-3
|Y(f)|
Frequency (Hz)
0
0.2
0.4
0.6
0.8
1
2000 4000 6000 8000 10000 12000 14000

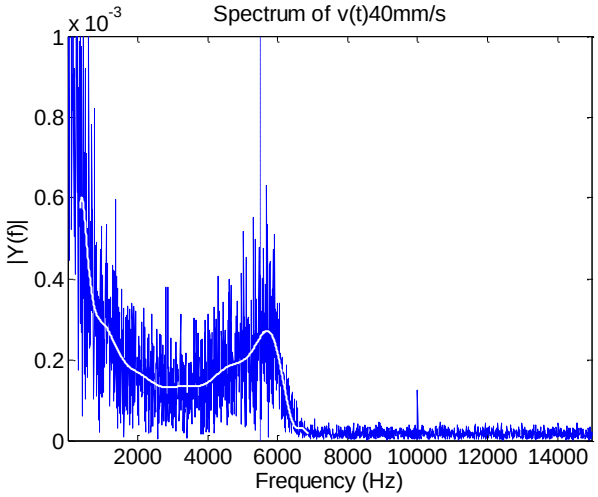
Spectrum of v(t)40mm/s
x 10^-3
|Y(f)|
Frequency (Hz)
0
0.2
0.4
0.6
0.8
1
2000 4000 6000 8000 10000 12000 14000

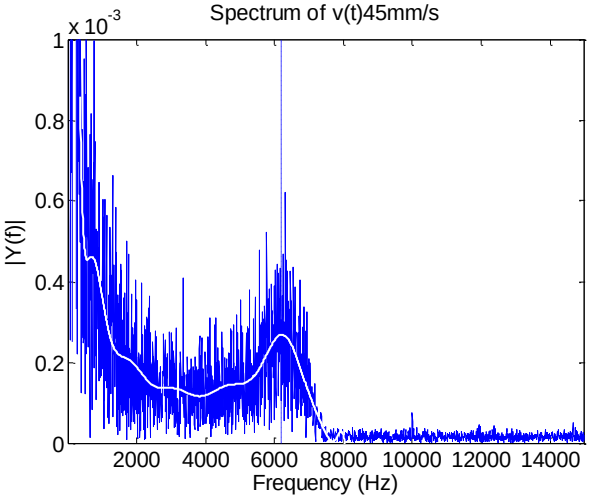
Spectrum of v(t)45mm/s
x 10^-3
|Y(f)|
Frequency (Hz)
0
0.2
0.4
0.6
0.8
1
2000 4000 6000 8000 10000 12000 14000

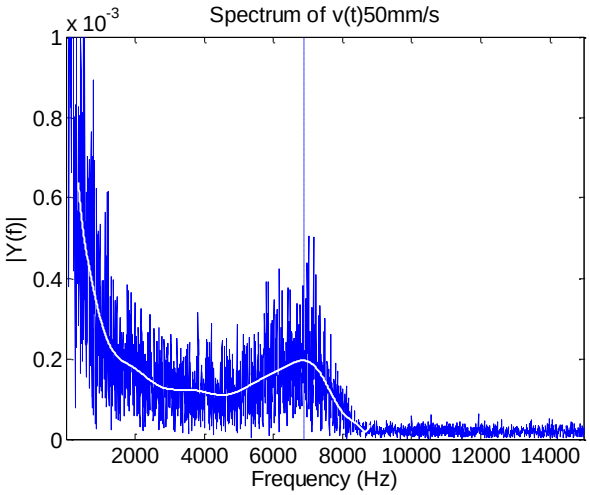
Spectrum of v(t)50mm/s
x 10^-3
|Y(f)|
Frequency (Hz)
0
0.2
0.4
0.6
0.8
1
2000 4000 6000 8000 10000 12000 14000

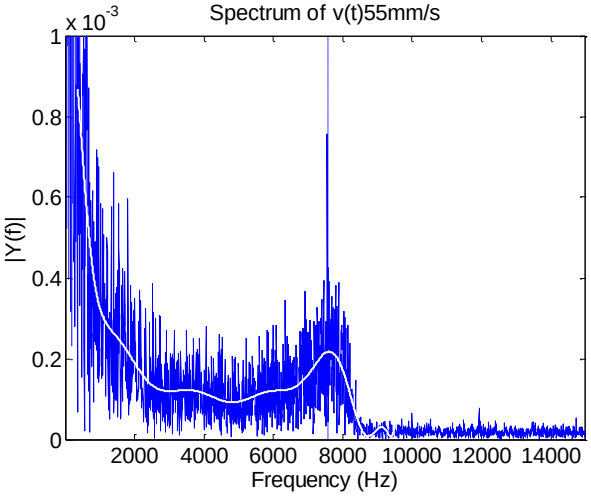
Spectrum of v(t)55mm/s
x 10^-3
|Y(f)|
Frequency (Hz)
0
0.2
0.4
0.6
0.8
1
2000 4000 6000 8000 10000 12000 14000

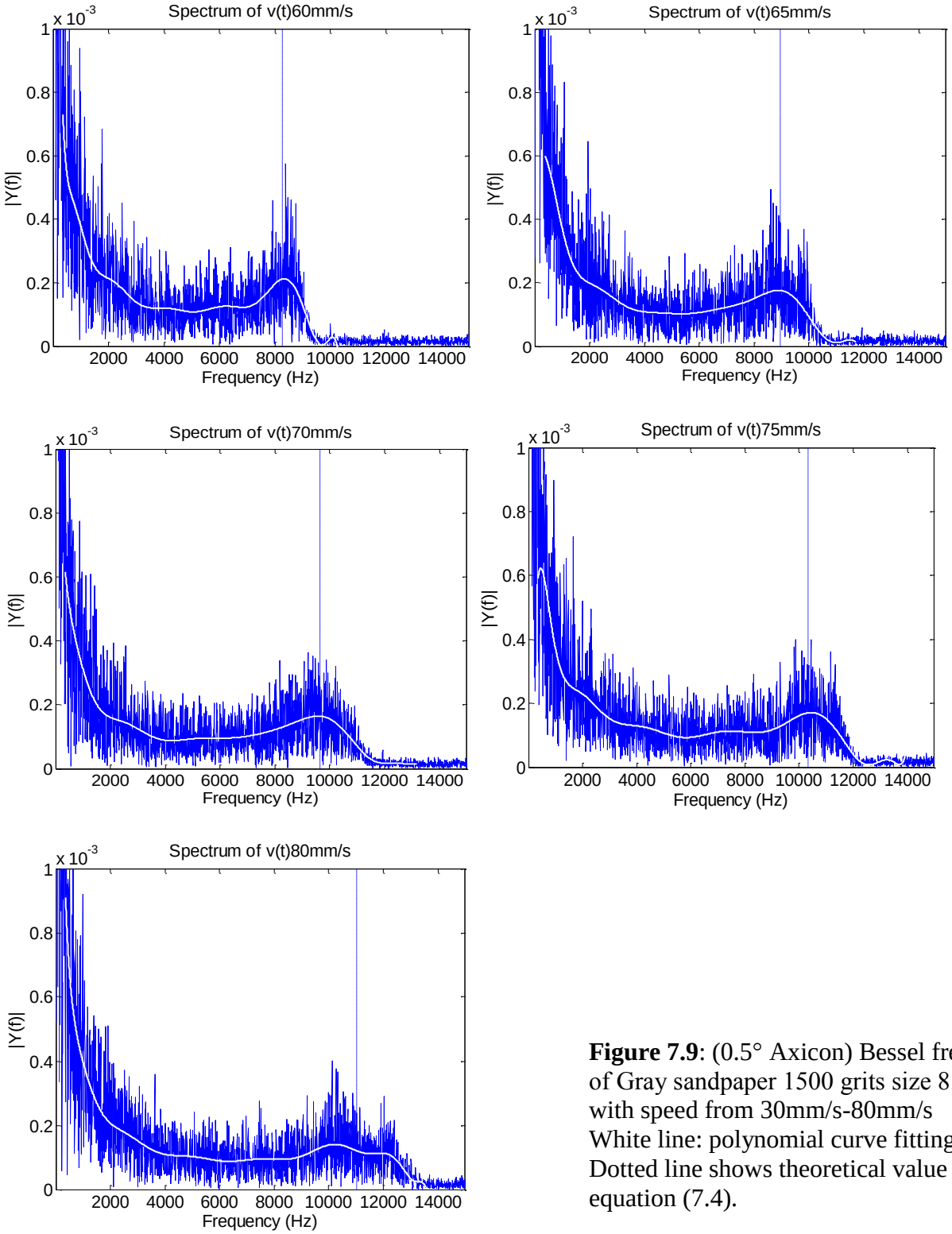

Figure 7.9: (0.5° Axicon) Bessel frequency of Gray sandpaper 1500 grits size 8.4μm with speed from 30mm/s-80mm/s
White line: polynomial curve fitting.
Dotted line shows theoretical value from equation (7.4).

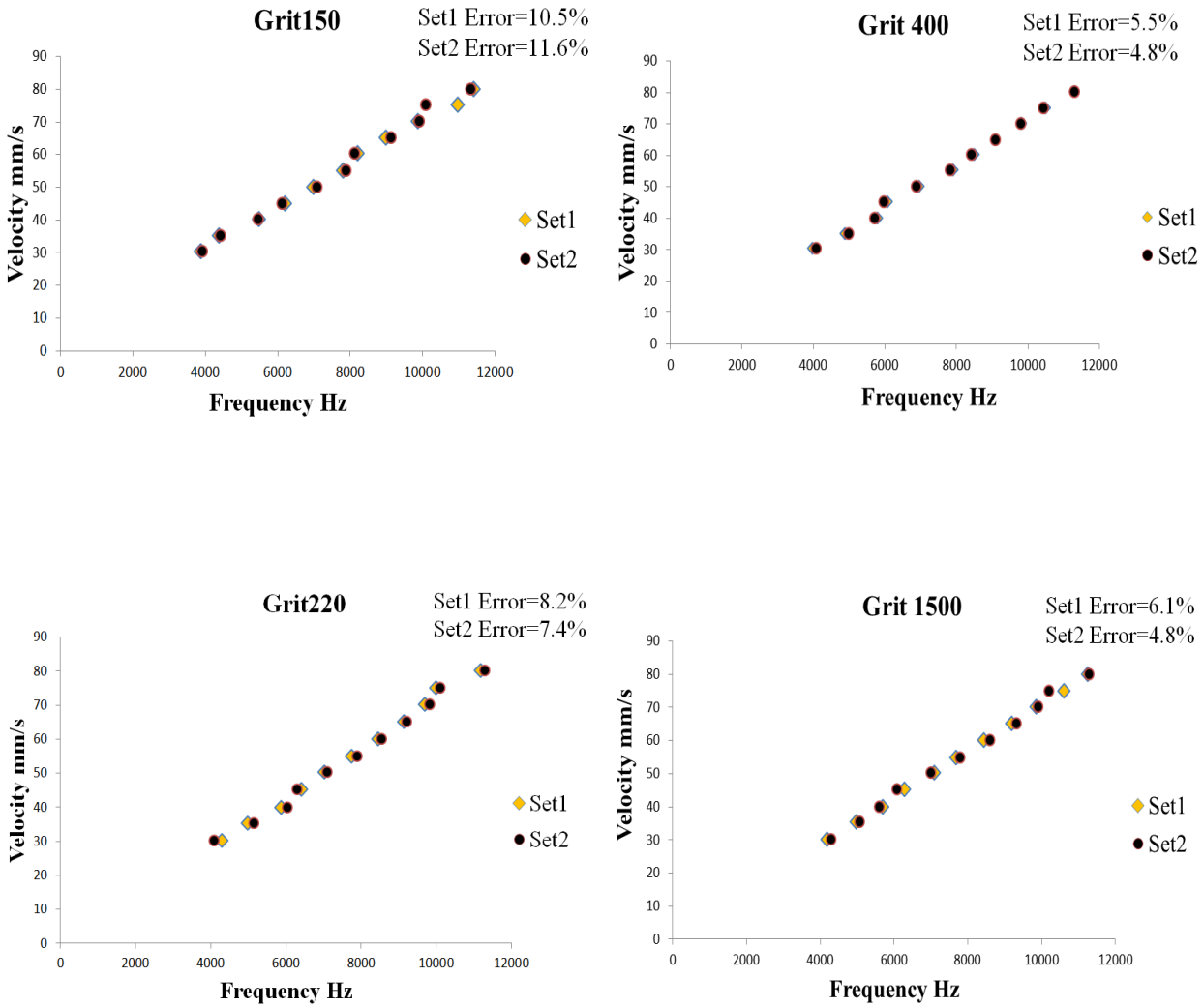

Figure 7.10: Velocity vs frequency of two sets of measurements of 5° axicon with the relative error of each set

7.2.2 Measurements results with 0.5° Axicon

The results with sandpapers 150-grit, 400-grit, 220-grit and 1500-grit are presented in figures 7.11, 7.12, 7.13 and 7.14 respectively**.** These results yielding the spectra of the scattered light intensity for velocities ranging between 30 and 80 mm/s. Comparing the results corresponding to the four sandpapers, the frequencies measured by the LBV and the theoretical frequency closely agree, as expected with almost the same trend. The spectra start decreasing at a frequency equal to the Bessel frequency after presenting a plateau of nearby constant value. The plots show that there is a slight variation from theoretical values, but this could be due to differences in the depth of field and fringe spacing of the two axicons as described in table 6-2 and 7-3. The measurements with 0.5° were less noisy than with 5° axicon. This is because the DOF generated with 0.5° was longer and the fringe spacing (average =71μm) was larger than with 5° axicon (average=7μm) that was close to the particle size in sandpaper. The larger fringe spacing allowed the particle to scatter light more efficiently from the fringes that produced signals with lower noise. The effect of ambient light and the reflection from the optical components may have been collected by the focusing lens and then detected by the photodetector that affected the signals to include noise. Every effort was made to eliminate stray reflections from the laser optics or from any possible light sources, to make the area where the system was being used safer and to also try to eliminate possible sources of noise in the system while these measurements were being performed and while the optical setup was being adjusted. These stray reflections could easily be acquired by the receiving optics. The small sand particles contribute to the detected scattered signal, and it cannot ensure a unique particle passing through the fringe pattern.

The measurement tests as part of this research were performed in several attempts to demonstrate the optical system could perform as a viable velocity measurement system for solid surfaces. In figure 7.15, where the velocity vs. frequency is plotted for two sets of repeated experiments, the % error between the measurements is also displayed and shows that the experiments have good repeatability.

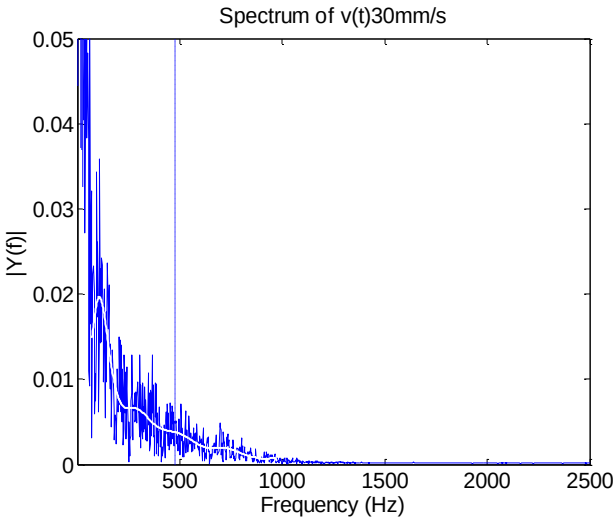
Spectrum of v(t)30mm/s
|Y(f)|
0.05
0.04
0.03
0.02
0.01
0
500
1000
1500
2000
2500
Frequency (Hz)

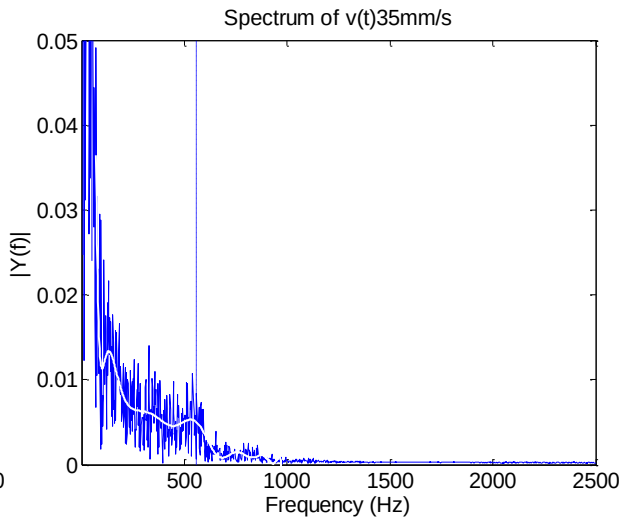
Spectrum of v(t)35mm/s
|Y(f)|
0.05
0.04
0.03
0.02
0.01
0
500
1000
1500
2000
2500
Frequency (Hz)

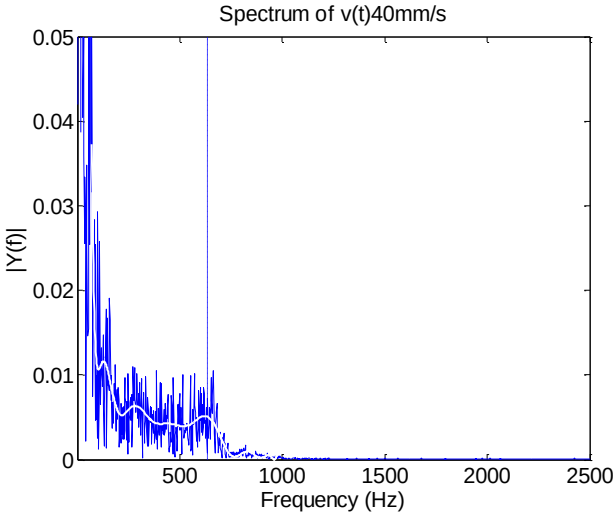
Spectrum of v(t)40mm/s
|Y(f)|
0.05
0.04
0.03
0.02
0.01
0
500
1000
1500
2000
2500
Frequency (Hz)

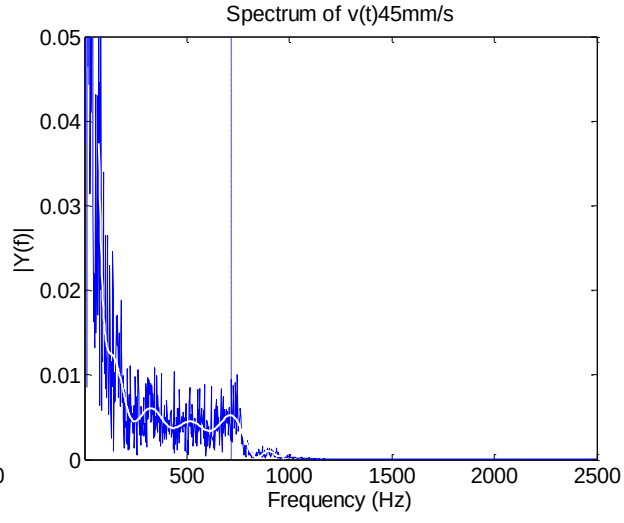
Spectrum of v(t)45mm/s
|Y(f)|
0.05
0.04
0.03
0.02
0.01
0
500
1000
1500
2000
2500
Frequency (Hz)

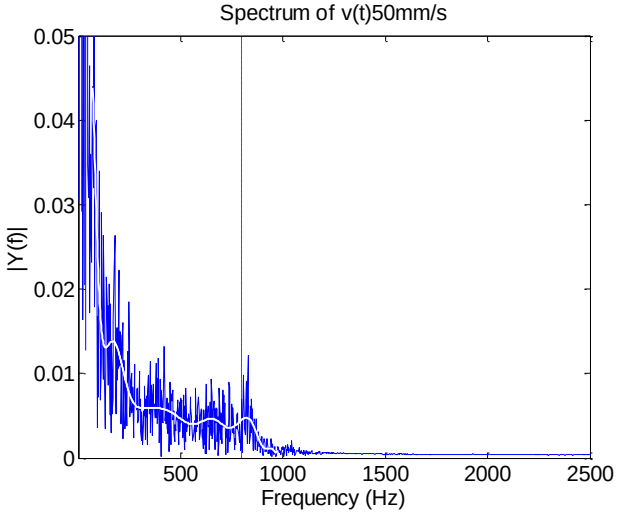
Spectrum of v(t)50mm/s
|Y(f)|
0.05
0.04
0.03
0.02
0.01
0
500
1000
1500
2000
2500
Frequency (Hz)

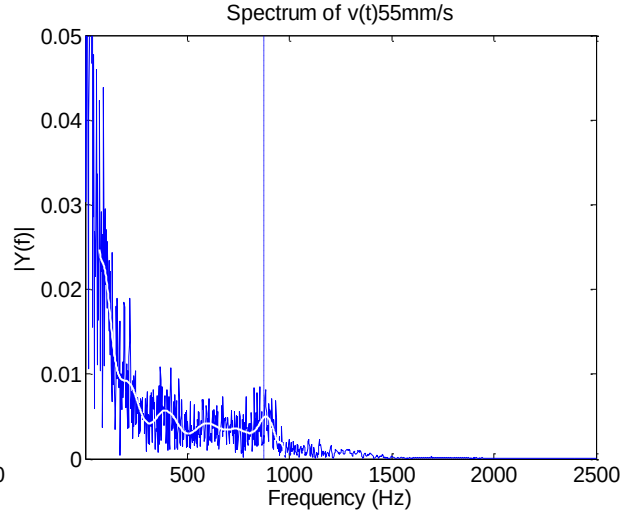
Spectrum of v(t)55mm/s
|Y(f)|
0.05
0.04
0.03
0.02
0.01
0
500
1000
1500
2000
2500
Frequency (Hz)

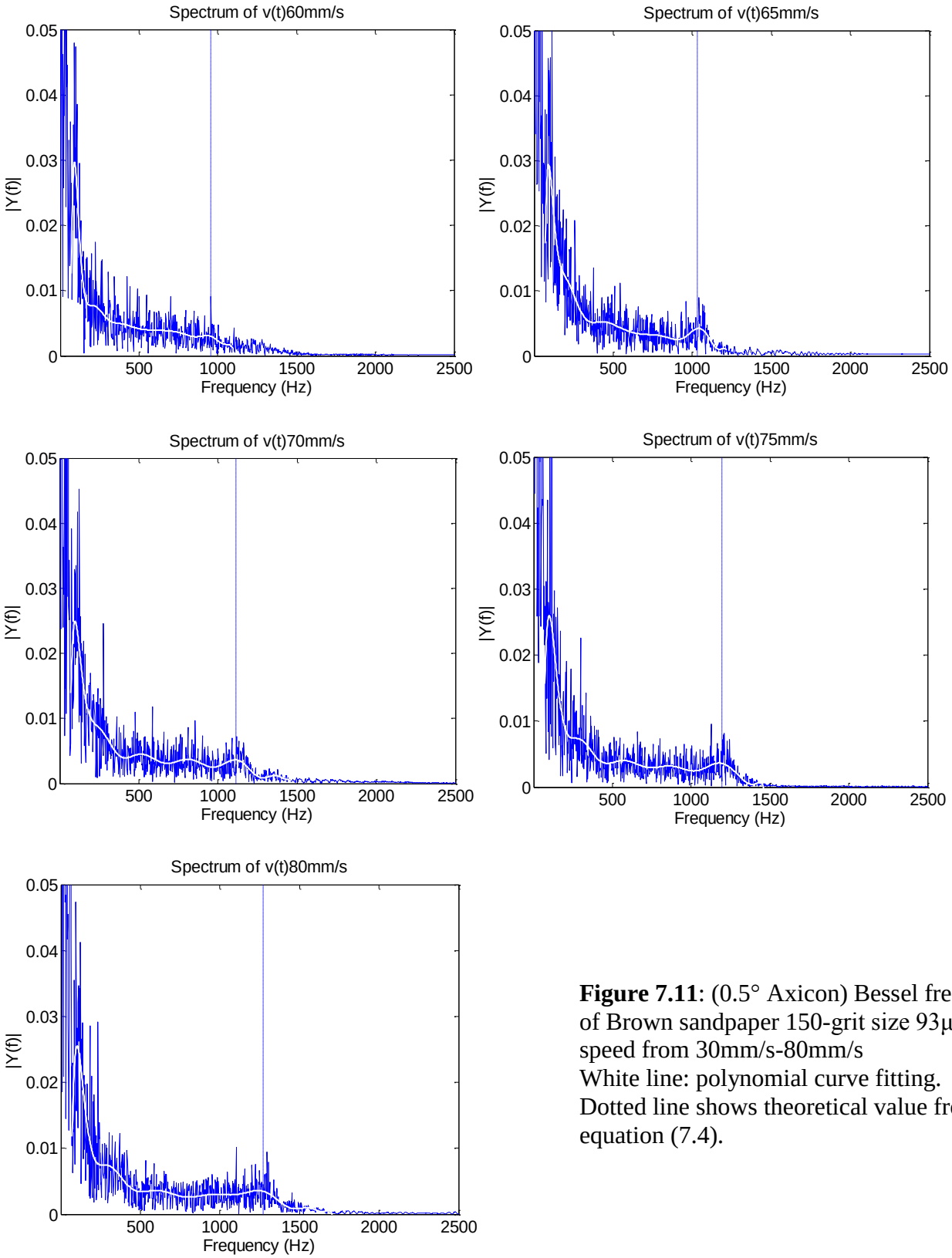

Figure 7.11: (0.5° Axicon) Bessel frequency of Brown sandpaper 150-grit size 93µm with speed from 30mm/s-80mm/s
White line: polynomial curve fitting.
Dotted line shows theoretical value from equation (7.4).

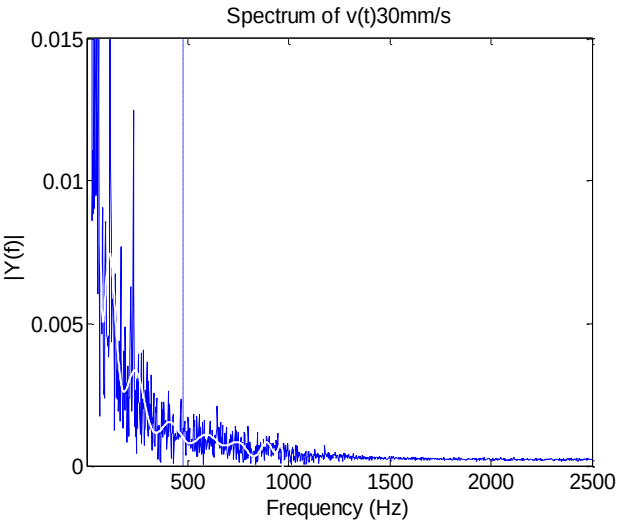
Spectrum of v(t)30mm/s
|Y(f)|
Frequency (Hz)
0.015
0.01
0.005
0
500
1000
1500
2000
2500

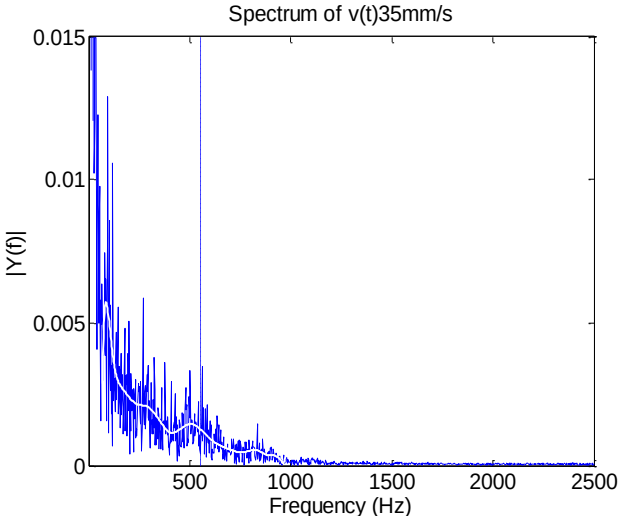
Spectrum of v(t)35mm/s
|Y(f)|
Frequency (Hz)
0.015
0.01
0.005
0
500
1000
1500
2000
2500

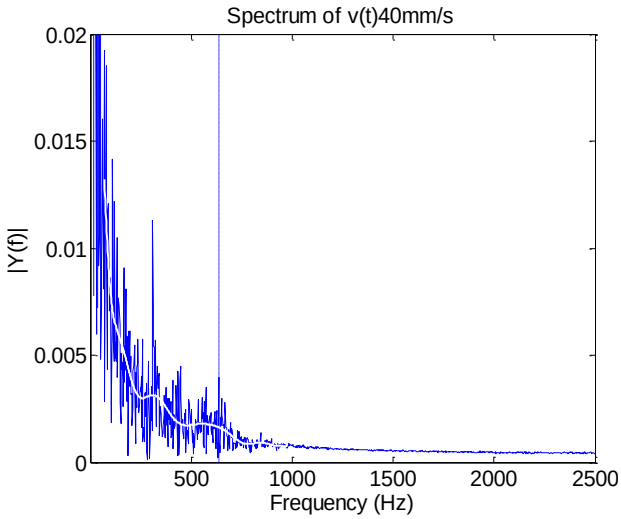
Spectrum of v(t)40mm/s
|Y(f)|
Frequency (Hz)
0.02
0.015
0.01
0.005
0
500
1000
1500
2000
2500

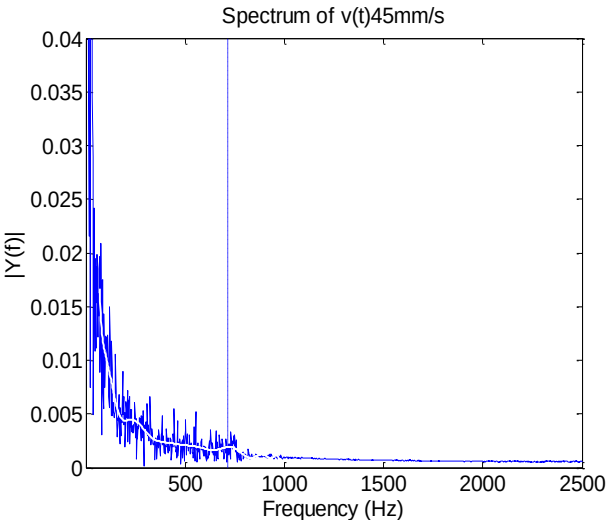
Spectrum of v(t)45mm/s
|Y(f)|
Frequency (Hz)
0.04
0.035
0.03
0.025
0.02
0.015
0.01
0.005
0
500
1000
1500
2000
2500

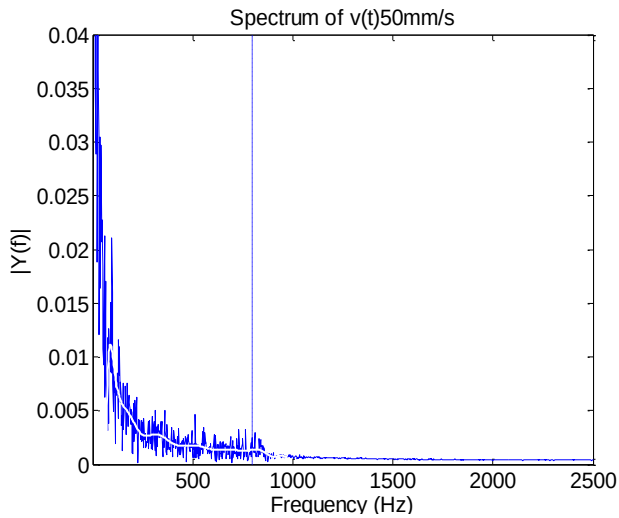
Spectrum of v(t)50mm/s
|Y(f)|
Frequency (Hz)
0.04
0.035
0.03
0.025
0.02
0.015
0.01
0.005
0
500
1000
1500
2000
2500

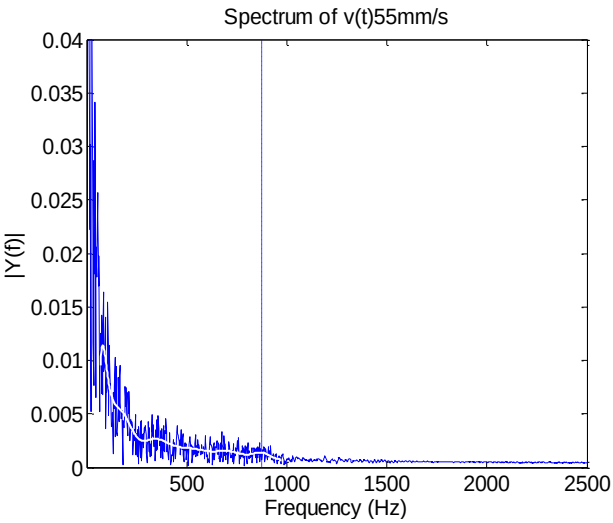
Spectrum of v(t)55mm/s
|Y(f)|
Frequency (Hz)
0.04
0.035
0.03
0.025
0.02
0.015
0.01
0.005
0
500
1000
1500
2000
2500

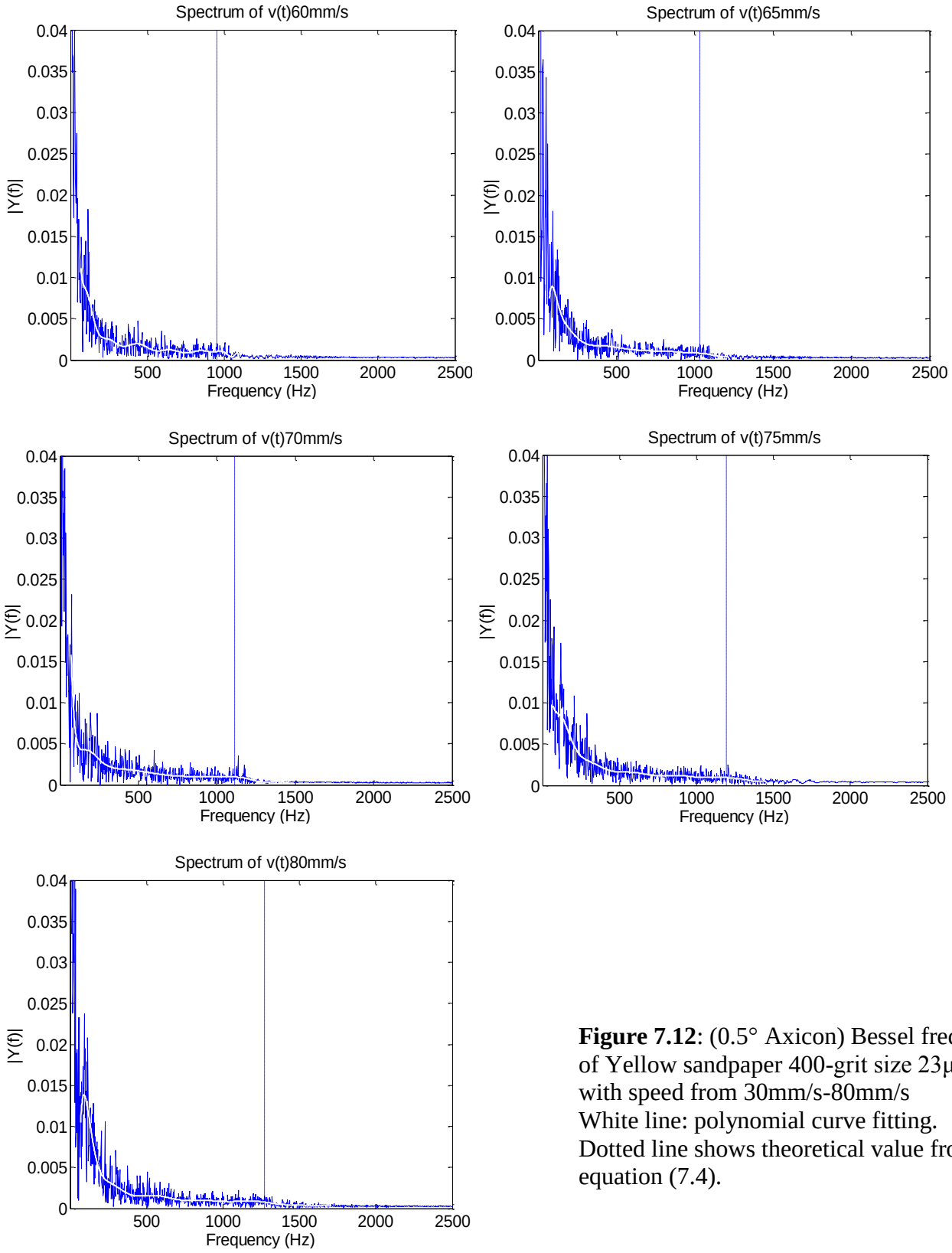

Figure 7.12: (0.5° Axicon) Bessel frequency of Yellow sandpaper 400-grit size 23µm with speed from 30mm/s-80mm/s
White line: polynomial curve fitting.
Dotted line shows theoretical value from equation (7.4).

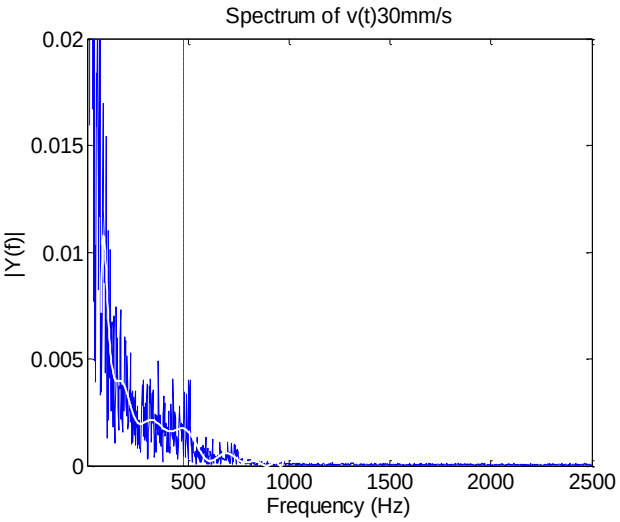
Spectrum of v(t)30mm/s
|Y(f)|
Frequency (Hz)
0.02
0.015
0.01
0.005
0
500
1000
1500
2000
2500

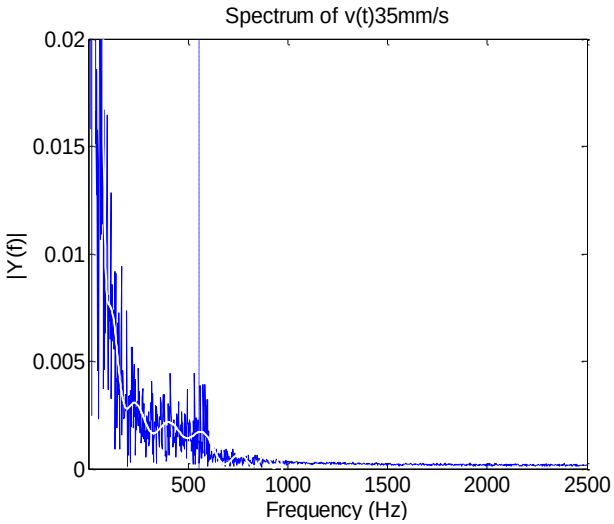
Spectrum of v(t)35mm/s
|Y(f)|
Frequency (Hz)
0.02
0.015
0.01
0.005
0
500
1000
1500
2000
2500

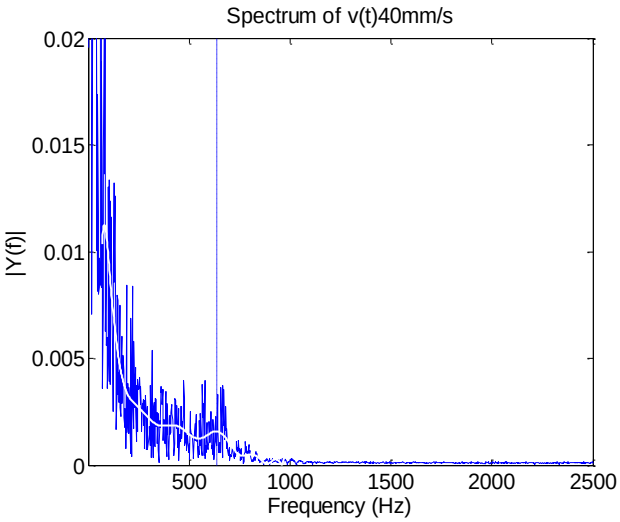
Spectrum of v(t)40mm/s
|Y(f)|
Frequency (Hz)
0.02
0.015
0.01
0.005
0
500
1000
1500
2000
2500

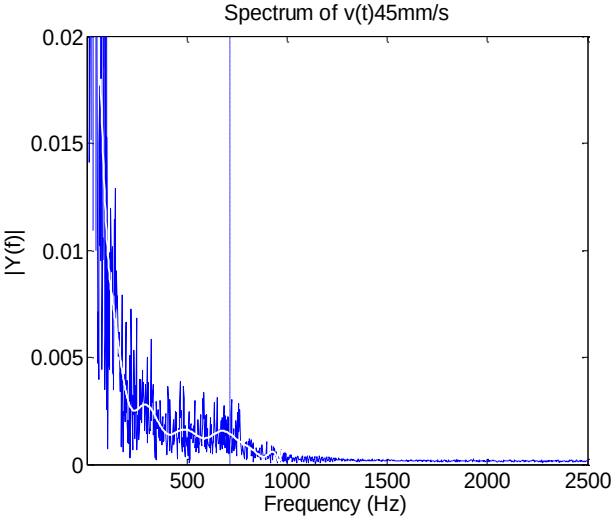
Spectrum of v(t)45mm/s
|Y(f)|
Frequency (Hz)
0.02
0.015
0.01
0.005
0
500
1000
1500
2000
2500

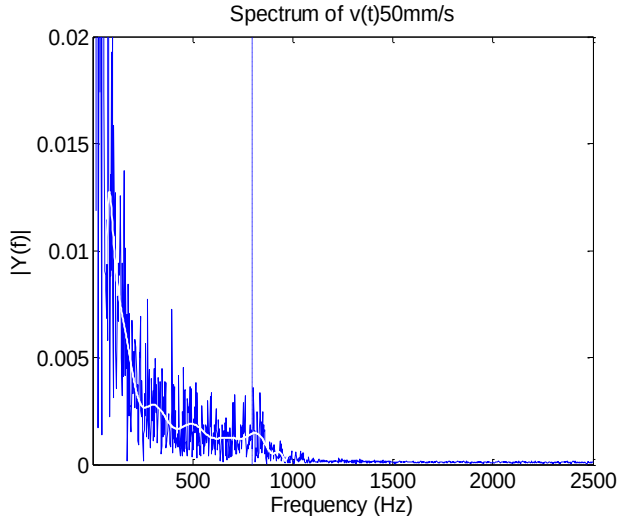
Spectrum of v(t)50mm/s
|Y(f)|
Frequency (Hz)
0.02
0.015
0.01
0.005
0
500
1000
1500
2000
2500

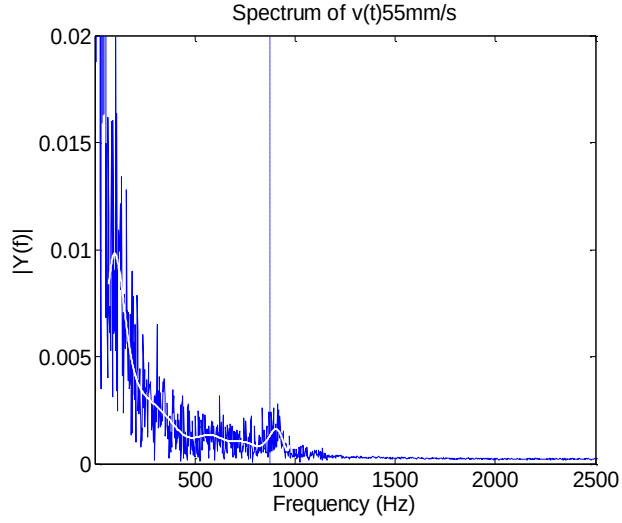
Spectrum of v(t)55mm/s
|Y(f)|
Frequency (Hz)
0.02
0.015
0.01
0.005
0
500
1000
1500
2000
2500

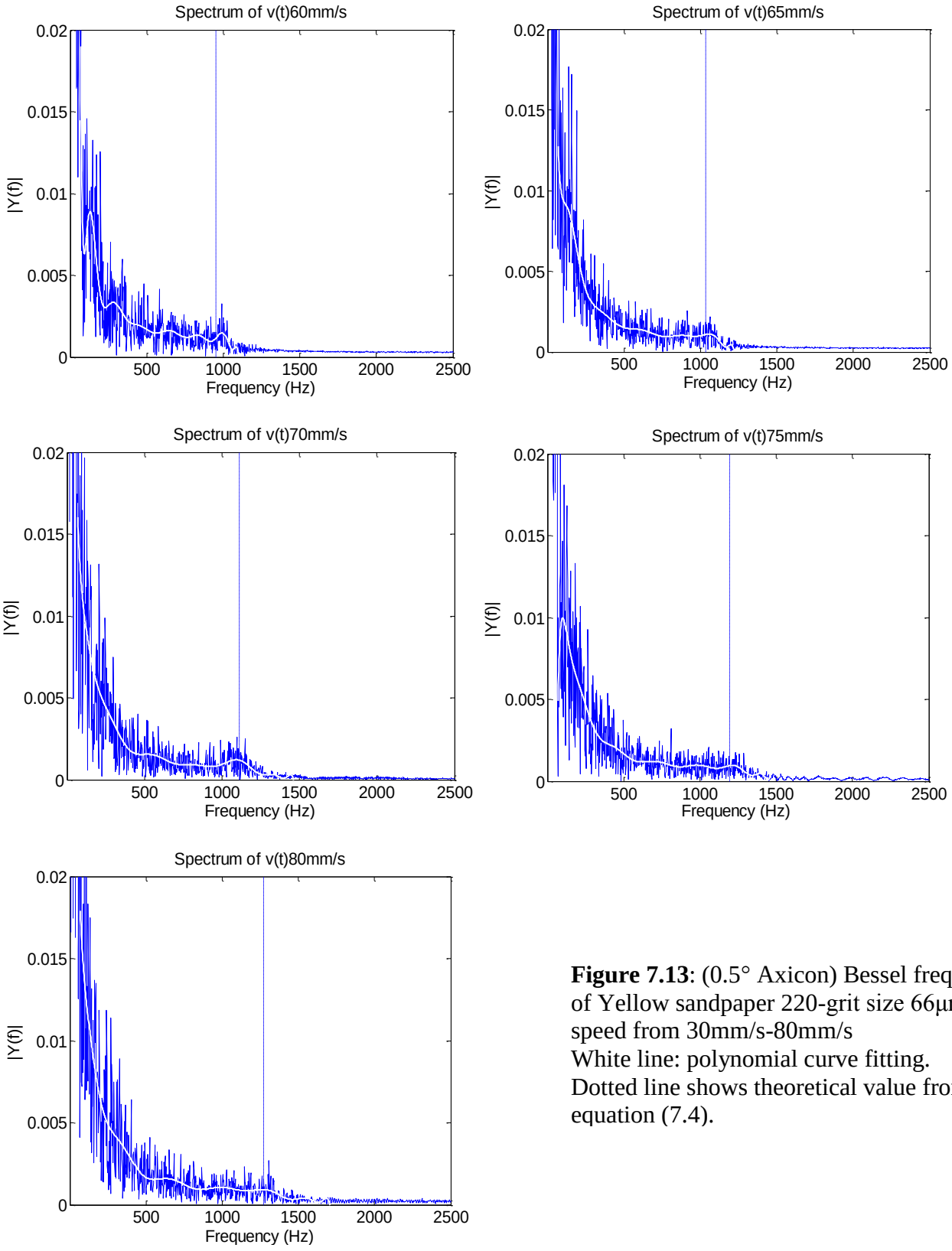

Figure 7.13: (0.5° Axicon) Bessel frequency of Yellow sandpaper 220-grit size 66μm with speed from 30mm/s-80mm/s
White line: polynomial curve fitting.
Dotted line shows theoretical value from equation (7.4).

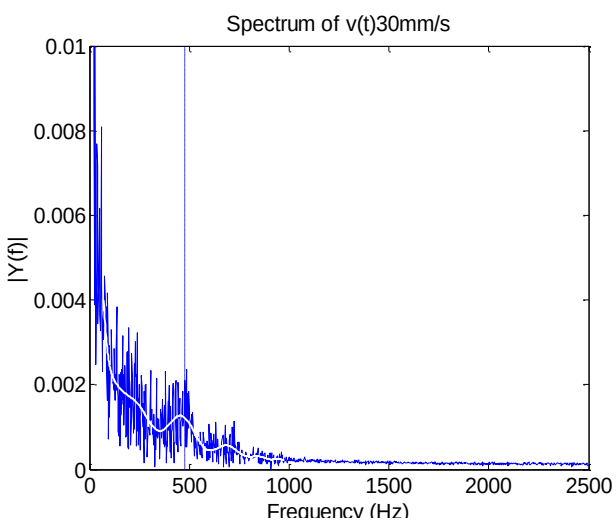
Spectrum of v(t)30mm/s
|Y(f)|
0.01
0.008
0.006
0.004
0.002
0
0
500
1000
1500
2000
2500
Frequency (Hz)

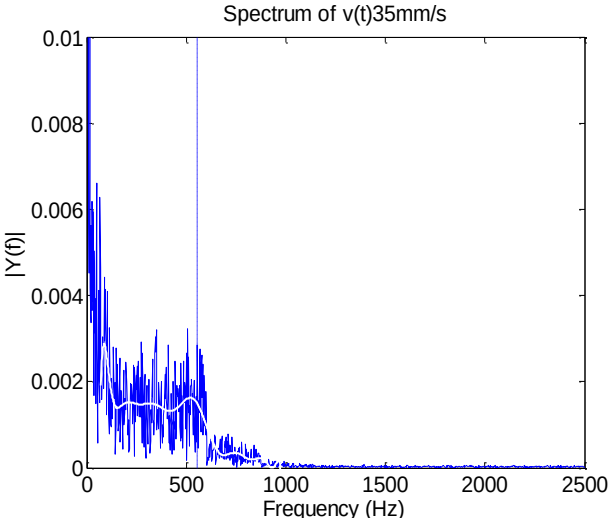
Spectrum of v(t)35mm/s
|Y(f)|
0.01
0.008
0.006
0.004
0.002
0
0
500
1000
1500
2000
2500
Frequency (Hz)

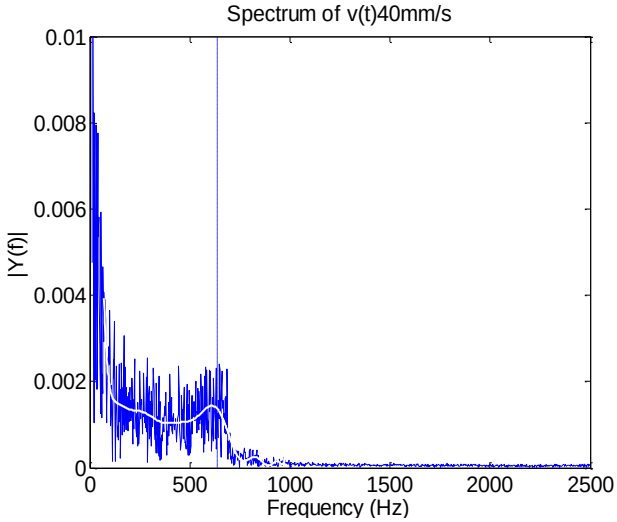
Spectrum of v(t)40mm/s
|Y(f)|
0.01
0.008
0.006
0.004
0.002
0
0
500
1000
1500
2000
2500
Frequency (Hz)

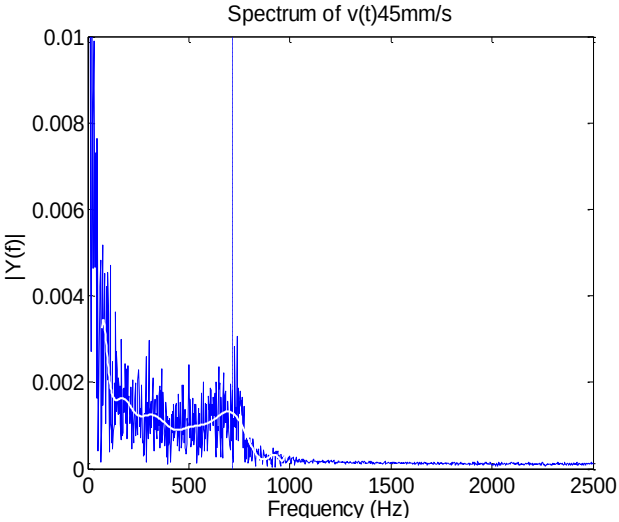
Spectrum of v(t)45mm/s
|Y(f)|
0.01
0.008
0.006
0.004
0.002
0
0
500
1000
1500
2000
2500
Frequency (Hz)

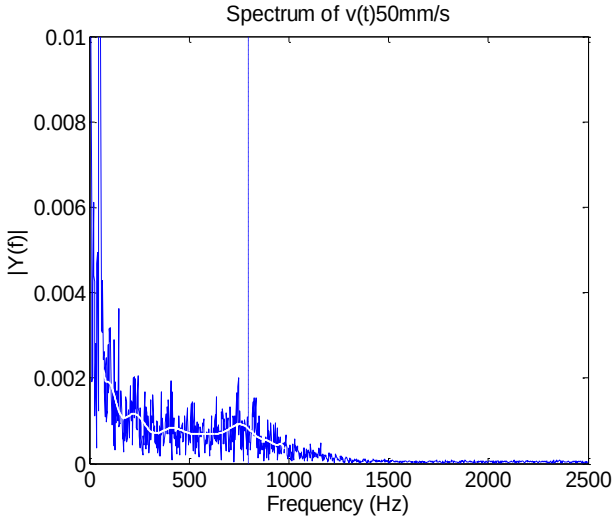
Spectrum of v(t)50mm/s
|Y(f)|
0.01
0.008
0.006
0.004
0.002
0
0
500
1000
1500
2000
2500
Frequency (Hz)

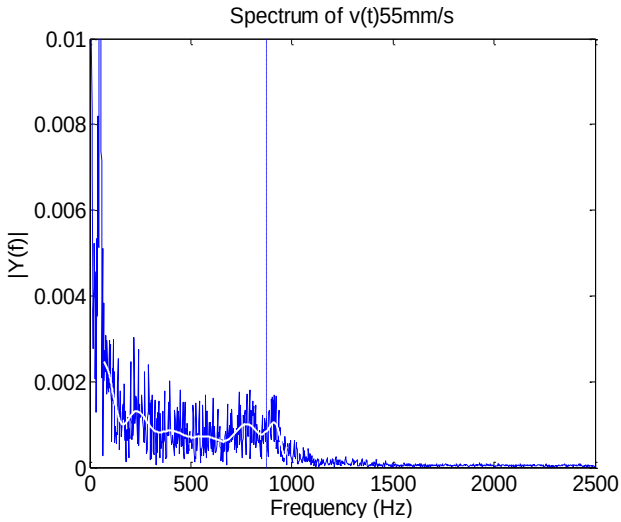
Spectrum of v(t)55mm/s
|Y(f)|
0.01
0.008
0.006
0.004
0.002
0
0
500
1000
1500
2000
2500
Frequency (Hz)

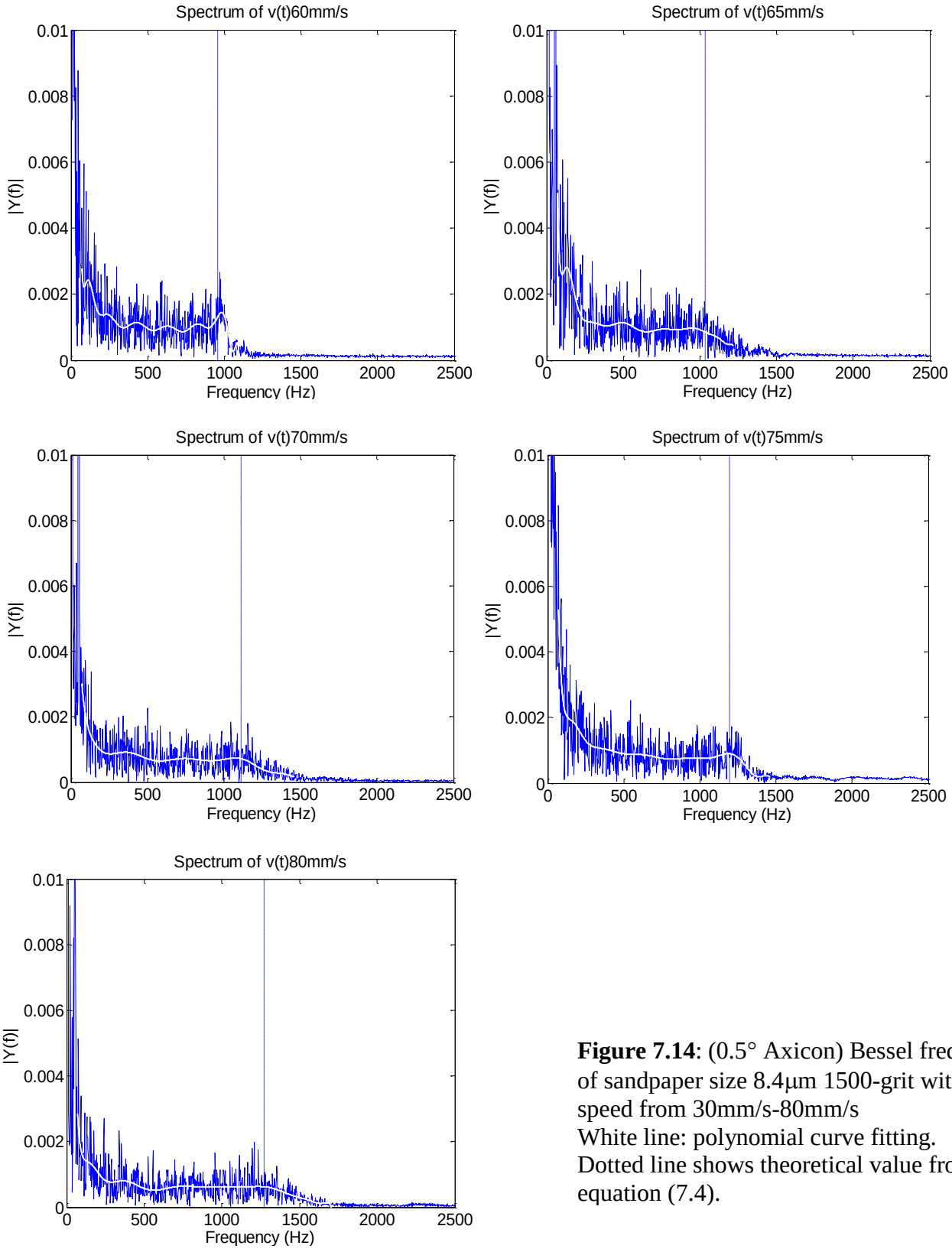

Figure 7.14: (0.5° Axicon) Bessel frequency of sandpaper size 8.4μm 1500-grit with speed from 30mm/s-80mm/s
White line: polynomial curve fitting.
Dotted line shows theoretical value from equation (7.4).

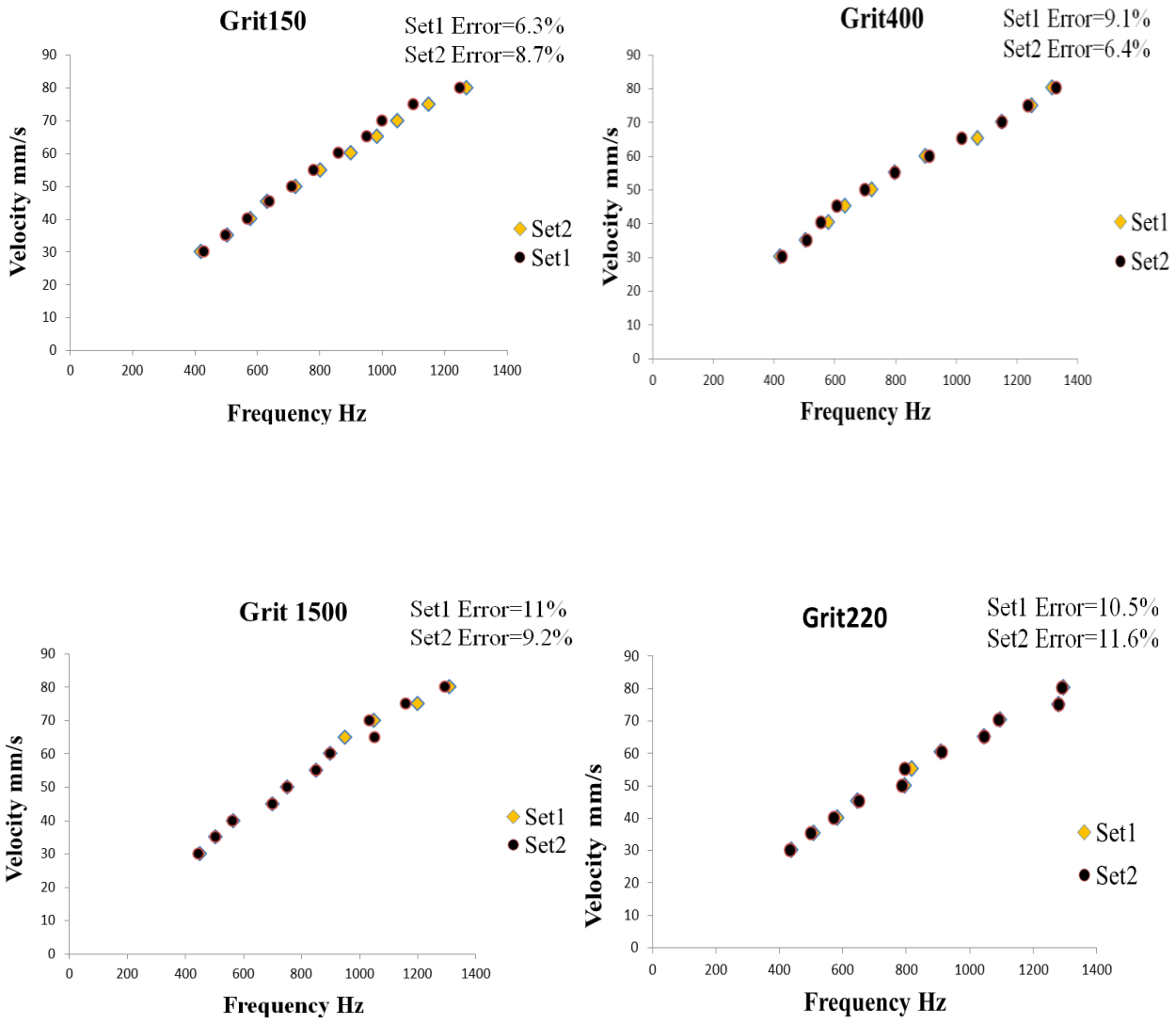

Figure 7.15: velocity vs frequency of two sets of measurements of 0.5° axicon with the relative error of each set

7.3 Analysis of measurement results with wires

Another set of experiments with single wires crossing the fringes at constant velocities were undertaken. In this case the wires are much larger than the fringes. These measurements could have applications in solid surfaces or objects velocity measurements in manufacturing, automation or biological experimentation. A time signal of scattered light intensity was generated by allowing the wires to move at constant velocity in the horizontal direction from any starting point and cross Bessel beam fringes. The signals generated by spaced 150μm diameter moving copper wires are completely different from the measured signals with the moving abrasive rough surface. In this case the time signal was used to measure the velocity of the wires. A single wire crossing the Bessel beam emits a single signal burst presenting the velocity of the wire, and its profile exhibits one well-defined peak corresponding to the central spot and other peaks corresponding to the fringes. The fringe spacing is well known, and depends only on the axicon and the wavelength of the laser used. Also, the time T to cross these fringes can be obtained from the time signal of the scattered light, so the velocity can be simply calculated by dividing the fringe spacing by the time difference between the fringes.

$$\text{Velocity} = \frac{\text{fringe spacing}}{\text{time}} = \frac{d_f}{\text{T}} \qquad (7.5)$$

Table 7-1: The first 16 roots of zero order Bessel function of the first kind

m	Values of r such that $J_0^2(r)=0$	Non-dimensional fringe spacing	0.5° Fringe Spacing (μm)	5° Fringe Spacing (μm)
1	2.404825	3.115253	70.537201	7.0271680
2	5.520078	3.133649	70.953733	7.0686645
3	8.653727	3.137807	71.047881	7.0780438
4	11.791534	3.139383	71.083566	7.0815988
5	14.930917	3.140146	71.100842	7.083320
6	18.071063	3.140573	71.11051	7.0842832
7	21.211636	3.140835	71.116443	7.0848742
8	24.352471	3.141008	71.12036	7.0852644
9	27.493479	3.141127	71.123054	7.0855330
10	30.634606	3.141214	71.125024	7.0857291
11	33.775820	3.141278	71.126473	7.0858735
12	36.917098	3.141327	71.127583	7.0859840
13	40.058425	3.141366	71.128466	7.086072
14	43.199791	3.141397	71.129168	7.086142
15	46.341188	3.141421	71.129711	7.086196
16	49.482609	3.141442	71.130187	7.086243

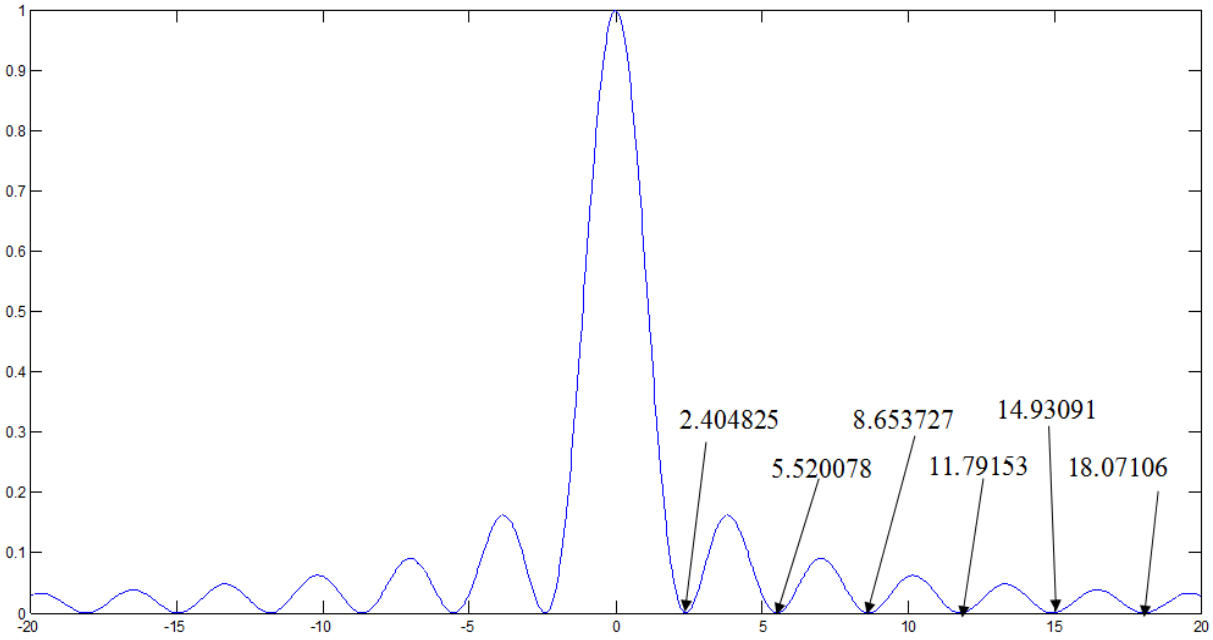

Figure 7.16: Bessel beam fringe spacing

The fringe spacing was simply calculated from equation

$$d_f = \left(\frac{\text{Non-dimensional Fringe spacing}}{k\beta}\right) \qquad (7.6)$$

Figure 7.16 and Table 7-1 give the values of Bessel beam fringes in the current LBV configuration as well as the calculated fringe spacing for 658nm.

7.3.1 Processing of 0.5° Axicon Measurements

The measurements were performed with velocities from 10 to 70mm/s with three wires. To illustrate the calculation procedure, the velocity of 50mm/s was chosen and its time signal is shown in figures 7.17 and 7.18. Results corresponding to other velocities are summarized in Table 7-2.

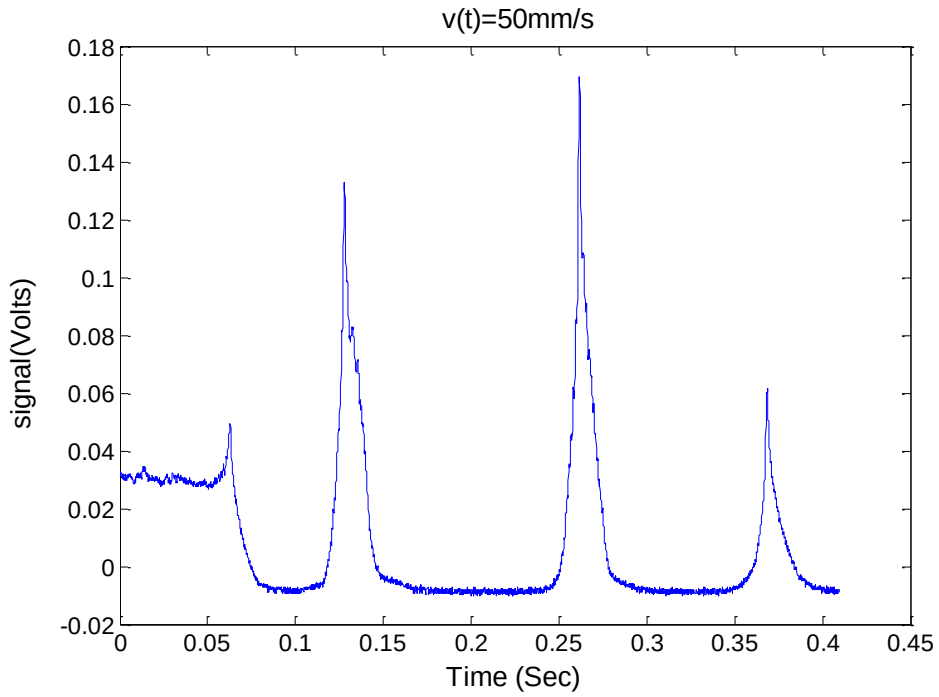

Figure 7.17: Time signal of 3 wires crossing Bessel beam fringes of 0.5° axicon at 50mm/s

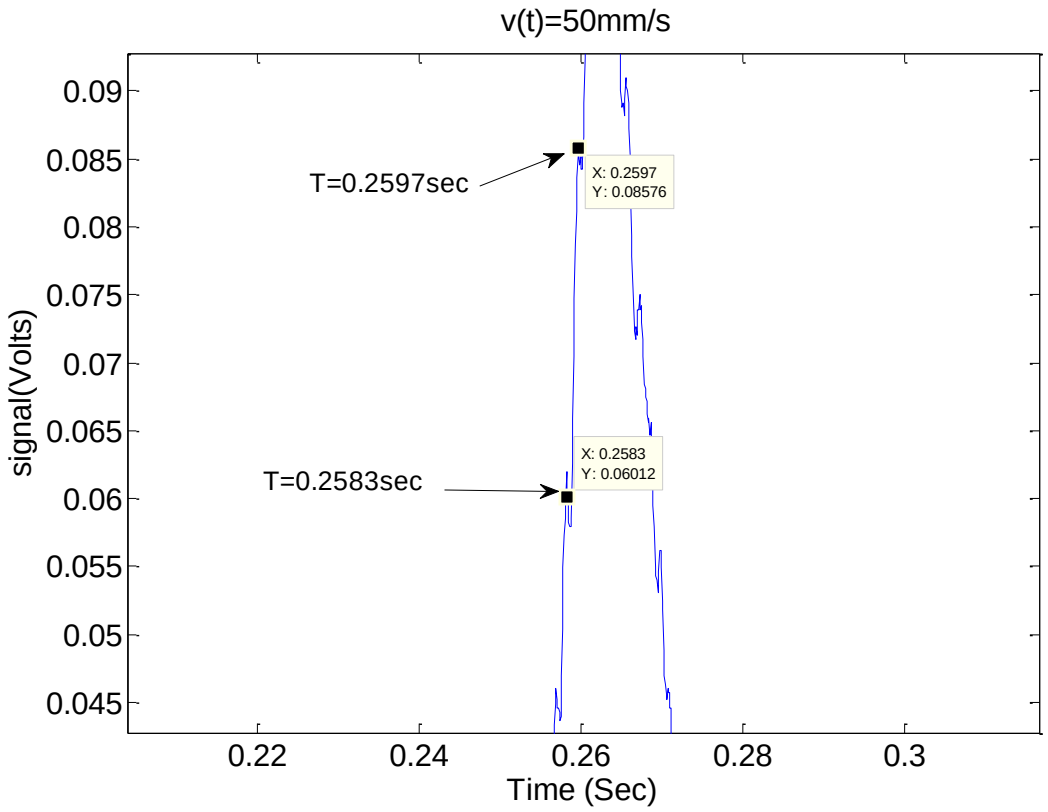

Figure 7.18: Two peaks representing the first two fringes of the time signal of 0.5° axicon (50mm/s)

In figure 7.18 we show a part of the time signal of figure 7.17 where we focus on two peaks corresponding to two adjacent fringes. The time for the particle to pass from the first fringe to the second can be found as:

Period between two fringes: T = 0.2597-0.2583 = 0.0014seconds

The corresponding fringe spacing between these two fringes from table 7-1: d_f =70.537201μm

Then calculating the velocity

$$v = \left(\frac{70.537201\text{x}10^{-3}}{0.0014}\right) = 50.384\text{mm/s}$$

The calculated velocity is very close to the set velocity of the stage. The difference of 0.384mm/s is likely due to the wires used were not exactly vertical while taking measurements when crossing the fringes. Also the wires are 150μm in size compared to the fringe spacing d_f =70.537201μm which can cause some errors.

The sampling frequency and number of points for each velocity were carefully chosen to capture the passage of the three wires through the measurement volume and to have a sampling time small enough to resolve the fringes. For measurements corresponding to all velocities shown in table 7-2, in general, as the velocity increases the relative error decreases.

Table 7-2: Measured speeds with 0.5° axicon

Actual set speed (mm/s) ±0.1	**Measured speed (mm/s)**	**% error**
10	8.9	11.0
20	19.2	4.0
30	29.6	1.3
40	40.5	1.4
50	50.4	0.8
60	62.9	4.7
70	70.7	1.0

7.3.2 Processing of 5° Axicon Measurements

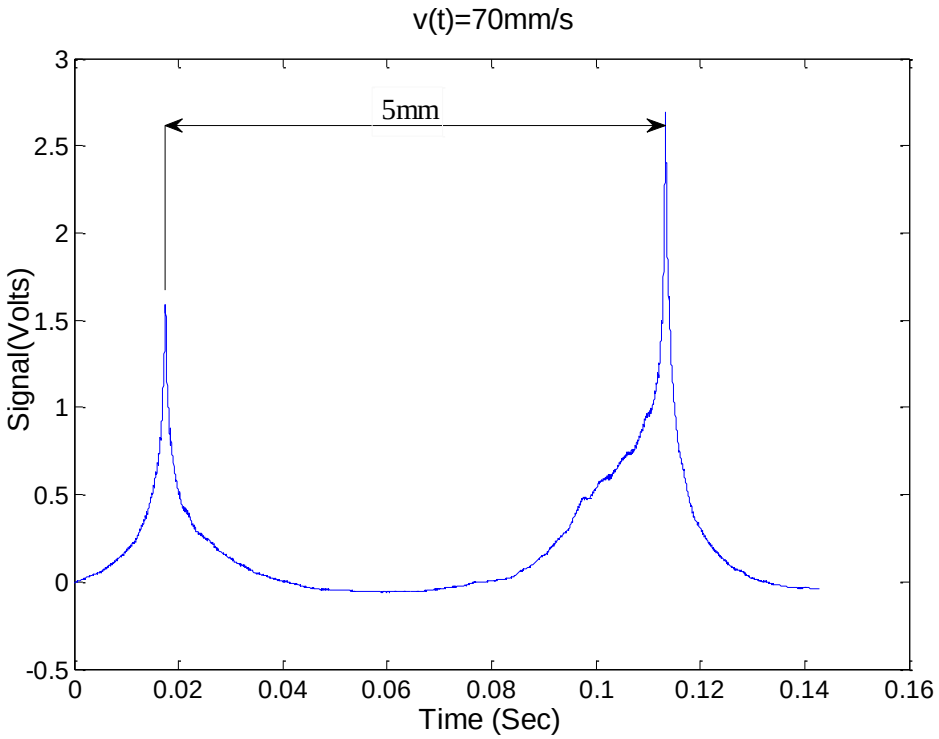

Figure 7.19: Time signal of 2 wires crossing Bessel beam fringes of 5° axicon at 70mm/s

Table 7-3: Measured speeds with 5° axicon

Actual set speed (mm/s) ±0.1	**Measured speed (mm/s)**	**% error**
10	11.8	11.8
20	18.2	9.2
30	33.7	12.2
40	43.7	9.2
50	50.6	1.1
60	58.9	1.7
70	70.8	1.2

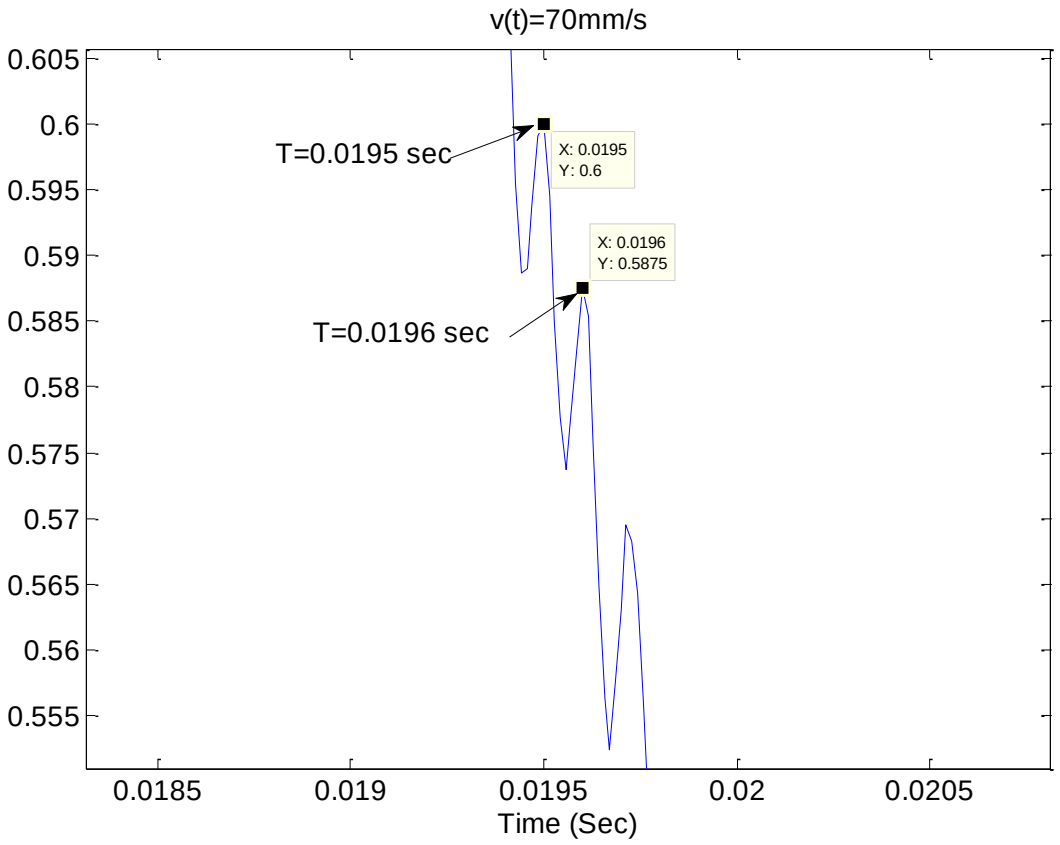

Figure 7.20: Two peaks representing the first two fringes of the time signal of 5° axicon (70mm/s)

The same procedure described for the 0.5° axicon was repeated for the 5° axicon. In this case two wires were used. A velocity of 70mm/s is selected to illustrate the calculations. The corresponding time signal is shown in figures 7.19 and 7.20. Considering the time between the fifth and sixth fringes of the Bessel beam,

Period between two fringes: T = 0.0196-0.0195 = 0.0001sec

The corresponding fringe spacing between these two fringes from table 7-1 d_f = 7.0271680μm

Then calculating the velocity

$$v = \left(\frac{7.083320\text{x}10^{-3}}{0.0001}\right) = 70.8332\text{mm/s}$$

Results for all other velocities are summarized in table 7-3. From these results, it can be seen that as the velocity increases the relative error decreases. Overall the results show that the Bessel beam fringe can be used for measurement of the velocity of the moving wires with the time

signal analysis. It should be mentioned that even though the wires are not perfectly straight or may had tiny bends and have larger diameter than fringe spacing, the results obtained were reasonably accurate.

Chapter 8

CONCLUSIONS AND RECOMMENDATIONS

In this work, an experimental setup was developed and built to conduct measurements of the velocity of moving rough surfaces. A prototype laser Bessel velocimetry optical system was built, characterized and validated. The fringes of a Bessel beam were used for this purpose. For the signal obtained from the moving rough surfaces a frequency signal analysis, based on the FFT method, was used. A time signal analysis, based on the time of flight, was used for measurement of the velocity of the wires. The LBV technique is a promising technique for velocity measurement. Some of the aspects that still require investigation are as follows:

- Measuring the negative velocity of particles in the flow with Bessel beam.
- Developing more accurate and computationally efficient models especially for real time applications in turbulent and laminar fluid flow.

The theory of working of the axicons presented helped in understanding the principle of using the LBV system. One of the inherited difficulties in LBV is performing accurate measurements of velocity directions and components. Based on the findings described in Chapter 7, the Bessel beam velocimetry method gave measurements very close to the expected values confirming that this optical technique is suitable for good measurements. Due to all the claimed advantages, time and energy were devoted in an effort to the development of this technique. As can be expected, nothing is ever so easy, and many issues have to be faced and overcome before reaching a satisfactory level of robustness.

The technique for measuring velocity with Bessel beam has many similarities with laser Doppler velocimetry. In both cases, the frequency of the signal produced by the photodetector or photomultiplier is proportional to the velocity of the particles. The equations relating to velocity are derivable from first principles, so calibration is not necessary in both cases. The difference is in the manner in which the fringe patterns are produced. The laser Doppler velocimeter has the advantage that small measuring volume with uniform fringe spacing and the velocity of smaller particles can be measured in submicron range. The Bessel beam technique, however, is simple but with larger depth of field and non-uniform fringe spacing. The Bessel frequency, f_b is similar to the expression of the Doppler frequency shift, f_D, for the LDV dual beam mode, where β is

the half angle between the two intersecting beams. The difference is that in the case of the f_b marks the edge of the hut shaped frequency distribution, while in LDV the spectrum shows a peak at f_D. One of the main disadvantages of the present technique compared to LDV is the lack of measurement of different velocity components. However, by observing the scattered light from different directions, or by repeating the measurements with different direction of the laser illumination, the component velocity measurements may be obtained.

References

[1] J. Hecht, "Beam: The Race to make the laser," *Opt. and photon. news*, vol. 16, no. 7, pp. 24-29, 2005.

[2] Yeh,Y; Cummins,H.Z., "Localized fluid flow measurements with an He–Ne laser spectrometer," *Appl. Phys. Lett.*, vol. 4, no. 10, pp. 176-178, 1964.

[3] J. Durnin., "Exact solutions for non-diffracting beams.I. The scalar theory," *JOSA* , vol. A4, no. 4, pp. 651-654, 1987.

[4] L. Paterson, E. Papagiakoumou, G. Milne, V. Garcés-Chávez, S. A. Tatarkova, W. Sibbett, F. J. Gunn-Moore, P. E. Bryant, A. C. Riches and K. Dholakia, "Light-induced cell separation in a tailored optical landscape," *Appl. Phys. Lett.*, vol. 87, no. 12, p. 123901, 2005.

[5] J.-y. L. a. J. F. Greenleaf, "Ultrasonic nondiffracting transducer for medical imaging," *Ultrason., Ferroelec., Freq. Cont.,* Vols. 37, no. 5, p. 438–447, Sept. 1990.

[6] A. Voigt, S. Heitkam, L. Büttner and J. Czarske, "A Bessel beam laser Doppler velocimeter," *Opt. Commun.,* vol. 282, no. 9, pp. 1874-1878, 2009.

[7] J. Y. Lu, X. L. Xu, H. Zou and J. F. Greenleaf, "Application of Bessel beam for Doppler velocity estimation,Ultrasonics, Ferroelectrics, and Frequency Contro," *IEEE Transactions on* , vol. 42, no. 4, pp. 649-662, 1995.

[8] A. K. B. Geselsch, "C. Doppler," vol. 2, p. 466, 1842.

[9] E. d. C. Andrade, "Doppler and the Doppler effect.," *Endeavour 18*, no. 69, 1959.

[10] L. E. Drain, "The laser Doppler Technique", USA: John Wiley and Sons, 1980.

[11] E. a. M. F. Huber, "Light scattering by small particles," *Aqua 47*, pp. 87-94, 1998.

[12] C. F. Bohren and D. R. Huffman, Absorption and scattering of light by small particles, John Wiley & Sons, 2008.

[13] Hulst, Hendrik Christoffel, and H. C. Van De Hulst, " Light scattering by small particles," *Courier Dover Publications,* 1957.

[14] Ichikawa, Tadashi, Hiroshi Ito, Manabu Kagami, and Satoru Kato, "Laser doppler velocimeter," *U.S. Patent 5,587,785,* December 24, 1996.

[15] Rogers, Philip L., and Kerry J. Vahala. , "Laser doppler velocimeter," *U.S. Patent 6,141,086,* October 31, 2000.

[16] H. Albrecht, N. Damaschke, M. Borys and C. Tropea, Laser Doppler and Phase Doppler Measurement Techniques, Springer, 2002.

[17] F. Durst, A. Melling and J. H. Whitelaw, Principles and practice of laser Doppler anemometry, 1981.

[18] F. Durst, A. Melling and J. Whitelaw, "Principles and practice of laser–Doppler anemometry," *NASA STI/Recon Technical Report A,* vol. 76, p. 47019, 1976.

[19] S. Tavoularis, "Measurement in Fluid Mechanics Paperback", 2009.

[20] T. Aruga, "Generation of long-range nondiffracting narrow light beams," *Apll.Opt.,* vol. 36, no. 16, pp. 3762-3768, 1997.

[21] Z. Jaroszewicz, "Axicons Design and Propagation Properties," Res. Dev. Treatisesv. 5, SPIE Polish Chapter, 1997.

[22] J. Sochack, A. Kołodziejczyk, Z. Jaroszewicz and A. S. Bar, "Nonparaxial design of generalized axicons," *Appl. Opt.,* vol. 31, no. 25, pp. 5326-5330, 1992.

[23] L. Soroko, "Axicons and meso-optical imaging devices," *in Progress in Optics,* vol. 27, pp. 109-160, 1989.

[24] L. Soroko, Meso-Optics – Foundations and Applications, Singapore: World Scientific, 1996.

[25] V. E. Peet and R. V. Tsubin, "Third-harmonic generation and multiphoton ionization in Bessel beams," *Phys. Revi.,* vol. A 56, no. 2, 1997.

[26] J. H. McLeod, "Axicons and their uses," *J. Opt. Soc. Am.,* vol. 50, p. 166–169, 1960.

[27] J. H. McLeod, "The axicon: a new type of optical element," *J. Opt. Soc. Am. ,* vol. 44, p. 592–597, 1954.

[28] J. Durnin, J. H. Eberly and J. J. Miceli, "Comparison of Bessel and Gaussian beams," *Opt. lett.,* vol. 13, no. 2, pp. 79-80, 1988.

[29] J. Arlt and K. Dholakia, "Generation of high-order Bessel beams by use of an axicon," *Opt. Commun.,* vol. 177, no. 1, pp. 297-301, 2000.

[30] Z. Bouchal, J. Wagner and M. Chlup, "Self-reconstruction of a distorted nondiffracting beam," *Opt. Commun,* vol. 151, no. 4-6, pp. 207-211, 1998.

[31] R. MacDonald, S. Boothroyd and T. C. Okamoto, "Interboard optical data distribution by Bessel beam shadowing," *Opt. Commun.,* vol. 122, no. 4-6, pp. 169-177, 1996.

[32] J. Durnin, J. Miceli and J. Eberly, *Opt. Lett.,* vol. 13, pp. 79-80, 1998.

[33] Y. Lin, W. Seka, J. H. Eberly, H. Huang and D. L. Brown, "Experimental investigation of Bessel beam characteristics," *Appl. opt.,* vol. 31, no. 15, pp. 2708-2713, 1992.

[34] D. McGloin and K. Dholakia, "Bessel beams: diffraction in a new light," *Contemp. Phys.,* vol. 46, no. 1, pp. 15-28, 2005.

[35] C. A. McQueen, J. J. Arlt and K. Dholakia, "An experiment to study a “nondiffracting” light beam.," *Amer. J. of Phys.,* vol. 67, no. 10, pp. 912-915, 1999.

[36] D. J. Fischer, C. J. Harkride and D. T. Moore, "Design and manufacture of a gradient-index axicon," *Appl. Opt.,* vol. 39, p. 2687–2694, 2000.

[37] E. B. Li, A. K. Tieu and W. Y. D. Yuen, "Measurements of velocity distributions in the deformation zone in cold rolling by a scanning LDV," *Opt. and las. in Eng.* vol. 35, no. 1, pp. 41-49, 2001.

[38] Li, Yajun and J. Katz., "Laser beam scanning by rotary mirrors. I. Modeling mirror-

scanning devices," *Appl. opt.,* vol. 34, no. 28, pp. 6403-6416, 1995.

[39] H. Albrecht, M. Borys, N. Damaschke and C. Tropea, "Laser Doppler and phase Doppler measurement techniques", Springer, 2003.

[40] F. Durst, A. Melling and J. Whitelaw, "Principles and practice of laser–Doppler anemometry", London:Academic Press, 1976.

[41] R. J. Adrian, "Particle-imaging techniques for experimental fluid mechanics," *Ann. Rev. of fluid mech.,* vol. 23, no. 1, pp. 261-304, 1991.

[42] A. Boutier, Laser Velocimetry in Fluid Mechanics, John Wiley & Sons, 2013.

[43] J. A. Monsoriu, C. J. . Zapata-Rodrıguez and W. D. Furlan, "Fractal axicon," *Opt. Commun.,* vol. 263, pp. 1-5, 2006.

[44] I. Golub and R. Tremblay, " Light focusing and guiding by an axicon-pair-generated tubular light beam," *J. Opt.Soc. Am. B,* vol. 7, no. 7, p. 1264–1267, 1990.

[45] M. Lei and B. Yao, "Characteristics of beam profile of Gaussian beam passing through an axicon," *Opt. Commun.,* vol. 239, pp. 367-372, 2004.

[46] Belanger and M. P.A. Rioux, "Ring pattern of a lens-axicon doublet illuminated by a gaussian beam," *Appl. Opt.,* vol. 17, no. 7, p. 1080–1086, 1978.

[47] Z. Jaroszewicz, A. Burvall and T. Friberg, "Axicon – The Most Important Optical Element," *Optics and Photonics News,* vol. 16, no. 4, p. 34–39, April 2005.

[48] M. De Angelis, L. Cacciapuoti, G. Pierattini and G. Tino, "Axially symmetric hollow beams using refractive conical lenses," *Optics and Lasers in Engineering,* vol. 39, no. 3, p. 283–291, 2003.

[49] B. Dépret, P. Verkerk and D. Hennequin, "Characterization and modelling of the hollow beam produced by a real conical lens," *Opt. Commun.,* vol. 211, no. 1-6, p. 31–38, 2002.

[50] K. Thewes, M. A. Karim and A. A. S. Awwal, " Diffraction free beam generation using

refracting systems," *Opt. Laser Technol.,* vol. 23, no. 2, p. 105–108, 1991.

[51] A. J. Cox and D. C. Dibble., "Nondiffracting beam from a spatially filtered Fabry-Perot resonator," *JOSA A,* vol. 9, no. 2, pp. 282-286, 1992.

[52] G. Scott and N. McArdle, "Efficient generation of nearly diffraction-free beams using an axicon," *Opt. Eng.,* vol. 31, no. 12, pp. 2640-2643, 1992.

[53] W.-X. Cong, N.-X. Chen and G. Ben-Yuan, "Generation of nondiffracting beams by diffractive phase elements," *JOSA A,* vol. 15, no. 9, pp. 2362-2364, 1998.

[54] J. Turunen, A. Vasara and A. T. Friberg, "Holographic generation of diffraction-free beams," *Appl. opt.,* vol. 27, no. 19, pp. 3959-3962, 1988.

[55] M. Couture and M. Piché, ""Focusing properties of an axicon pair," *Canadian journal of physics,* vol. 71, no. 1-2, pp. 70-78, 1993.

[56] N. Davidson, A. A. Friesem and E. Hasman, "Holographic axilens: high resolution and long focal depth," *Opt. lett.,* vol. 16, no. 7, pp. 523-525, 1991.

[57] J. Arlt, V. Garces-Chavez, W. Sibbett and K. Dholakia, " Optical micromanipulation using a Bessel light beam," *Optics Communications,* vol. 197, no. 4, pp. 239-245, 2001.

[58] L. Staroński, J. Sochacki, Z. Jaroszewicz and A. Kołodziejczyk, " Lateral distribution and flow of energy in uniform-intensity axicons," *J. Opt. Soc. Am. ,* vol. 9, no. 11, pp. 2091-2094, 1992.

[59] T. Čižmár and K. Dholakia, "Tunable Bessel light modes: engineering the axial propagation," *Opt. exp.,* vol. 17, no. 18, pp. 15558-15570, 2009.

[60] P. L. Overfelt and C. S. Kenney, "Comparison of the propagation characteristics of Bessel, Bessel-Gauss, and Gaussian beams diffracted by a circular aperture," *JOSA A,* vol. 8, no. 5, pp. 732-745, 1991.

[61] R. Arimoto, C. Saloma, T. Tanaka and S. Kawata, "Imaging properties of axicon in a scanning optical system," *Appl. opt.,* vol. 31, no. 31, pp. 6653-6657, 1992.

[62] P. Dufour, N. McCarthy and Y. De Koninck, "Two-photon microscopy with high depth of field using an axicon," in *Lasers and Electro-Optics*, Baltimore, Maryland United States, 2005.

[63] I. Golub, "Solid immersion axicon: maximizing nondiffracting or Bessel beam resolution," *Opt. Lett.*, vol. 32, no. 15, pp. 2161-2163, 2007.

[64] E. J. Botcherby, R. Juškaitis and T. Wilson, "Scanning two photon fluorescence microscopy with extended depth of field," *Opt. commun.*, vol. 268, no. 2, pp. 253-260, 2006.

[65] R. Arimoto, C. Saloma, T. Tanaka and S. Kawata, "Imaging properties of axicon in a scanning optical system,," *Appl. opt.*, vol. 31, no. 31, pp. 6653-6657, 1992.

[66] O. Bryngdahl, " Shearing interferometry with constant radial displacement.," *JOSA*, vol. 61, no. 2, pp. 169-172 , 1971.

[67] M. Rioux, R. Tremblay and P.-A. Belanger, "Linear, annular, and radial focusing with axicons and applications to laser machining," *Appl. opt.*, vol. 17, no. 10, pp. 1532-1536, 1978.

[68] R. M. Herman and T. Wiggins, "Production and uses of diffractionless beams," *J Opt Soc Amer(JOSA)*, vol. 8, no. 6, pp. 932-942, 1991.

[69] C. Altucci, R. Bruzzese, D. D'Antuoni, C. de Lisio and S. Solimeno, "Harmonic generation in gases by use of Bessel–Gauss laser beams," *JOSA B*, vol. 17, no. 1, pp. 34-42 , 2000.

[70] I. Manek, Y. B. Ovchinnikov and R. Grimm, "Generation of a hollow laser beam for atom trapping using an axicon," *Opt. Commun.*, vol. 147, no. 1-3, p. 67–70, 1998.

[71] E. M. Wright, J. Arlt, K. Dholakia and J. Soneson, "Optical dipole traps and atomic waveguides based on Bessel light beams," *Physical Review A*, vol. 63, no. 6, p. 8, 2001.

[72] Z. Ding, H. Ren, Y. Zhao, J. Nelson and Z. Chen, " High-resolution optical coherence tomography over a large depth range with an axicon lens," *Opt. Lett.*, vol. 27, no. 4, pp. 243-245, 2002.

[73] Z. Bouchal, J. Wagner and M. Olivik, "Bessel beams in the focal region," *Opt. Eng.,* vol. 34, no. 6, p. 1680–1688, 1995.

[74] S. De Nicola, "On-axis focal shift effects in focused truncated J0 Bessel beams," *Pure and Appl. Opt.,* vol. 5, no. 6, p. 827–831, 1996.

[75] B. Lü, W. Huang, B. Zhang, F. Kong and Q. Zhai, "Focusing properties of Bessel beams," *Opt. Commun.,* vol. 131, no. 4-6, pp. 223-228, 1996.

[76] S. Chávez-Cerda and G. H. C. New, "Evolution of focused Hankel waves and Bessel beams," *Opt. Commun.,* vol. 181, no. 4, p. 369–377, 2000.

[77] J. C. Gutiérrez-Vega, R. Rodríguez-Masegosa and S. Chávez-Cerda, "Focusing evolution of generalized propagation invariant optical fields," *Journal of Optics A* , vol. 5, no. 3, p. 276–282, 2003.

[78] G. Bickel, G. Hausler and M. Maul, "Triangulation with expanded range of depth," *Opt. Eng.,* vol. 24, no. 6, pp. 246975-246975, 1985.

[79] A. G. Saikaley, "Imaging, characterization and processing with axicon derivatives," PhD diss., Laurentian University, Sudbury, 2013.

[80] E. Dowski and W. Cathey, " Extended depth of field through wave-front coding," *Appl. Opt.,* vol. 34, no. 11, pp. 1859-1866, 1995.

[81] J. Ojeda-Castaneda, E. Tepichin and A. Diaz, "Arbitrarily high focal depth with a quasioptimum real and positive transmittance apodizer," *Appl. opt.,* vol. 28, no. 13, pp. 2666-2670, 1989.

[82] B. Chebbi, S. Minko, N. Al-Akwaa and I. Golub, " Remote control of extended depth of field focusing," *Opt. Commun.,* vol. 283, no. 9, p. 1678–1683, 2009.

[83] Z. Zhai, S. Ding, Q. Lv, X. Wang and Y. Zhong, "Extended depth of field through an axicon," *Journal of modern Optics,* vol. 56, no. 11, pp. 1304-1308, 2009.

[84] Z. Bouchal, "Nondiffracting optical beams: physical properties, experiments and applications," *Czechoslovak journal of physics* , vol. 53, no. 7, pp. 537-624, 2003.

[85] V. Garcés-Chávez, D. McGloin, H. Melville, W. Sibbett and K. Dholakia, "Simultaneous micromanipulation in multiple planes using a self-reconstructing light beam," *Nature* , vol. 419, no. 6903, pp. 145-147, 2002.

[86] T. Aruga and S. W. Li, "Super high resolution for long-range imaging," *Appl. opt.,* vol. 38, no. 13, pp. 2795-2799., 1999.

[87] S. Monk, J. Arlt, D. A. Robertson, J. Courtial and M. J. Padgett, "The generation of Bessel beams at millimetre-wave frequencies by use of an axicon," *Opt. commun.,* vol. 170, no. 4, pp. 213-215, 1999.

[88] K. Wang, L. Zeng and C. Yin, "Influence of the incident wave-front on intensity distribution of the nondiffracting beam used in large-scale measurement," *Opt. Commun.,* vol. 216, no. 1-3, p. 99–103, 200.

[89] S. C. Tidwell, D. H. Ford and W. D. Kimura, "Transporting and focusing radially polarized laser beams," *Opt. commun.*, vol. 31, no. 7, pp. 1527-1531, 1992.

[90] D. Li, K. K. Imasaki, S. Miyamoto, S. Amano and T. Mochizuki, "Conceptual design of Bessel beam cavity for free-electron laser.," *International journal of infrared and millimeter waves* , vol. 27, no. 2, pp. 165-171, 2006.

[91] S. P. Tewari, H. Huang and R. W. Boyd, "Theory of third-harmonic generation using Bessel beams, and self-phase-matching," *Phys. Rev. A,* vol. 54, no. 3, p. 2314, 1996.

[92] S. Hughes and J. M. Burzler, "Theory of Z-scan measurements using Gaussian-Bessel beams," *Phys. Rev.* , vol. 56, no. 2, pp. R1103-R1106, 1997.

[93] "www.thorlabs.com/thorcat/16000/PDF10A-Manual.pdf," Thorlabs, 21 3 2012. [Online]. [Accessed 10 01 2015].

[94] MSE, "http://measurementsci.com/wp-content/uploads/2014/10/miniLDV_brochure.pdf," Measurement Science Enterprise. [Online].

[95] "www.seabean.com/polish/GritScales.pdf-scale sandpaper grit," Sandpaper Grid Scales. [Online]. [Accessed 22 9 2014].

[96] I. H. Malitson and M. J. Dodge, "Refractive-Index and Birefricence of Synthetic Sapphire," *JOSA,* vol. 62, no. 11, pp. 1405-1405, 1972.

[97] S. Wolfram, " www. wolframalpha. com," Wolfram Alpha, 2009. [Online]. [Accessed 10 January 2015].